Copyright is owned by the Author of the thesis. Permission is given for a copy to be downloaded by an individual for the purpose of research and private study only. The thesis may not be reproduced elsewhere without the permission of the Author.

Doctoral Thesis

THE INVESTIGATION OF NON-CONTACT VITAL SIGNS DETECTION

MICROWAVE THEORETICAL MODELS AND SMART SENSING SYSTEMS

Nguyen Thi Phuoc Van

Department of Mechanical & Electrical Engineering

School of Food and Advance Technology

Massey University, New Zealand

2019

THE INVESTIGATION OF NON-CONTACT VITAL SIGNS DETECTION MICROWAVE THEORETICAL MODELS AND SMART SENSING SYSTEMS

A thesis presented in partial fulfilment of the requirements for the degree of

Doctor of Philosophy

in

Department of Mechanical and Electrical Engineering, SF&AT at Massey University, Palmerston North, New Zealand.

Nguyen Thi Phuoc Van

2020

Recommended Citation

Nguyen Thi Phuoc Van (2020) The investigation of non-contact vital signs detection microwave theoretical models and smart sensing systems, School of Food and Advance Technology, Massey University, New Zealand

Declaration

The thesis complies with the 'Guidelines for Doctoral Thesis by Publications' and with the requirements from the Handbook for Doctoral Study by the Doctoral Research Committee (DRC), Massey University. January 2011. Version 7.

Disclaimer

The opinions, figures and conclusions in the thesis are solely those of the author(s). Under no circumstances will the author(s) be responsible for any loss or damage of any kind resulted from the use of these methods and techniques presented in the thesis.

Contents

Abstract **x**

Acknowledgements **xiii**

1 Introduction **1**

1.1 Need for microwave sensing system 2
1.2 Motivation 4
1.3 Objectives 5
1.4 Challenges 6
1.5 Contributions 7
1.6 Thesis organization 8
1.7 Research outcomes 9

2 Literature review **12**

2.1 Introduction 12
2.2 Antennae system for microwave radar sensor 14
2.3 Signal processing techniques and mathematical models 17
2.3.1 Signal processing techniques 17
2.3.2 Related mathematical models 19
2.4 Hardware developments 20
2.4.1 Single tone CW radar sensor 22
2.4.2 Frequency modulation continuous wave (FMCW) radar sensor 26
2.4.3 Hybrid FMCW-CW radar sensor 29
2.4.4 Stepped-Frequency Continuous Wave (SFCW) Radar . . . 30
2.4.5 Random noise UWB radar sensor 32
2.4.6 Pulse-Based radar sensors 34
2.5 Conclusion 38

2.6 Related Publications 38

3 Extra Wide Band Antennae System for Vital Sign Detection 40
3.1 Introduction 40
3.2 Antenna design 41
3.2.1 Two dimensions (2D) transceiver antennae 43
3.2.2 Three-dimensional (3D) transceiver antennae 45
3.3 Vital signs sensing using extra wide band $3D$ antennae 48
3.3.1 System and performance analysis 48
3.3.2 Measurement and discussions 50
3.4 Conclusions 52
3.5 Related Publications 53

4 False alarm, Detection Probabilities of Microwave Doppler Sensing System 55
4.1 Introduction 55
4.2 System Model 56
4.3 SNR Analysis 60
4.3.1 Signal Power 60
4.3.2 Residual Phase Noise 60
4.3.3 Additive White Gaussian Noise 62
4.3.4 $1/f$ Noise 62
4.3.5 SNR 62
4.4 Detection and False Alarm Probabilities 63
4.4.1 Detection Probability 63
4.4.2 False Alarm Probability 65
4.5 Simulation Result 65
4.5.1 SNR and Detection/False Alarm Probabilities under Rayleigh Fading Channel 66
4.5.2 Detection/False Alarm Probabilities of the System under the Nakagami-2 Channel Model 69
4.6 Measurement Results 69
4.7 Conclusion 73
4.8 Related Publications 74

5 Nature-inspired Sensor System for Vital Sign Detection 75
5.1 Introduction . . . 75
5.2 System Model . . . 78
5.2.1 Theoretical model . . . 78
5.2.2 System Signal to Noise Ratio (SNR) . . . 80
5.3 Error detection probability . . . 82
5.4 Simulation Results . . . 85
5.5 Measurement Result . . . 87
5.6 Conclusion . . . 91
5.7 Related Publications . . . 92

6 Smart Radar Sensing System for Vital Signs Detection 93
6.1 Introduction . . . 93
6.2 Proposed system . . . 95
6.2.1 Operating principle of CW radar sensor . . . 96
6.2.2 AI module . . . 97
6.3 Experiment and Data . . . 102
6.3.1 Measurement set up . . . 102
6.3.2 Data sets . . . 104
6.3.3 Evaluation Metric . . . 105
6.4 Results . . . 105
6.5 Conclusion . . . 109
6.6 Related Publications . . . 109

7 Conclusion and Future work 110
7.1 Conclusion . . . 110
7.2 Future studies . . . 111

References 114

List of Tables

2.1 Parameters of UWB radar [1] 37

4.1 System parameters used for simulation. 66
4.2 Respiratory rates and signal-to-noise ratio (SNR) from five objects at different distances. 70

5.1 Parameters of the proposed system used for simulation 86
5.2 Respiratory rates from five objects at different distances 91

6.1 Data set description 104
6.2 Classification accuracy of proposed system 108

List of Figures

1.1 Applications of the microwave Doppler sensing system 2
1.2 Microwave sensing system is used to find people under debris . . 3

2.1 (a) Arrays antennae system. (b) Topology of the sequential-phase feed network © 2012 IEEE [2] 15
2.2 Topology of designed antennae arrays (a) 2×1 patch elements, (b) 3×2 patch elements, (c) 6×2 patch elements [3] 16
2.3 Block diagram to test multiple targets detection [4] 18
2.4 Traditional FFT method (a) versus VMD based method (b) [4] 19
2.5 Error probability of radar sensing system © 2012 IEEE [5] . . . 20
2.6 Received signal in time domain (a) and in frequency domain (b) at the distance of 0.5 m [6] 21
2.7 System overview and real-life application example with measured performance [7] 22
2.8 Continuous Wave System diagram. 23
2.9 Schematic of 1.15 GHz microwave radar [8] 24
2.10 Testing performance of Kum-Mu Chen *et al.* [8] system at the earthquake rubble model of Michigan State University 25
2.11 Schematic of life-detector system [9] 26
2.12 Frequency versus time of transmitting and receiving signal at $FMCW$ radar 27
2.13 Topology of $FMCW$ radar used to detect a human through the wall [10] 28
2.14 Experiment setup of $FMCW$ radar to detect a human through the wall [10] 28
2.15 Transmitting and receiving signal at $FMCW$-CW radar in (a) frequency domain and (b) time domain [11] 29

2.16 Experiment setup of $SFCW$ radar to detect a human through the brick: (a) size view, (b) top view, (c) postures [12]. 30
2.17 Breathing rate of a face-up posture person at different time resolutions [12] 31
2.18 Diagram of a basic random noise UWB radar sensor 32
2.19 A schematic of a digital random noise UWB radar sensor [13] . . 33
2.20 Detecting human movement through a wall using a digital random noise UWB radar sensor [13] 34
2.21 Block diagram of a typical UWB radar system 35
2.22 Vital signs detection experiments for a human subject by UWB radar sensor (a) outdoors, (b) indoors [1] 36
2.23 Detection algorithm [1] 37
2.24 The STFT in the case of 9 m human location [1] 38

3.1 Feeding methods for patch antennae: (a) Coaxial feed, (b) Microstrip line feed, (c) Aperture coupled feed, and (d) Proximity coupled feed [14, 15] 42
3.2 Structures of the designed antennae 4× patch for RX and 3× patch for TX [16] 44
3.3 3D Geography of proposed antennae [16] 46
3.4 Fabricated antenna system [16] 47
3.5 Reflection at the input and Isolation between two antennae [16] . 47
3.6 Block model of the radar sensor system [16] 48
3.7 The measurement setup to detect the vital signs [16] 51
3.8 Amplitude versus respiratory rate in frequency domain when the distance between the antennae and the object is 80 cm [16] . . . 52
3.9 Amplitude versus respiratory rate when 3 cm of wood between the antennae and the object in frequency domain [16] 53
3.10 Receiving signal in time domain and in frequency domain [16] . . 54

4.1 System diagram. 56
4.2 Power of signal and noise of the system. 67
4.3 Signal-to-noise ratio (SNR) versus the distance from the radar system to the human body. 67
4.4 Detection probabilities of the system under different threshold levels of receiver filter. 68

4.5 False alarm of the system under different threshold levels of receiver filter. . . . 68
4.6 False alarm/detection probabilities of the system under Nakagami-2 channel model. . . . 69
4.7 Measurement setup to detect the breathing rate. . . . 70
4.8 Receiving signals in time domain. . . . 71
4.9 Receiving signals in frequency domain. . . . 71
4.10 Signal-to-noise ratio (SNR) of the system. . . . 72
4.11 Detection capability of the system in time domain. . . . 73
4.12 Detection probability of the system at different distances. . . . 73

5.1 System diagram. . . . 76
5.2 SNR at the receiver 1 86
5.3 Error probability of the system when the distance changes 87
5.4 Experimental setup 88
5.5 Measurement setup for proposed system 88
5.6 Receiving signal in time domain 89
5.7 Receiving signal in frequency domain 89
5.8 Error probability of system vs distance of measurement 89
5.9 $SNR_{left} - SNR_{right}$ at different distances when the object is in the left side 90
5.10 Directional detecting capability of the proposed system 90

6.1 Simulation for Dysthymic respiration. . . . 94
6.2 Simulation of Cheyne Stokes Respiration signal. . . . 94
6.3 Block diagram. . . . 95
6.4 The steps implemented in the AI module. . . . 97
6.5 Linear Support Vector illustration. . . . 100
6.6 Decision tree model. . . . 101
6.7 Measurement setup. . . . 103
6.8 Experimental procedure. . . . 104
6.9 Measured signal in the time domain. . . . 105
6.10 Measured signal in the frequency domain. . . . 106
6.11 Relationship between Feature # 2 and Feature # 66 in the Data set I. . . . 107

6.12 Relationship between Feature # 62 and Feature # 65 in the Data set III. 107

Abstract

Natural disasters, such as floods, landslides and earthquakes, occur frequently around the world. The consequences of such disasters in developing countries tend to be more severe due to the lack of effective life detector systems. Life signs detecting has been an active and challenging research field that has great potential in the applications such as finding human lives under debris and non-invasive diagnosis and health monitoring. There are obvious limitations of conventional devices such as optical or acoustic detectors. The optical equipment requires operation from experts, while the acoustics need a quiet environment. The detectors with the thermal sensors and wireless tracking systems are also insufficient when the "non line of sight" problem appears. In addition, vital signs information (such as heartbeat and breathing rate) from non-invasive microwave sensors are very important to locate people or predict health conditions in the cases of defence, smart home applications, and baby monitoring. Since NASA proposed the use of microwave radar sensing system for life detecting, research and implementation on sensitive, effective, and economic vital signs sensing systems based on microwave signals have become very active. Until now, most research on life detectors has concentrated on hardware development, signal processing, and development of new algorithms to improve accuracy of vital signs detection.

The present study has focused on microwave sensors, studying microwave theoretical models and searching for life detecting, health care and smart home applications. In this research, the antennae systems for vital signs detection, such as breathing rate, were first investigated to validate their performance in a system at different frequencies. The antennae system had an extremely large band width, operating from L band to the X band. Based on the proposed antennae system, models to evaluate the false alarm/detection probabilities of a microwave sensing system were then developed and validated to examine the accuracy of the system

in advance. These models are very useful for hardware development of microwave radar sensors. Further investigation into the theoretical models, proposed a novel system that was inspired by the microbat animal's physical structure. This system showed an enhancement in the accuracy and directional signals of the microwave sensing system. Artificial intelligence was then integrated with the radar sensing system to develop the smart microwave radar sensing system. The machine learning/ deep learning models based on the collected data were developed. The study indicated high accuracy in classifying different types of breathing disorders.

This page is intentionally left blank.

Acknowledgements

During the tough but worthwhile journey of my Ph.D, there are countless people for me to say thanks. First of all, I would like to thank my primary supervisor Dr. Liqiong Tang for her patient guidance and valuable support throughout my study. I am very grateful to my co supervisors Dr. Faraz Hasan, Prof. Subhas Mukhopadhyay and A.Prof. Nguyen Duc Minh for encouraging, and giving me freedom in my research.

I would like to thank for New Zealand Scholarship and Slumberger Faculty for the Future programs which offered generous support to me to pursue my study, and my dreams at Massey University.

In general, I wish to thank my friends Amardeep Singh, Achinthya Perera, Chanjief Chandrakumar, Paturkar Abhipray, Syed Shan, Thu Nguyen, Nisansala Pallawala, Nasrin Afsarimanesh, Md. Eshrat E Alahi, Anindya Nag, and Kanwal Zaidi for their cheerful sharing and support to make my life in New Zealand nicer and more enjoyable. I also thank to Massey staff Jamie Hooper, Saba Azeem, Dandan Wang, Dilantha, Sherryl, Sharon, Karen, Sharlene and Glenda for always helping me.

A special thanks is given to my great proof reader Dr. Ruth Mortimer for always helping me through my publications and my thesis.

I acknowledge the Editors and anonymous referees for carefully reading, giving feedback and suggestions on five presented works here to help me improve the thesis substantially.

Finally, I would like to take this opportunity to thank my family for their unconditional love and support.

Chapter 1

Introduction

The first microwave Doppler sensing system to detect vital signs was released in the 1970s. This sensing system was able to trigger a warning signal when apnoea appeared in an infant [17]. The fast development in the semiconductor industry opened an application avenue for Doppler radar sensors. Microwave sensing is non-invasive. This non-invasive property of the Doppler radar sensor makes it ideal for detecting and monitoring human vital signs and has attracted a lot of research interest in the field of smart home applications, health care, defense, and rescue after natural disasters. Figure 1.1 illustrates the popular research areas involving Doppler radar sensing over the past decade. The research work presented in this thesis has focused on improving the signal quality of the radar-sensing system through the study of microwave theoretical models for the applications such as detecting vital signs in rescue work for life searching and non-invasive health care. Such radar-sensing systems and equipment, especially the economic ones, are of significant value for life searching during natural disasters and have great potential in future smart systems.

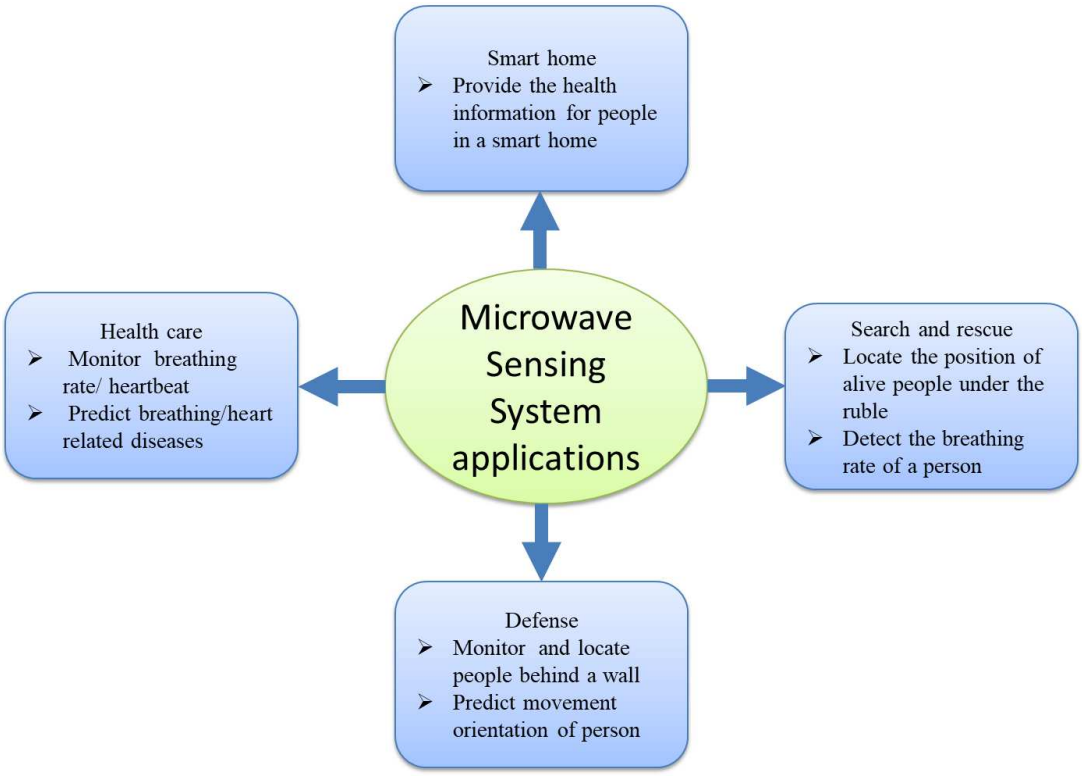

Figure 1.1: Applications of the microwave Doppler sensing system

1.1 Need for microwave sensing system

Natural hazards, such as landslides and earthquakes, cause many deaths all over the world. For example, in Nepal's earthquake in 2015, the number of deaths was around 8000 [18]. During this disaster, many people covered by debris could not be found in time. The conventional methods, such as using dogs to find people who are buried, are inefficient due to the time consumption and uncertainty [19]. Moreover, other methods such as optical-based detectors that require operation by experts, or the sound-based system that is significantly affected by noises from the environment, have their limitations and drawbacks. The camera/thermal sensors lack detecting ability to find location information in the smoking environment [20]. The microwave sensing system has great potential for such applications. Figure 1.2 presents an illustration of the potential for using the microwave sensing system to find people under debris.

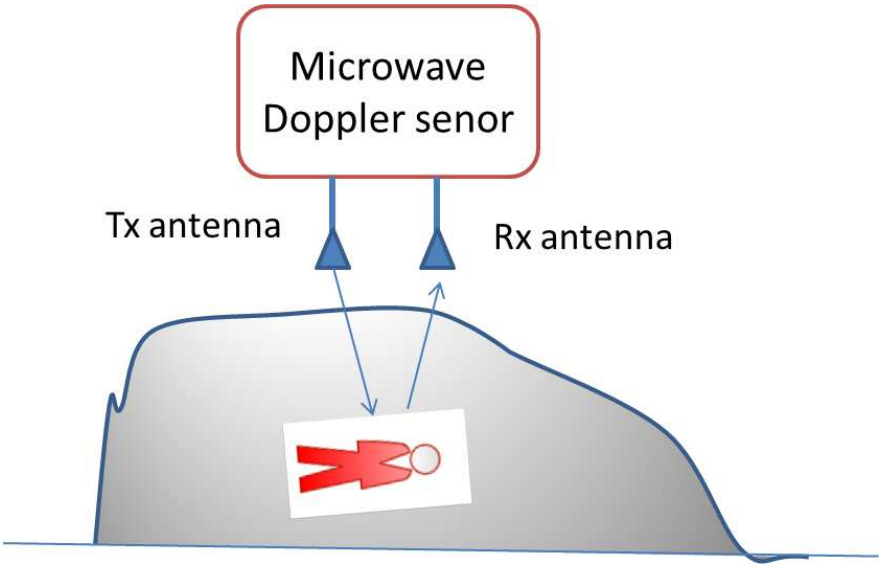

Figure 1.2: Microwave sensing system is used to find people under debris

The vital signs detecting system, based on the Doppler radar, has been attracting much attention in recent studies [19, 21–25]. It is understood that in a vital sign radar detecting system, the transmitter sends waves to the human body; these waves are modulated by the chest displacement and reflect to the receiving antenna [26]. By comparing the transmitting waves and the receiving waves from the human body, one can extract useful information such as the respiratory rate, heart beat and the location of the people. An important application field of microwave radar sensing is to detect people who are trapped alive under debris, rubble or behind a wall. Such a system ,not only can detect the presence of people via a respiratory signal, but is also able to locate where they are by comparing the transmitted signals and received signals. In the health-care applications, microwave sensors can be used to measure the breathing rate and heartbeat, especially in cases like burned patients. Microwave sensing equipment can also continuously monitor the sleeping of babies to prevent sudden unexpected infant deaths [27]. Reference [28] discussed the effect of antennae characteristics, filters to the quality of vital signs measured by microwave radar sensor for medical application. Their work introduced a deep relationship between hardware configuration of radar sensor and the quality of measured breathing rates and heartbeat.
For smart home applications, the microwave radar sensor is integrated with other sensors to provide more information. For example, by collecting the breathing

rate of a person during sleep, a smart home system can even generate warning signals or messages to remind people for medical checking.
Although there are a lot of reports on microwave sensing, few studies have focused on theoretical models and economic smart systems. The challenge is to find theoretical models to evaluate the accuracy of microwave radar sensing systems. These have led to the interest of this research.

1.2 Motivation

In the vital signs detecting radar sensor, transceiving antennae play the role of sensing probes in a microwave sensing system. Shen [2] introduced an antenna design of 60 GHz frequency, which can operate from 50 GHz to 60 GHz. The size of the antennae is quite small since its operating frequency is high, and this high frequency operation is more useful for medical applications than for search and rescue purposes. Another development was a wide band antenna with the gain of 5 dB in the range $[4.5 - 6.5]$ GHz [29], which has the advantage of quite large bandwidth ($2Ghz$). However, it has the limitations of operating at L band or X band. The literature search shows little work has been conducted on using extra wide band (from L band to the X band) to validate the performance of microwave radar sensing for search and rescue purposes. The first motivation of this research was to find the feasibility to develop an extremely wide band antennae system.
When it comes to the channel link to describe the transmission between a person and the radar sensing system, there are no models available that can evaluate the accuracy of a radar sensing system when it operates in different environments. Most of the current research uses the Friis channel model for the links. This model considers that there are line-of-sight (LOS) transmissions between the detecting system and the human body. The model is too simple to describe the environment in which the life detector needs to operate. Obviously, to detect the location of living people under the debris or the rubble of fallen buildings, the signal of a life detecting system has to go through a very dense environment. The considerations of the channel model for the links transmitter-to-human-to-receiver are crucial when establishing a mathematical model to predict the accuracy of a sensing system. This research conducted a study on false alarm, detection or outage probability of radar sensing systems and also considered the design of a radar

sensing system to increase the three-dimensional detection capability.
A nature-inspired system from the micro bat animal was proposed to enhance the accuracy and the directional ability of the radar sensing system. To prove the outperforming ability of the proposed system ,the detection probability of the conventional and proposed systems are developed and compared.
To make the microwave sensing system smarter for life searching devices and medical applications, this research introduced a novel artificial intelligence (AI) microwave radar sensing model. This model, which is based on machine learning/ deep learning can be further developed to make the microwave radar sensing system intelligent for different applications.

1.3 Objectives

To realise the aim of this research, the following objectives have to be fulfilled.

- Develop an extra wide band antennae system that is able to detect tiny movements like human chest displacement.
- Conduct a study on available models and establish the mathematical models to evaluate the accuracy of the radar sensing system when it operates in different media. The false alarm/detection probabilities for the microwave sensing system will be investigated when the frequency and transmitting power changes. Those probabilities are the important factors for the hardware development, especially for search and rescue since the sensing system has to operate in the non-line of sight (NLOS) environments.
- Develop a life detector system that can enhance the detection and directional capabilities. The mathematical model of detection probability will be compared with the performance of conventional systems. Establish a measurement system to validate the theoretical/simulation results.
- Conduct a study on artificial intelligence to develop an AI-based microwave radar sensing system. Different machine learning/deep learning techniques will be explored for vital signs detection.

1.4 Challenges

This research has to face the following challenges before finding viable solutions for the potential applications mentioned in Section 1.1.

Extra wide band antennae

- Identify adequate equipment including software to design an extra wide band antennae system
- Find a solution to reduce the size and weight of the antennae
- Develop a portable antennae system (narrow beam) to use for vital signs detection purposes.

Mathematical models to evaluate the accuracy of the microwave sensing system

- Develop a mathematical model on the false alarm, detection and outage probabilities of a portable life detector when it operates in different environments.
- Validate the developed mathematical model with the simulation/measurement results
- Process the measured signals to get the desired information in order to validate developed models.

Nature-inspired radar sensing system

- Study the behavior and physical structure of the micro bat animal
- Find similar physical properties in the micro bat animal which inspires the development structure of a microwave radar sensing system
- Investigate a mathematical model of detection probability of this proposed system and compare with the conventional one
- Establish a measurement system to validate the performance of the proposed system.

Smart radar sensing system

- Study machine learning/deep learning techniques and the application possibilities for vital signs data
- Collect enough data to build different types of AI models
- Build data sets to validate AI models
- Set up different types of measurement to collect meaningful data.

1.5 Contributions

This research, through the investigations, simulations and experiments, completed the initially set objectives, established useful models for smart system development and made the following contributions.

Antennae system

- An extra wide band antennae system was developed
- The antennae can operate at different frequencies, from the L band to the X band to detect vital signs such as breathing rate
- The antennae were able to carry out experiments at various frequencies
- A novel three dimensional orthogonal design was proposed and successfully implemented to reduce the size of the antennae.

Mathematical model to evaluate the accuracy

- Examined the signal-to-noise ratio (SNR) on the basis of different types of noise such as phase noise, Gaussian noise, leakage noise between the transmitting and receiving antennae.
- Investigated the derivation on the false alarm, detection and outage probabilities of the radar sensing system in detecting the chest movement.
- Studied and compared different channel models presented for various media to derive the alarm/detection/outage probabilities.

- Conducted experiment to compare the proposed theoretical model with the measured data.

Nature-inspired sensor system

- Inspired by Microbat, proposed a novel nature-inspired vital signs detecting microwave sensing system.
- Investigated the derivation on the error probability of the radar sensing system in breathing rate detection.
- Conducted a validation and comparison between the proposed system and the conventional system.
- Carried out the experiment to compare and evaluate the proposed system with the five-point touching sensor.
- Validated that the proposed system enhances the $3D$ detection capability of the microwave radar sensing system.

Smart microwave Doppler sensing system

- Proposed an AI-based microwave sensing system.
- Conducted the experiment to collect data for different applications using smart radar sensing.
- Built a statistical model-based machine learning to diagnose breathing problems.
- Investigated the feasibility of a smart sensing system to enable more functions for search and rescue purposes.

1.6 Thesis organization

The literature related to this research and the research outcomes are discussed in the following chapters. The organization of the thesis is presented as follows: **Chapter 2: Literature review**. In this chapter, different types of Doppler vital sign radar systems, with a focus on search and rescue purposes, are discussed

carefully. Chapter 2 presents a background of microwave Doppler sensors. The hardware structures (from on chip to the circuit level) are reviewed. Different signal processing methods for vital signs detection of radar sensing system are surveyed.

Chapter 3: Extra Wide Band Antennae System for Vital Signs Detection. The principles of patch antennae are discussed. The beam-enhanced capability and an extreme wide band antennae was designed in $FR4$ substrate. The orthogonal structure to reduce the size of the antennae system is presented in this chapter. The measurements through the line of sign (LOS) and non-line of sign ($NLOS$) media to detect the respiratory rate to check the performance of antennae are discussed.

Chapter 4: False alarm/ Detection Probabilities of Microwave Doppler Sensing System. In chapter 4 the mathematical model of false alarm/ detection probabilities are investigated. The power of different noises was considered to derive SNR. The SNR and probabilities derivations are validated by the simulation and measurement results.

Chapter 5: Nature-inspired Radar Sensing System for Vital Sign Detection. This chapter introduces a novel vital signs detecting system which is inspired by the micro bat animal. The derivation of error detection probability is developed. The performance in detection ability of the proposed system is evaluated and compared with the conventional systems.

Chapter 6: Smart Radar Sensing System for Vital Signs Detection. Chapter 6 discusses the smart sensing system. The AI-based microwave radar sensor has the potential to enable more functions in medical and rescue applications. The smart radar sensing system can be used for health-care diagnosis such as for a breathing disorder problem and predicts the action of people or categorizes subjects in search and rescue operation.

The conclusions are drawn and prospective research recommendations are given in Chapter 7.

1.7 Research outcomes

This research has produced the following peer-reviewed publications.

Book chapter

- **Van Nguyen Thi Phuoc**, Liqiong Tang, Duc Minh Nguyen, Faraz Hasan, and Subhas Mukhopadhyay. "Wide Band Antennae System for Remote Vital Signs Detecting Doppler Radar Sensor." In Modern Sensing Technologies, pp. 47-62. Springer, Cham, 2019.

Journal publications

- **Van Nguyen Thi Phuoc**, Liqiong Tang, Veysel Demir, Faraz Hasan, Duc Minh Nguyen, and Subhas Chandra Mukhopadhyay,. " Review-Microwave Radar Sensing Systems for Search and Rescue Purpose" Sensors 2019, 19(13), 2879, **Q1**, **Impact Factor 3.03**

- **Van Nguyen Thi Phuoc**, Liqiong Tang, A. Singh, N. D. Minh, S. C. Mukhopadhyay and S. F. Hasan, "Self-Identification Respiratory Disorder Based on Continuous Wave Radar Sensor System," in IEEE Access, vol. 7, pp. 40019-40026, 2019. doi: 10.1109/ACCESS.2019.2906885, **Q1**, **Impact Factor 4.098**

- **Van Nguyen Thi Phuoc** Liqiong Tang, Faraz Hasan, Nguyen Duc Minh, and Subhas Mukhopadhyay. "Nature-inspired sensor system for vital signs detection." Sensors and Actuators A: Physical 281 (2018): 76-83. **Q1**, **Impact Factor 2.739**

- **Van Nguyen Thi Phuoc**, Liqiong Tang, Subhas Chandra Mukhopadhyay, Duc Minh Nguyen, and Faraz Hasan. "Probabilities of False Alarm for Vital Sign Detection on the Basis of a Doppler Radar System." Sensors 18, no. 3 (2018): 694. **Q1**, **Impact Factor 3.03**

Conference publications

- **Van Nguyen Thi Phuoc**, Liqiong Tang, Nguyen Duc Minh, Faraz Hasan, and Subhas Mukhopadhyay. "Extra wide band 3D patch antennae system design for remote vital sign Doppler radar sensor detection." In 2017 Eleventh International Conference on Sensing Technology (ICST),1-5, 2017

- **Van Nguyen Thi Phuoc**, Liqiong Tang, Nguyen Duc Minh, Faraz Hasan, and Subhas Mukhopadhyay. "Outage Probability of Vital Signs Detecting

Radar Sensor System." 12th International Conference on Sensing Technology (ICST), 358-362, 2018

- **Van Nguyen Thi Phuoc**, Liqiong Tang, Faraz Hasan, Subhas Mukhopadhyay, and Nguyen Duc Minh. "Combination of Artificial Intelligence and Continuous Wave Radar Sensor in diagnosing breathing disorder" The 4th International Conference on Research in Intelligent and Computing in Engineering (RICE 2019) - Accepted paper

Other Publications

- **Van Nguyen Thi Phuoc**, Syed Faraz Hasan, Xiang Gui, Subhas Mukhopadhyay, and Hung Tran. "Three-step two-way decode and forward relay with energy harvesting." IEEE Communications Letters 21, no. 4 (2017): 857-860. **Q1**, **Impact Factor 2.723**

- Hoang, P. Chi, T. Ngoc Nguyen, Quyet Nguyen, Q. Toan Bui, **Van Nguyen Thi Phuoc**, D. Minh Nguyen, and Loan Pham-Nguyen. "Dynamic error correction technique for wide-band 0.4–4 GHz direct receiver." In Recent Trends in Telecommunications Research (RTTR), Workshop on, pp. 1-4. IEEE, 2017.

Chapter 2

Literature review

2.1 Introduction

The non-invasive detection feature of radar sensor systems has raised much research attention and led to many interesting applications of the microwave sensing systems, such as health care monitoring, defense, security, smart homes, and live person search and rescue. The Doppler radar sensor system can be used to detect and monitor the movement of human tissues and organs without touching the body, and provides a non-invasive technique to diagnose diseases related to heart, lungs, vascular system, and other organs [30]. The first vital signs sensing system was introduced by Caro *et al.* in 1971 [17]. This system was used to determine the apnoea phenomenon of infants, which could turn on an alarm when the apnoea lasted more than 30 seconds. The recommended distance from human to antennae of this system was around 50 cm. Following this invention, many studies tried to improve the quality of the vital signs sensing system by advancing hardware structures and signal processing techniques [23, 24, 31–69].
In [33], Lee and Lin proposed an arterial pulse wave analyzer based on a CW Doppler microwave which operated at a frequency of 24.125 GHz. Their system could accurately detect the movement of the arterial wall. From 1990 to 1996, two patents [38, 42] were registered in the USA. Both focused on medical applications using radar sensors. In a radar sensing system, the antennae play an important role in increasing the sensing ability. References [56, 60, 63, 70–73] focused on improving the sensitivity of the antenna system in order to detect cancer tumors or thorax movements. Hall *et al.* [68] presented a survey on an intelligent phased-array CW sensor system for monitoring vital signs continuously. In recent years,

non-contact radar sensor has been combined with artificial intelligence (AI) to predict clinical events in [69,74]. Research in this field suggests a strong potential for the smart radar sensor.

To improve the quality of vital sign detection, many researchers focused on signal processing methods to achieve high accuracy of the breathing rate and heartbeat [4, 75–95]. Reference [82] presented the maximum likelihood estimator (MLE) and generalized likelihood ratio test ($GLRT$) techniques that were used to estimate the breathing rate and heartbeat. Their signal processing showed the ability to separate multiple vital signals. The attempts to calibrate for signal spectrum and to remove the breathing harmonics were discussed in [83,87]. Additionally, in [87] the clutter suppression of random body movements was proposed to increase the quality of vital sign signal detection. Similarly, Gu *et al.* [84] investigated a random body movement cancellation ($RBMC$) technique by combining a camera system with the microwave sensor. The random body movements recorded by the camera were used to compensate for the phase shift in the radar sensor. Another approach to enhance the breathing rate and heartbeat detection in the radar sensor is cyclostationary [86,93]. The author in the references [86,93] reports that the result of extracting signals depended less on signal to noise ratio (SNR) or the filtering technique by their novel cyclic technique. To consider the mathematical model to evaluate SNR value, the Friis model is used for a transmission link between the radar sensing system and the human. This model suggests the line-of-sight (LOS) link between the measured subject and the radar sensing system.

Besides the signal processing techniques for vital signs detection of a radar sensor system, the hardware development is crucial to make these systems more reliable. The development of semi-conductor technology has conferred many advantages on radar systems. The size of the radar system is significantly reduced. Radar sensors can now be integrated with other circuits (signal processing circuit, ADC, control circuits and so on) on the same board. Many studies have paid attention to making radar sensors even smaller, saving power, increasing sensing sensitivity [96–102], and detecting distance or direction [1, 8, 9, 103–112]. Most on-chip radar sensor systems operate at quite high frequencies (above 5 Ghz). The research has made contributions to various applications in daily life such as observing respiratory/sleeping patterns of humans [113, 114], diagnosing respiratory diseases [115,116], collecting cardia/respiration of rats [117], and monitoring

the heartbeat of cows [118] on a dairy farm.
Another important application of Doppler radar sensor is to search and locate the position of victims under the rubble of collapsed buildings. Owing to the obstacles between the living victim and the radar sensor, the penetration property of a microwave radar sensor for such application is an important factor to consider. The penetration ability of a microwave sensor system depends on operating frequency and transmitting power. Therefore, several studies chose the L and S band as the operating frequencies for their system [9] [8]. This chapter reviews this crucial application of radar sensor. The first part is the essential probes of the radar sensor - antennae system, then the signal processing and theoretical models related to the radar sensing system are discussed. In addition, the hardware structure of the radar sensing system is considered carefully based on two general types of radar sensors - continuous wave (CW) and pulse-based systems. Finally, the conclusion and future ideas are presented.

2.2 Antennae system for microwave radar sensor

The antennae system of Doppler vital sign detector is essential to improve the quality of a non-contact Doppler sensor system. The antennae should have high gain, good efficiency, and low coupling between transmitting and receiving antennae. It seems that the horn antennae are better than patch antennae in terms of efficiency, direction and gain [19, 26]. However, for weight and size, the patch antennae systems are superior to the horn antennae. Moreover, the gain in patch antennae can be improved by increasing the number of batches. Therefore, in this work, the patch antennae for radar sensing systems are reviewed carefully in the research presented in this thesis to find suitable antennae for search and rescue purposes of the radar sensing system.
The antennae design work presented in [2] and [3] is concentrated on the frequencies around 60 GHz. It is obvious that, with very high frequency, the size of the antennae does not create any problems for the system. In [2], the antennae system was built on the low-temperature co-fired ceramic ($LTCC$) substrate. The structure of this system is shown in Figure 2.1. Each antenna consists of four patches. The size of the antenna is quite small (9×9) mm due to the high operating frequency. The range of operating frequency is from 50 GHz to 60

GHz. The return loss is around -10 dB and the isolation between two antennae is around -30 dBm.

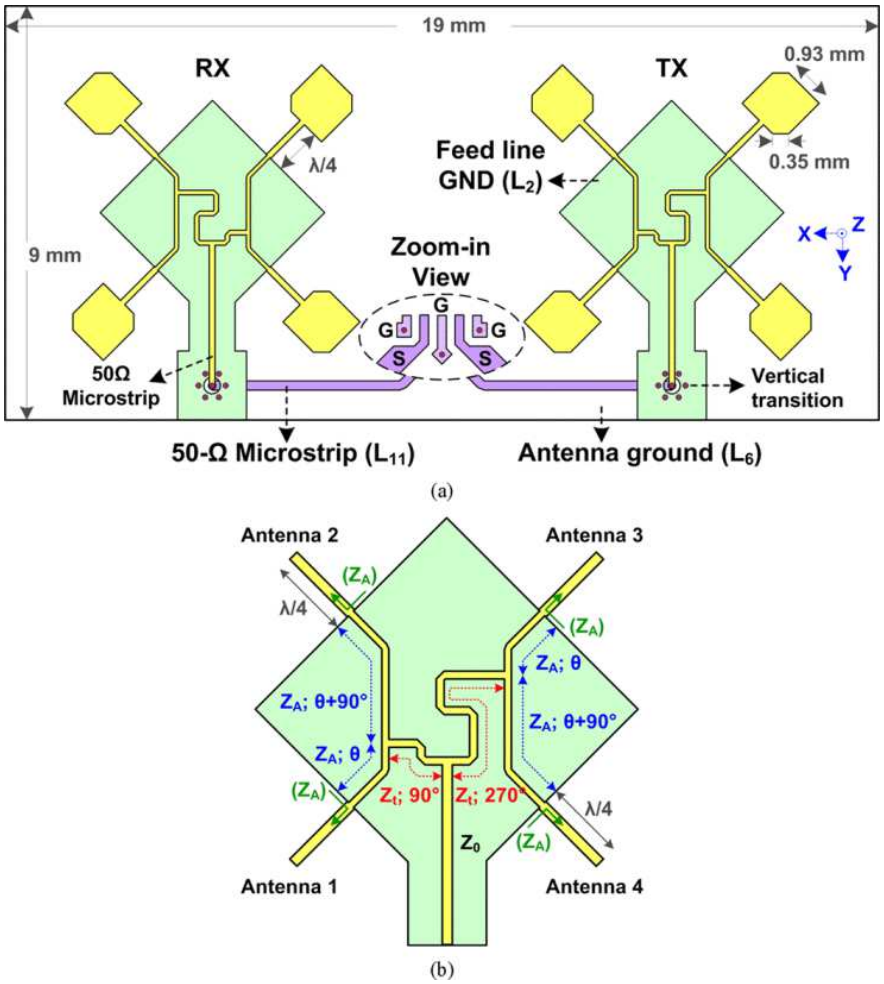

Figure 2.1: (a) Arrays antennae system. (b) Topology of the sequential-phase feed network © 2012 IEEE [2]

The reference [3] presented another design structure of the patch antennae for the radar sensing system with a range of frequency from 57.24 GHz to 65.88 GHz. The reflection at each antenna is lower than -10 dB and the isolation between two antennae was around -30 dB. The maximum dimension of fabricated antennae is around 1.5×5.5 mm. Most of the studies have tried to reduce the beam width of an antenna to around 60 $degrees$.

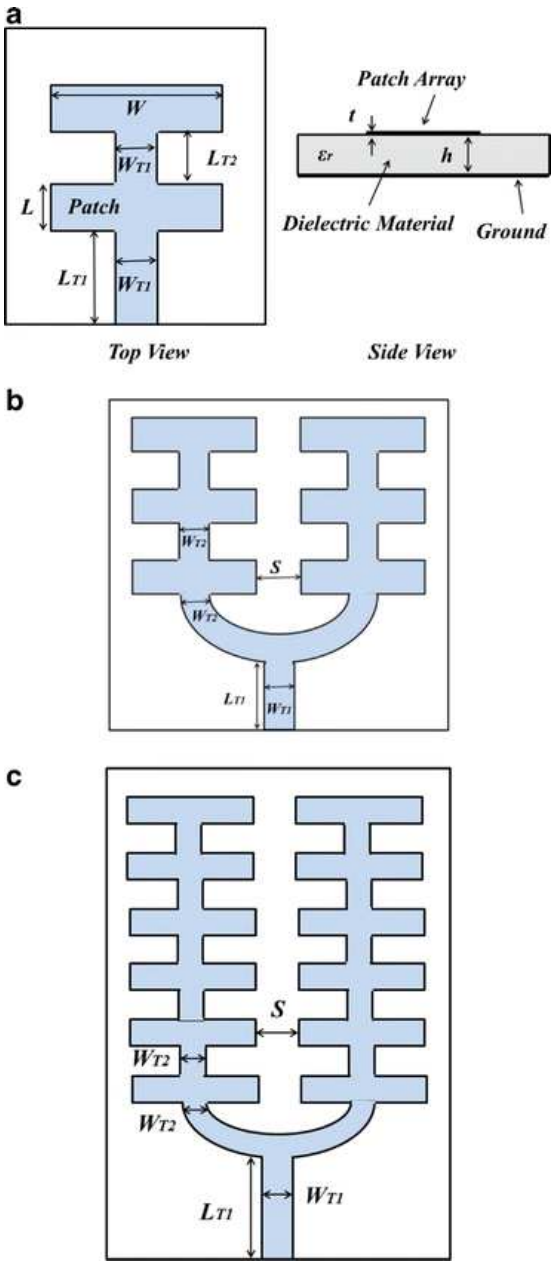

Figure 2.2: Topology of designed antennae arrays (a) 2×1 patch elements, (b) 3×2 patch elements, (c) 6×2 patch elements [3]

It is obvious that the size of the antennae is proportional to the wavelength of operating frequency. When the sensing system operates at a high frequency, the size of antennae does not cause any problem for the whole system. However, for the go-through materials applications, such as finding survivors, we need to use the lower frequencies. This means that the wave length will be large. In this case, patch antenna size is a big issue [119]. Moreover, the radar sensor

systems might need to operate in different frequencies for specific circumstances as the dual-band transmitter [99]. Therefore, investigation of the portable multiple bands antenna with a novel structure to improve the beam direction and isolation used for vital signal detecting sensor system, is a significant need for the vital sensor radar detector. The motivation to investigate the multiple bands antennae system comes from the fact that (1) little previous study has investigated the $3D$ multiple bands (from L-band to X-band) patch antennae for the vital Doppler radar detector, (2) the designed antennae can then be used to check the ability to detect the vital signs at various bandwidths for line-of-sign (LOS) and non-line-of-sign (NLOS) transmission to find the potential applications of different frequencies in different situations. (3) the $3D$ design reduces the size of the antennae system which is used for the portable life-detecting sensor system.

2.3 Signal processing techniques and mathematical models

2.3.1 Signal processing techniques

There are many techniques to obtain and classify the breathing rate/heartbeat from the baseband received signal of the microwave sensor. The Fast Fourier transform (FFT) and continuous Wavelet transform (CWT) [4, 88–95, 120–123] are considered very basic methods to retrieve respiratory rate. These techniques can find the frequency spectrum of received signals, based on the peak of spectrum in a specific frequency range, and the breathing rate or heartbeat can thus be estimated. However, the microwave radar sensor operates in a noisy environment with a variety of noises such as random body movements, flicker noise, clutter noise, leakage noises between transmitting antennae and receiving antenna and so on. Therefore, in many applications, simply applying FFT or CWT on the received signal is not sufficient in obtaining the desired signals (vital signs).
Another popular technique to find the pattern in the data is principal component analysis (PCA). In this method, principal components of a vector data can be found by forming the orthogonal matrix in which rows are eigenvectors of covariance matrix of the vector data [124]. This method was then combined with WT or short time Fourier transform ($STFT$) to process multivariate statistical data [125]. This signal processing method can extract the respiratory rate from

the pulse oximeter's photoplethysmographic signals with high accuracy.
In the received signal of the radar sensor, the breathing signal has higher energy than the heartbeat signal. To reduce the effect of breathing rate harmonic on the heartbeat signal, the chest displacement signal is firstly broken down into intrinsic components. The breathing rate and heartbeat can be restructured from those components in the time domain. This technique is called empirical mode decomposition (EMD) [126]. After applying the EMD on the received signal the simple FFT can be applied to find the breathing rate and heartbeat.
To reduce the random body movement, Li *et at* [58,127] proposed a method that detects signals from both sides of the person. These signals are combined to cancel out the noise caused by random body movement, then arctangent or complex signal demodulations are applied before using FFT to find the breathing rate and heartbeat. Similarly, [87] also used two receiving antennae to detect the vital signs. However, they just simply chose the strongest signal to process. The moving filter is applied to the selected signal to remove the quasi-static clutter.
Another technique to reduce the flicker noise was mentioned in [85] by using the harmonic radar. This work proposed a harmonic CW radar sensing system that operates at two frequencies (fundamental and harmonic). They reported that in their system, the flicker noise was reduced significantly while SNR was increased.
Recently, Yu *et al.* [93] proposed an approach based on higher order cyclostationary to detect the heartbeat and respiration of a person. The third-order cyclic cumulant was applied to detect the vital signs. This method could reduce the harmonic interferences, random body movements, and clutter noise. It also allowed the radar sensor to detect the weak signals with low SNR values.

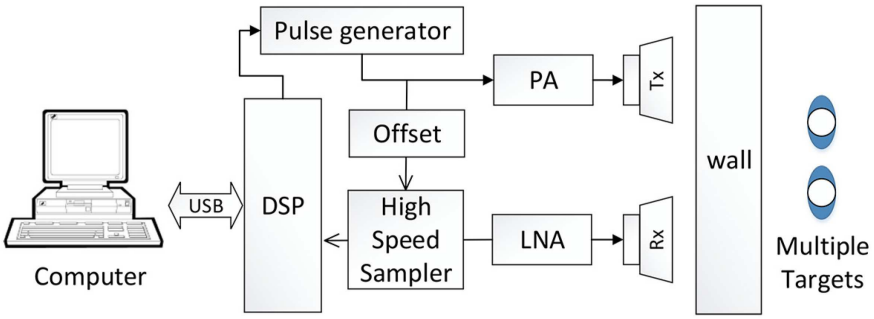

Figure 2.3: Block diagram to test multiple targets detection [4]

Besides the vital sign detection techniques, target tracking based on radar

sensor is also very important in search and rescue or defense applications. Yan *et al.* [4] have proposed an approach based on an algorithm called variational mode decomposition (VMD) to track different targets behind a wall. The setup of the testing system is shown in Figure 2.3. This method decomposed the breathing signals into various sub-signals. The separated signals can be tracked by the VMD algorithm. The tracking algorithm consists of four steps: determine traversed range bins, VMD algorithm, breathing recognition, and Hilbert Transform. The result of this proposed algorithm is compared to the conventional FFT in Figure 2.4. It is obvious that the VMD algorithm approach is a good choice in the case of multiple target detection based on microwave radar sensor.

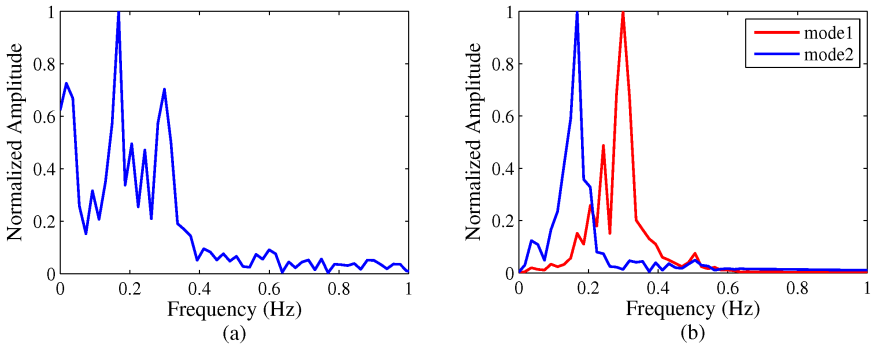

Figure 2.4: Traditional FFT method (a) versus VMD based method (b) [4]

Another powerful algorithm to detect breathing rates of multiple subjects is the independent component analysis (ICA) [128, 129] technique. This method allows blind segregation of data into independent sources and is applied to successfully separate the breathing rates of three people by a $SFCW$ radar sensor [128].

2.3.2 Related mathematical models

The SNR is an important parameter in the radar sensing system. To evaluate the received power signal, we have to consider the transmission link between the radar sensor and the measured human. The reference [130] used the Friis model for the transmitting antenna- human- receiving antenna links. The Friis model suggests that there is a LOS link between the sensor and the subject. Based on this transmission model, the received power signal and the power of phase noise

were calculated to evaluate the SNR of the radar sensing system in breathing rate and heartbeat detection.

The Friis model in the work [130] does not regard the multi-path signals to the receiver. Jeong et al. [5] enhanced the precision for this transmission link by using the log-normal model. Formed on this model, the mathematical derivation to evaluate the accuracy of the radar sensing system was developed. The false alarm, miss detection and total error probabilities were investigated to determine the integrity of the radar sensor. The $3D$ error probability of the radar sensing system is shown in Figure 2.5. The amplitude of cluster is proportional to the error probability value.

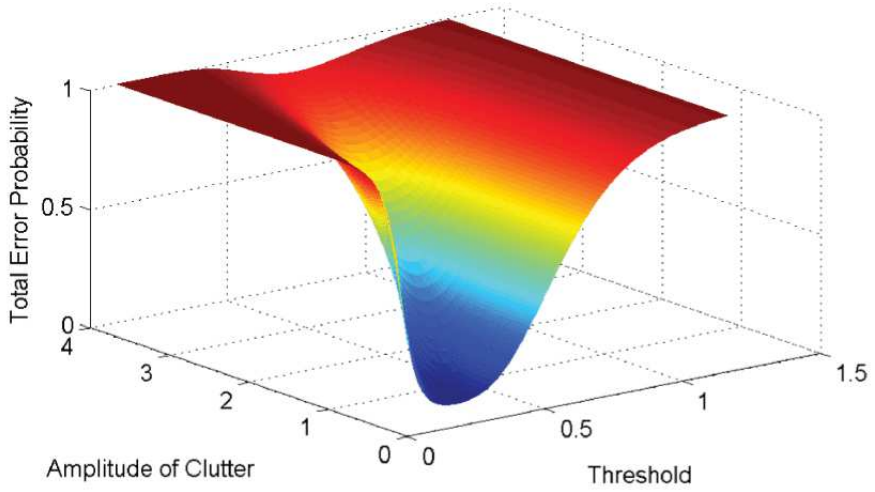

Figure 2.5: Error probability of radar sensing system © 2012 IEEE [5]

2.4 Hardware developments

In the past five decades, the improvement of semi-conductor technology, embedded computing, and artificial intelligence (AI) techniques have enabled significant improvement in the vital signs detection Doppler sensor systems. The cumbersome microwave radar sensor of the past has been replaced by smaller, smarter, and higher sensitivity systems. An early respiratory monitoring system [32] was attached to an X-ray and triggered this machine automatically by instance of respiration. This system is quite simple. It consists of an oscillator, quadrature mixer, direction detector circuit, differentiators, and trigger circuit. Another CW

microwave radar for vital signs detection was discussed in [36] with the size of 20 $cm \times 28\ cm \times 18\ cm$ and large attached antennae. Later, the burgeoning of semi-conductor technology helped to reduce the size of vital signs detecting radar sensor systems. For example, the 5.8 GHz radar sensor receiver chip of 0.13 μm $CMOS$ [6] is as small as $1.2mm \times 1.2mm$. This system can detect the breathing rate of a human at the distance of $1.5m$. The detection results of breathing rate and heartbeat, when a person sits at the distance of $0.5m$, are displayed in Figure 2.6. The respiration and heartbeat can be found easily from the spectrum of the received signal.

Figure 2.6: Received signal in time domain (a) and in frequency domain (b) at the distance of 0.5 m [6]

The system on chip (SoC) radar sensor has become very popular as it has many applications. Reference [7] introduced a SoC radar sensor with RF interference rejection and integration of power management clock generation functions. To operate this system, the external antennae and crystal needs to be connected within this compact kit. The block diagram, the example module, and application results of this system are illustrated in Figure 2.7. The example module has a size of $5.8cm \times 3cm$ and can detect the breathing rate at a distance of 9 m and heartbeat at a distance of 5 m. When this system operates in a condensed environment, the detection distance might reduce, but it still has high potential for search and rescue applications.

The development in hardware of the microwave radar sensor goes along with processing techniques to improve the accuracy of vital signs detection. The next section discusses different kinds of radar sensor based on transmitting wave forms.

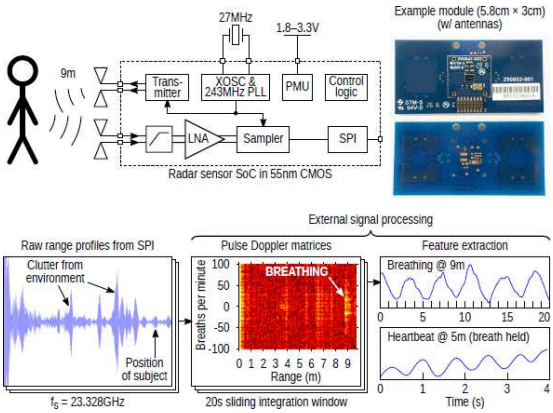

Figure 2.7: System overview and real-life application example with measured performance [7]

2.4.1 Single tone CW radar sensor

A typical functional block diagram of the CW radar sensor system is shown in Figure 2.8. The system consists of an oscillator (OSC), IQ demodulator, arctangent demodulator, analog to digital converter (ADC), digital signal processing and display unit. The OSC is the microwave signal source, and this signal is amplified by a power amplifier (PA) before being sent towards the human position through transmitting antenna Tx. The receiving antenna Rx of the sensor captures the reflected signal from the human. This signal is amplified by a linear amplifier (LNA). After that, the signal is down converted by a quadrature modulator to create two orthogonal signals, S_I and S_Q. The two orthogonal signals are used as the inputs for the arctangent demodulator. The analog signal from the arctangent modulation unit is digitalized by ADC before sending to the DSP to extract useful information. The results (vital signs such as breathing rate, heartbeat and so on) are shown in the display unit.

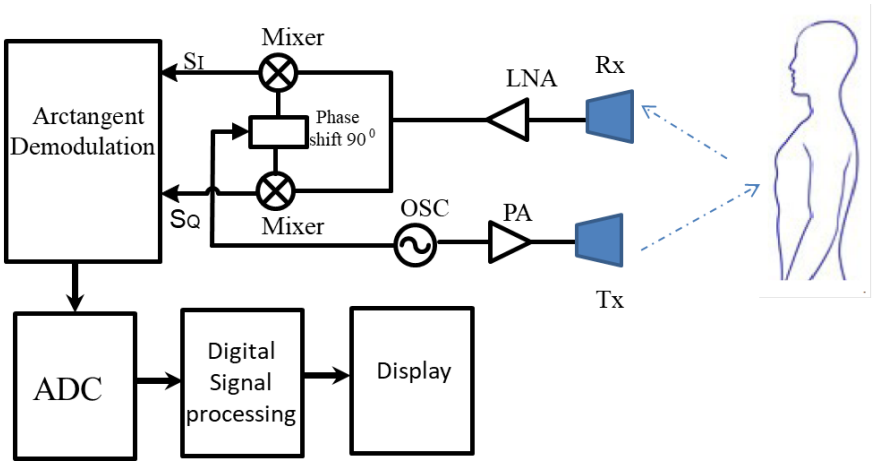

Figure 2.8: Continuous Wave System diagram.

The generated signal of the CW radar sensor system can be represented by:

$$V_T(t) = A_T \cos\left(2\pi f_0 t + \phi\left(t\right)\right) \tag{2.1}$$

where A_T is the amplitude of the transmitted signal, f_0 is the carrier frequency, t is the transpiring time, and $\phi\left(t\right)$ is the phase noise. The signal $V_T(t)$ is then reflected from the human's chest. The chest displacement can be considered as a periodic signal $l\left(t\right)$. At the receiver, this signal is down converted by the I/Q demodulator. The purpose of using I/Q demodulation is to alleviate the null-points problem [23]. The base band signal at the output of the demodulator can be written as:

$$B_O(t) \approx arctan\left(\theta_0 + \frac{4\pi l(t)}{\lambda} + \triangle\theta(t)\right) \tag{2.2}$$

The thorax displacement $l(t)$ is much smaller than the value λ therefore, the small angle rule can be used in Equation 2.2. The output signal of the radar sensor system is proportional to the chest movement.

$$B_O(t) \approx \theta_0 + \frac{4\pi l(t)}{\lambda} + \triangle\theta(t) \tag{2.3}$$

where θ_0 is the phase shift due to the distance from the human location to the antennae system and $\triangle\theta(t)$ is the phase noise.

CW radar topologies

In 2000, Kum-Mu Chen *et al.* [8] constructed two CW microwave life-detection systems which operated at 450 MHz and 1.15 GHz respectively. Their experiment results show that the 1.15 GHz microwave radar could penetrate deeper through the rubble with metallic wire. The block diagram of this life-detector is shown in Figure. 2.9. A stable CW signal (power 25.6 dBm) was generated by a phase-locked oscillator. This signal goes through a 10 dB directional coupler and a circulator before reaching the RF switch to the antenna. A 10 dB directional coupler divides the signal from OSC into two parts; 90% of the power goes to the circulator and 10% goes to the 3-dB directional coupler. At the second directional coupler, the 40 mW power is split into two equal parts which are used as a local reference for the mixer and to drive the clutter cancellation circuit. In this system, the two antennae are stimulated sequentially. The signals from both antennae are associated to decrease the background noise. The clutter noise is canceled by the combination of digital-controlled phase-shifter, fixed attenuator, amplifier, and digital-controlled attenuator. In addition, the system sensitivity is increased by a phase-shifter connected to the local port of the mixer [8].

Figure 2.9: Schematic of 1.15 GHz microwave radar [8]

This system was tested in the simulated earthquake rubble at the Electromagnetics Laboratory, Michigan State University (Figure 2.10). The system can detect the breathing rate and heartbeat over a distance of seven feet including three feet of rubble with metallic wire mesh. This system showed good results with the dual antennae system which helped to reduce the background noise and the noise created by the nearby moving operators.

Figure 2.10: Testing performance of Kum-Mu Chen *et al.* [8] system at the earthquake rubble model of Michigan State University

Another system was developed by Jalai Bidgoli *et al.* [9] with the same purpose of finding survivors. This system operated at the same frequency of reference [8] (1.15 GHz) with a similar transmitting power (26.5 dBm). Their system had the

ability to cancel the clutter and other noise sources, in which a microprocessor-based system was used to eliminate clutter. The computer was connected to the system to control and monitor the reflected signal. Two horn antennae were used in this work. The schematic presentation of their proposed system is shown in Figure 2.11. There are four main blocks in this system. The first block generates a transmitting signal, blocks 2 and 3 take the responsibility of noise cancelation, while block 4 down-converts the RF signal to the baseband signal. They report that this system can detect the breathing rate at a 10 m thickness with standard density materials.

Figure 2.11: Schematic of life-detector system [9]

2.4.2 Frequency modulation continuous wave (FMCW) radar sensor

The block diagram of the $FMCW$ radar sensor is similar to the CW sensor as shown in Figure 2.8, but the OSC should be replaced by a voltage control oscillator (VCO). The diagram of frequency versus time of $FMCW$ radar is displayed in Figure 2.12, where BW is the bandwidth of transmitting signal, $\triangle f$ is beat frequency, and $\triangle t$ is the time delay.

In the $FMCW$ radar system, the transmitter sends a linear frequency signal

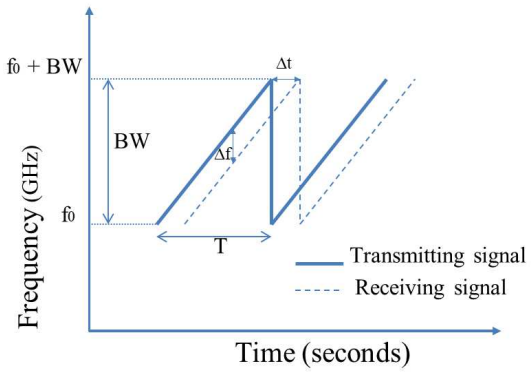

Figure 2.12: Frequency versus time of transmitting and receiving signal at $FMCW$ radar

from f_0 to $f_0 + B$ toward the person's position. Owing to the person's movement and the distance between the person and the radar sensor, the received signal was shifted in frequency and time domain, as illustrated in Figure 2.8. The distance from the target to the radar sensor and the range resolution can be estimated as [23, 131]:

$$d = \frac{cT\triangle f}{2BW} \tag{2.4}$$

$$\triangle d = \frac{c}{2BW} \tag{2.5}$$

where BW is the bandwidth of transmitted signal, $\triangle f$ is beat frequency, and $\triangle t$ is the time delay. c is light speed and T is pulse repetition period of the transmitted signal.

In the work of [10] Matthew *et al* applied the singular value decomposition (SVD) algorithm on the obtained signal from a so-called *Soprano* $FMCW$ system. The hardware schematic is shown in Figure 2.13. This system was first developed by Chen *et al* [132]. The central operating frequency of the sensor is 5.8 GHz with a bandwidth of 83.5 MHz. The transmitting power is 13 dBm and the antenna gain is 12 dBi. This system was set up outside a residential house with a 33 cm brick wall to detect people inside the living room (2.8 m × 4.7 m).

The measurement setup is shown in Figure 2.14. The received signals in this radar system were processed by singular value decomposition (SVD) and moving target indicator (MTI) techniques to detect location and the moving trend of the

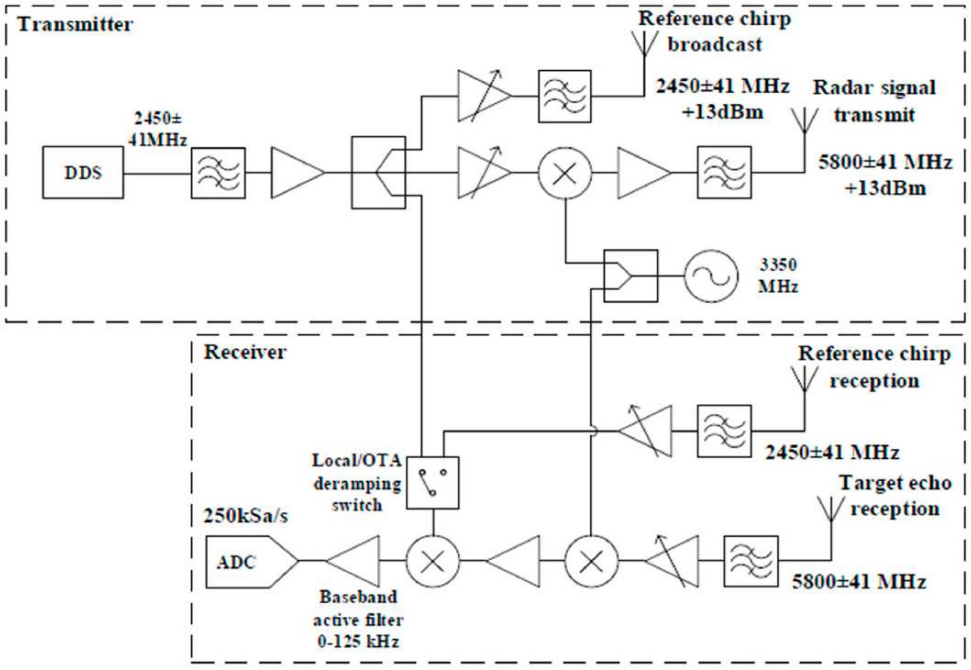

Figure 2.13: Topology of *FMCW* radar used to detect a human through the wall [10]

subject during the measurement.

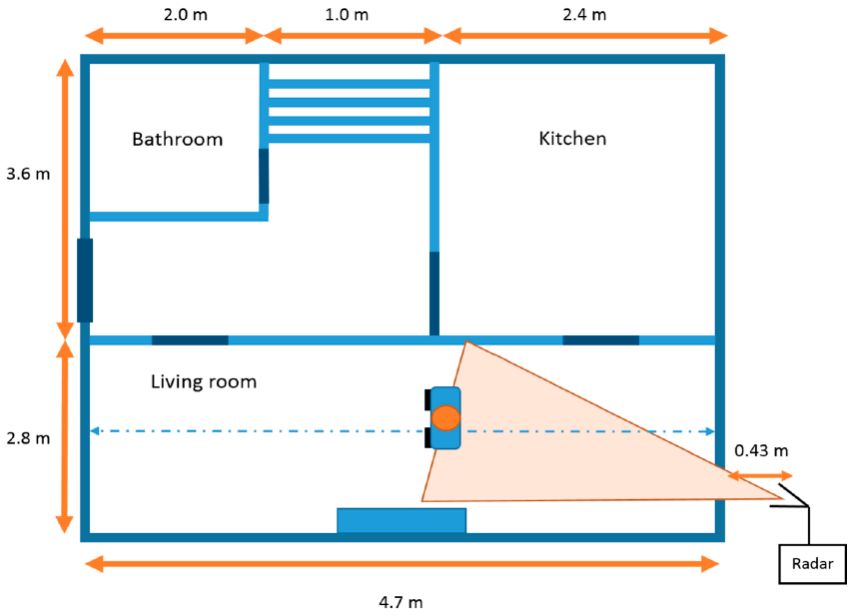

Figure 2.14: Experiment setup of *FMCW* radar to detect a human through the wall [10]

2.4.3 Hybrid FMCW-CW radar sensor

To combine the advantages of range detection in $FMCW$ radar and small displacements detection in the single tone CW radar sensor, Guochao Wang *et al.* [11] introduced a hybrid system which operates at $FMCW$ and CW alternatively to obtain the range and vital signs of a human. The transmitted and received signals in frequency and time domains are demonstrated in Figure 2.15. The $FMCW$ period provides the distance information, while the thorax displacements can be obtained from CW mode.

Figure 2.15: Transmitting and receiving signal at $FMCW$-CW radar in (a) frequency domain and (b) time domain [11]

Both references [8] and [9] introduced the life-detector with high penetration capability. Based on the high directional antennae system of these systems, the direction of the victim under the debris might be found, but the distance from human to the radar antennae cannot be estimated. In these studies, they did not mention the range detection ability of their system. To enable both functions of range and vital signs detection, the hybrid $FMCW$-CW microwave radar seems to be a good choice [11].

2.4.4 Stepped-Frequency Continuous Wave (SFCW) Radar

The SFCW has many advantages such as the frequency flexible controlling, high dynamic range, and it can be easily calibrated at different frequencies [12, 133]. The work in reference [12] performed some physical experiments which can simulate finding live people under the debris situations. The measurement set up of this work is described in Figure 2.16. The measured subject was asked to lie under bricks on the floor as in Figure 2.16 (a). The thickness of the brick layer was changed from 0 to 20 cm. The subject was asked to perform four postures as in Figure 2.16 (c). A total of 201 frequency steps from 300 to 1300 MHz were set-up. The combination of vector network analyser (VNA) Model $E5061A$, two antennae, and a PC were utilized as a $SFCW$ system.

Figure 2.16: Experiment setup of $SFCW$ radar to detect a human through the brick: (a) size view, (b) top view, (c) postures [12].

This work shows very encouraging results for human rescue application. The breathing rate of a human can be detected through the obstacle, and the posture of the subject is not critical. The measuring time to find the respiratory rate of a person is quite small (5 seconds) as shown in Figure 2.17. For search and rescue purposes, the breathing rate should be considered as the main signal to find the live subject. An alternative option to detect both location and respiratory rate of a person is to use pulse-based radar sensor systems. These types of radars are discussed in the next sections.

Figure 2.17: Breathing rate of a face-up posture person at different time resolutions [12]

2.4.5 Random noise UWB radar sensor

Another promising UWB radar is random noise or random signal UWB radar. Its operating principle is similar to the short-pulse UWB sensor, but the short-pulse generator block is replaced by a band-limited random noise generator. This remote sensing system has high range and velocity resolutions. The effect of the antennae leakage and the radio frequency interference in this system is eliminated by its own waveform signal [13, 134].
For searching and locating people under the debris when human-caused/natural disasters occur, UWB radar is a good choice since it can also detect the vital signs and the location of the target. In 2004, Narayanan *et al.* [135] introduced the basic block diagram of random noise UWB radar, as described in Figure 2.18. This sensing system can detect a trihedral reflector behind a wall.

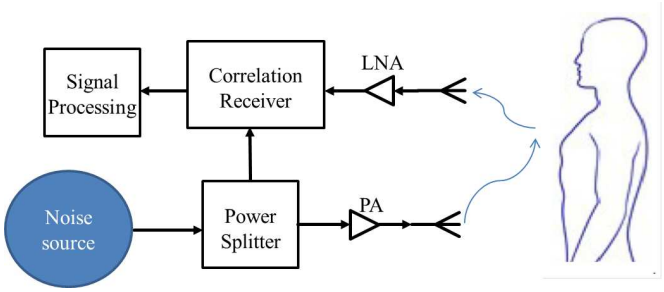

Figure 2.18: Diagram of a basic random noise UWB radar sensor

Later, in 2010, Chieh-ping Lai *et al.* [13] proposed a digital UWB random noise radar sensor system for search and rescue purposes. The topology of the system is shown in Figure 2.19. In this design, an FPGA-based receiver was developed. The operating bandwidth of the system from 350 MHz to 750 MHz corresponds to a 37.5 cm resolution. In this work, the chip-based generator is used as the source noise, and the software-defined technique was utilized to reduce the size and power consumption of the radar system.

Figure 2.19: A schematic of a digital random noise UWB radar sensor [13]

The results of Chieh-Ping Lai's human detection system is presented in Figure 2.20. We can see that this radar system can locate the human position at a distance of 6 m through the wall.

Figure 2.20: Detecting human movement through a wall using a digital random noise UWB radar sensor [13]

2.4.6 Pulse-Based radar sensors

A pulse-based UWB radar has two operating modes: emitting and silent. A short pulse is sent in the emitting mode and the echo signal returns to the radar in the silent mode. The range and velocity of the target can be detected by comparing the transmitted pulse and the received pulse. A basic block diagram of an UWB microwave radar sensor is shown in Figure 2.21. The desired waveform is created by the pulse generator. The pulse repeat frequency (PRF) is determined by a local oscillator. The pulse signal is modulated by a modulator before being amplified and emitted through the transmitting antenna (T_x). The echo signal is amplified by a linear amplifier before being down-converted to the baseband.

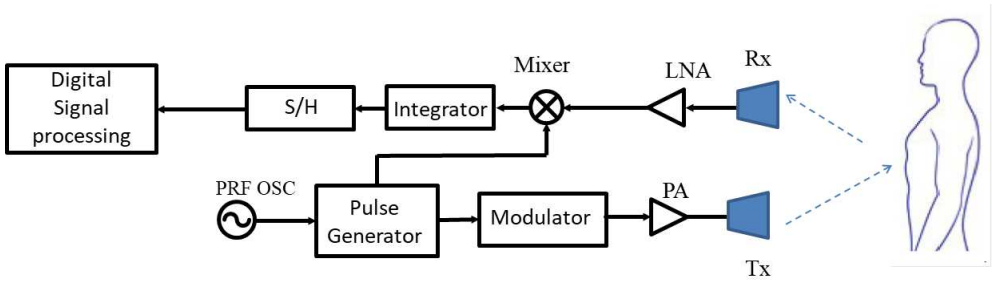

Figure 2.21: Block diagram of a typical UWB radar system

The transmitting signal $(s_i(t))$ in the time domain for the i^{th} frame can be written as [136].

$$s_i(t) = p(t - iT_f)cos(2\pi f_0(t - iT_f)) \tag{2.6}$$

where f_0 is the carrier frequency, $p(t - iT_f)$ is the impulse signal, and T_f is the duration of the frame $(T_f = \frac{1}{f_p})$. f_p is the pulse repetition frequency.
The received signal after being amplified by LNA is given as follows.

$$r_i(t) = Ap\left[t - iT_f - \tau(t)\right] cos\left[2\pi f_c(t - iT_f - \tau(t))\right] \tag{2.7}$$

where A is the amplitude of the signal and depends on the gain of LNA and the transmission loss due to the environment between radar and target. $\tau(t)$ is the propagation delay, equal to the round-trip time of a radar pulse.
The range to the target $(R(t))$ can be estimated from the propagation delay $\tau(t)$ as:

$$R(t) = \frac{c\tau(t)}{2} \tag{2.8}$$

The thorax movement of a human can be obtained by performing the Fourier transform on the received signal.
To improve the performance of the short pulse radar, a coding technique is utilized to increase resolution and avoid the multi-user interference. The transmitted signal is coded by the pseudo-noise code in the transmitting block. This radar is so-called as pseudo-random UWB radar to be used to detect vital signs of humans [137–139].

To enhance the penetration property in the pulse-based UWB radar, the transmitted power and the carrier frequency of the system should be considered carefully. Moreover, the signal processing method is more challenging in such a dense transmitting environment. References [92] and [1] report a de-noising method for detection of through-wall vital signs based on the UWB radar sensor. The experimental setup is shown in Figure 2.22. The thickness of the wall is 1 m, and the human target was measured at varying distances from 3 m to 12 m.

(a)

(b)

Figure 2.22: Vital signs detection experiments for a human subject by UWB radar sensor (a) outdoors, (b) indoors [1]

The parameters of the UWB radar are given in Table 2.1. There are two important points noted from Table 2.1. First, the center frequency of this system is quite low (400 MHz). Second, the amplitude of the transmitted signal is quite high (50 $volt$). Both conditions, low operating frequency and high power make sure that the signal can penetrate through the dense rubble to find live victims when there is a disaster. Moreover, Liang [1] also proposed a detection algorithm to provide range information and vital signs like breathing rate and heartbeat. The flow chart is displayed in Figure 2.23. Several de-noising techniques were applied: first the stationary clutter, linear trend, and non-stationary clutter are

Table 2.1: Parameters of UWB radar [1]

Parameter Value	Value
Center frequency	400 MHz
Transmitted signal amplitude	50 V
Pulse Repeat Frequency (PRF)	600 kHz
Number of averaged values (NA)	30
Time window	124 ns
Number of samples (M)	4092
Input bandwidth of the Analog to Digital Converter (ADC)	2.3 GHz
ADC sample size	12 bits
Receiver dynamic range	72 dB

suppressed. After that, the signal is filtered in range and in slow time. The next step is to analyze in slow time, then input this signal to FFT and window to find the frequency. The output signal of $STFT$ is used for range information.

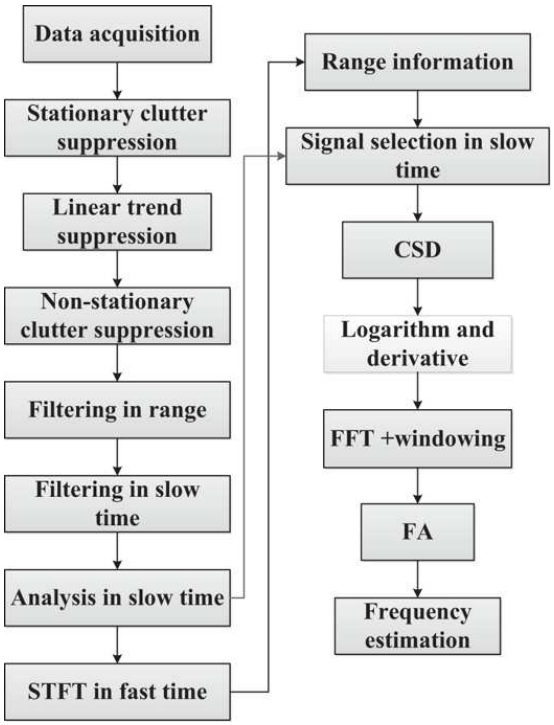

Figure 2.23: Detection algorithm [1]

Figure 2.24 displays the range information provided by this system when the

distance from the person to the radar system is 9 m. The estimated range by their proposed system is quite accurate.

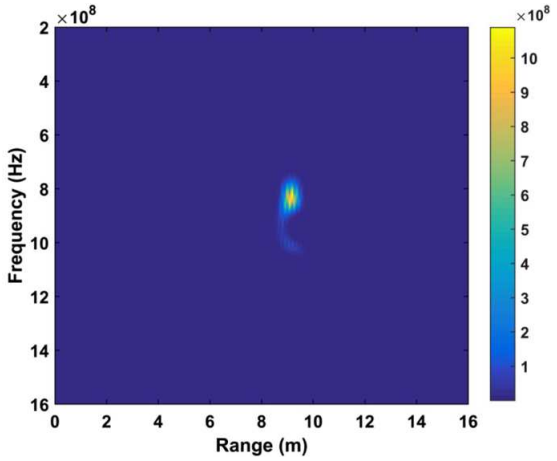

Figure 2.24: The STFT in the case of 9 m human location [1]

2.5 Conclusion

In this chapter, some representative microwave Doppler sensor systems for finding survivors are discussed. For this special purpose, most of the considered systems operated at S and L frequency bands. Therefore, the antennae should be developed for this purpose. The power of the radar systems for this application is also much higher than the systems used for medical applications. Moreover, the signal processing techniques are very important in order to remove noise and clutter to improve the accuracy of the radar sensor systems. The mathematical models to evaluate the accuracy of this system should be considered carefully to estimate any vital sign sensing system in advance.
In addition, optimized hardware structures can be combined with more efficient signal processing techniques to alleviate many of the issues with the radar vital sign sensing system.

2.6 Related Publications

- **Van Nguyen Thi Phuoc**, Liqiong Tang, Veysel Demir, Faraz Hasan, Duc Minh Nguyen, and Subhas Chandra Mukhopadhyay,. " Review-Microwave Radar Sensing Systems for Search and Rescue Purpose" Sensors 2019,

19(13), 2879

Chapter 3

Extra Wide Band Antennae System for Vital Sign Detection

3.1 Introduction

In the vital signs sensing radar system, the antenna system plays the role of probes to detect the vital signs. It is obvious that antennae should be small, have high directivity and gain. Authors in references [2,3] optimized the antenna system to detect vital signs with operating frequencies around 60 GHz. The size of antennae is proportional to the wavelength. Therefore, in such high frequency, the dimensions of antenna system are very small. For the rescue application to find live people under the debris, the lower frequency radio signal can go through the obstacle better than higher frequency signals. When the vital signs detecting radar system has to operate at low frequency, the size of its patch antennae is a significant problem [119]. In addition, to improve the flexibility of the life-detection system in terms of operating frequency, the antennae should have a very wide band width. Therefore, in this study, portable multiple bands antennae with a novel design structure is presented. This chapter discusses the investigation the $3D$ multiple bands (from L-band to X-band) patch antennae for the vital Doppler radar detector. The vital signs detecting ability of the system at different operating frequencies is tested through Line-Of-Sign (LOS) and Non-Line-Of-Sign ($NLOS$) environments.

This chapter presents a novel antenna system for human vital signs detection. In this work, system working principles and different types of patch antennae are introduced, along with the measurement set up of the vital signs detecting radar

sensor system. A wide band (from 900 MHz to 12 GHz) patch antenna system with beam-enhanced capacity is developed in $FR4$ substrate. This substrate has dielectric constant 4.4 and 1.2 mm of height. To reduce the size of the antenna system, a $3D$-orthogonal structure was utilized to design the transmitting and receiving antennae. The multi-patch elements transmitting antenna was placed orthogonally with the receiving antenna to decrease the size of the antenna system. Moreover, the bandwidth and the directional capacity of the antennae were put in high priority to identify the human's chest displacement at different frequencies, from L band to the X band. The measurement outcome shows that human vital signs could be revealed by the proposed $3D$ antenna system.
The remainder of this chapter is organized as follows. Section 3.2 states the design of the antennae, underlying the structure, simulation and measurement results. The detected vital signs using the developed antennae are presented in Section 3.3, and the conclusions are given in Section 3.4.

3.2 Antenna design

There are different types of antennae. The patch antenna is very popular in sensor systems because of its low cost, reasonable size, light, and easy to connect to the printed circuits. The microstrip antenna is composed of three layers. The metallic strip - patch is put on top of the substrate and the third layer is the ground plane [15]. There are many types of microstrip patch elements such as square, rectangular, dipole, circular, elliptical, triangular, disc sector, circular ring and ring sector. To enhance scanning capability and directivity of the antenna, the arrays of microstrip elements were considered.

With respect to the feeding method to the antennae, there are four main ways including coaxial probe, microstrip line, aperture coupling, and proximity coupling [140] [141] [142] [15] [143] as can be seen in Figure 3.1. The coaxial-line feed (Fig 3.1 (a)) has two conductors; the inner conductor is connected to the radiation patch and the other one is soldered to the ground plane. This type of feed is easy to fabricate, match, and has low spurious radiation. However, it has bandwidth limitations and difficulty in modelling. Similar to the advantages of the coaxial-line feed, the microstrip line feed (Figure 3.1 (b)) is simple to fabricate, match and model. However, the spurious radiation increases proportionally with the thickness of the substrate, and the bandwidth is quite narrow (around

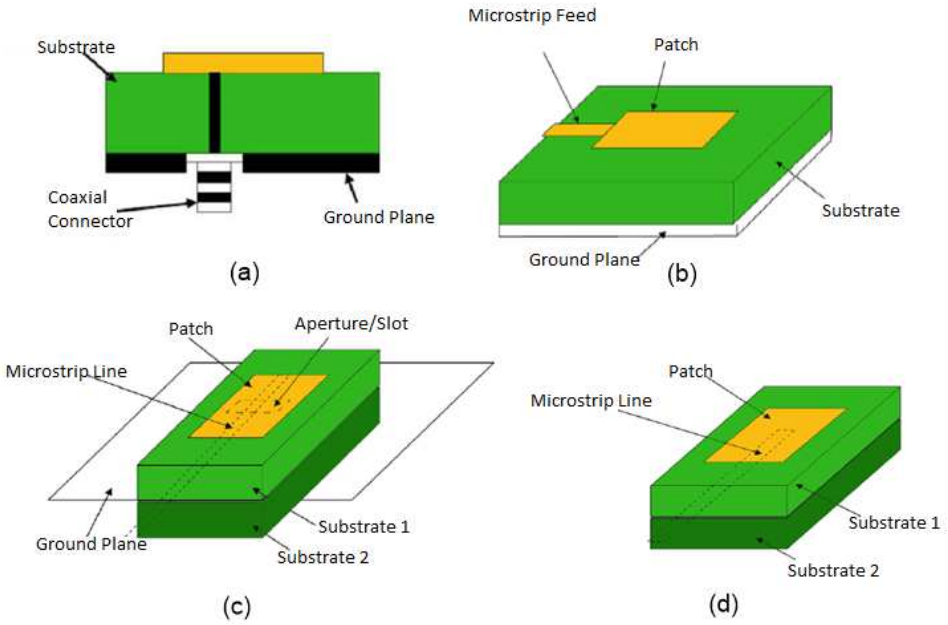

Figure 3.1: Feeding methods for patch antennae: (a) Coaxial feed, (b) Microstrip line feed, (c) Aperture coupled feed, and (d) Proximity coupled feed [14, 15]

2 - 5 %).

In the first two methods, coaxial probe and microstrip line, asymmetries always exist. This problem leads to the high order modes and cross-polarized radiation. These problems could be reduced by the non-contacting aperture-coupling feeds (Figure 3.1 (c), (d)). The aperture coupled feed (Figure 3.1 (c)) has two substrates separated by the ground plane in the middle. The patch is etched on the top substrate while the microstrip feed line is imprinted on the bottom of the lower substrate. The feed line is coupled to the patch by a slot on the ground. Obviously, the parameters of this type of feeding can be chosen separately. The independent choices of substrate dielectric constants, thickness, feed line width, slot size, and position support the optimized antenna design. The most popular advantages of the aperture coupled feed are easy to model, and have low spurious radiation. However, this method is very hard to fabricate and the bandwidth is not very wide. The last feeding method is proximity-coupled feed as shown in Figure 3.1(d). This feeding consists of two substrates; the upper and the lower ones. The radiation patch is on top of the substrate, while the feeding line is placed between two substrates. The optimization for the design can be achieved by

changing the parameters such as feeding stub, the width and length of the patch or the dielectric of substrates. The proximity coupling feed is more difficult to fabricate but has wider bandwidth and low spurious radiation [15, 144].

3.2.1 Two dimensions (2D) transceiver antennae

In the $2D$ transceiver antenna system, the transmitting antenna is placed in parallel with the receiving antenna. Each antenna might consist of several patch elements. The width (W) and the length (L) of each patch are calculated as [145, 146].

$$W = \frac{c}{2f\sqrt{\frac{\varepsilon_r+1}{2}}} \tag{3.1}$$

$$L = \frac{c}{2f\sqrt{\varepsilon_{reff}}} - 2\triangle L \tag{3.2}$$

where c, f, and ε_r are the light velocity, operating frequency, and dielectric constant respectively. ε_{reff} is the relative and effective dielectric constants. $\triangle L$ is the patch length extension [146].

Two basic equations (3.1) and (3.2) are used to estimate the size of antenna. If a $2D$ antenna with the gain around 10 dBi is developed, the size of the antenna can go up to $30cm \times 30cm$. Therefore, the size of the transceiving antennae is larger than $30cm \times 60cm$.

There are several important radiation characteristics which are considered carefully during design of the antenna system. They are antenna bandwidth, efficiency, directivity, and gain. The detail expressions for these parameters are discussed as follows [147, 148]

- Antenna bandwidth BW

$$BW = \frac{S-1}{Q_T\sqrt{S}} \tag{3.3}$$

  where S, Q_T are the voltage standing wave ratio ($VSWR$), and total quality factor respectively

- Antenna efficiency is the ratio between radiated power (P_r) and the fed

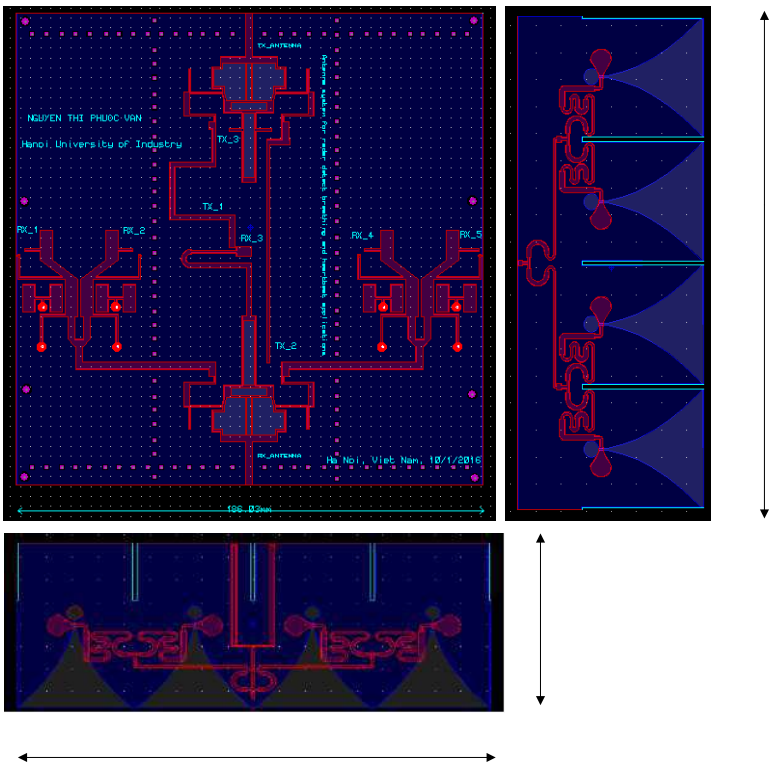

Figure 3.2: Structures of the designed antennae 4× patch for RX and 3× patch for TX [16]

power to the antenna P_T

$$\eta = \frac{P_r}{P_T} \tag{3.4}$$

- Antenna directivity is the proportion between maximum radiation intensity and the average radiation intensity

$$D = \frac{\frac{1}{2} Re\left(E_\theta H_\phi^\star - E_\phi H_\theta^\star\right)}{P_r / 4\pi r^2} \tag{3.5}$$

where E and H are the electrical and magnetic radiation, $\theta = 0$ or 90^0, $\phi = 90$ or 270^0, and r is the distance from the antenna to the considered point.

- Antenna gain is the product of directivity and efficiency

In the patch antenna, when the waves go through the feed point, they see the high impedance circuit (or near open circuit). This condition advocates that the

microstrip patch acts as a cavity, and most of the energy is echoed back. Based on this idea, the microstrip antenna is modeled as a cavity with its top and bottom are electric walls with the boundary conditions listed as follows:

- On electric walls the product of the unit vector normal to the cavity wall and the electrical radiation vector equal to zero
- On magnetic walls the product of the unit vector normal to the cavity wall and the magnetic radiation vector equal to zero

To design a microstrip patch antennae for the vital-sign sensing purpose, the high gain and the narrow directivity are required because the vital signals such as respiratory rate and heart rate are very small. The modified disc sector is chosen for each patch element. Disc sector geometry is defined by two parameters the angle α and the radius a of the disc sector. By tuning α, and a, we can get different outputs like gain, directivity and achieve extra band width. The detail of formula for this type of patch is presented in Chapter 14 [119]. Moreover, in the designed antenna system, the cost-effective factor can be achieved by using low-cost material- $FR4$ with substrate thickness 1.2 mm and dielectric constant $\varepsilon_r = 4.4$.

Figure 3.2 shows the 2-dimension ($2D$) structure of receiving, transmitting antennae, and the power splitter and combiner. The transmitting antenna consists of 4×3 patch elements (see Figure 3.3), so the total elements of transmitting antenna are 12. If the transmitting and receiving antennae are installed in the $2D$ configuration, the total area of the antenna system will be around 100 $cm \times$ 100 cm. This structure is too large for a portable vital signs detecting system. The $3D$ antennae structure could be a good solution for this problem.
The structure of each path is shown in the left and bottom of Figure 3.2, disc sector elements are impedance matching by the curve transmission line structure to reduce the size of the antenna. On the left side of this Figure is the power splitter and divider; the size of this circuit is 18.6 cm x 18.6 cm. These parts are designed on the same patch to save the space of the antenna system.

3.2.2 Three-dimensional (3D) transceiver antennae

Figure 3.3 is the receiving antennae contracted by 5×4 patch elements. The transmitting and receiving antennae are connected by the power splitter and power combiner. The feeding method is coaxial feed because it is easy to fabricate

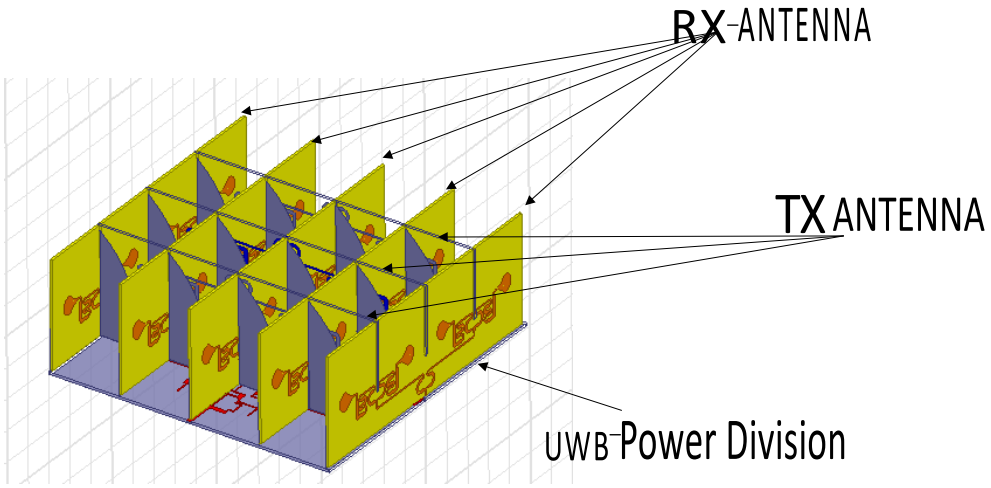

Figure 3.3: 3D Geography of proposed antennae [16]

and to connect to the radar sensor system through the cables. The power splitter and combiner are designed based on the idea adopted from [149, 150]. With the consideration of direction, gain, compact size, and extra wide band, an orthogonal antenna system was designed and fabricated as shown in Figure 3.4. In comparison with a $2D$ configuration, this novel design reduces the size about three times. The antennae development involves the use of HFSS and ADS softwares with the directivity of 54^0 . The comparison results of the simulation and measurements are presented in Figure 3.5. As can be seen, the antennae can operate in a very wide band, from around 900 MHz to 12 GHz with $S_{11} < -10\ dBm$. The measurement results of transmitter and receiver antennae on S_{11} show a better result in the frequency range from 800 MHz to 4.4 GHz and from 9.4 GHz to 12 GHz. The difference between the design and the simulation results of S_{11} might come from the variation of substrate permittivity at different frequencies. In simulation software the permittivity is chosen as 4.4. The isolation simulation result between two antennae $S_{21}$is quite close to the measurement result with the value of $S_{21} < -20\ dBm$.

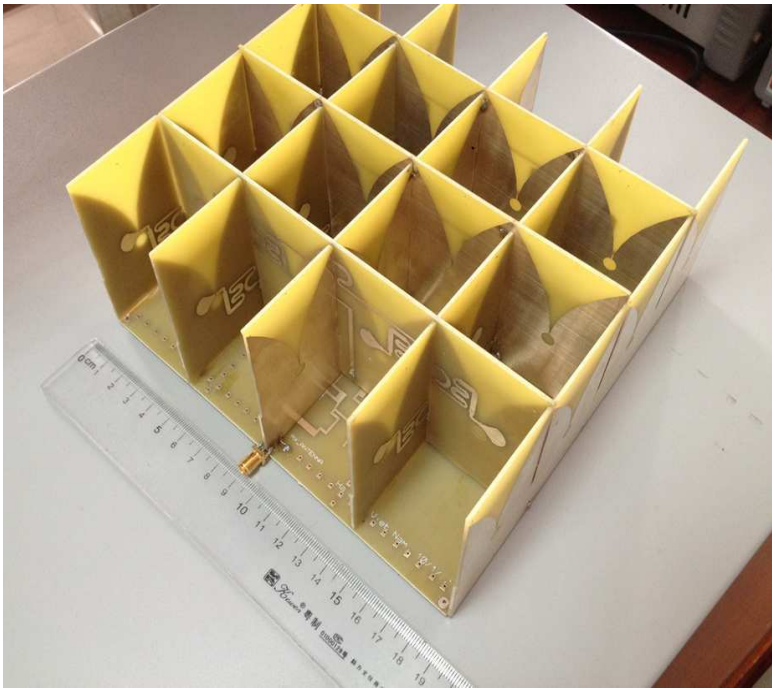

Figure 3.4: Fabricated antenna system [16]

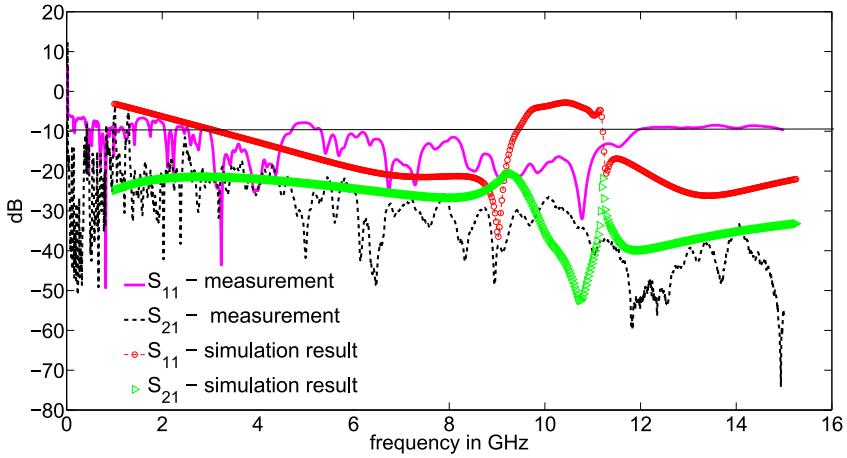

Figure 3.5: Reflection at the input and Isolation between two antennae [16]

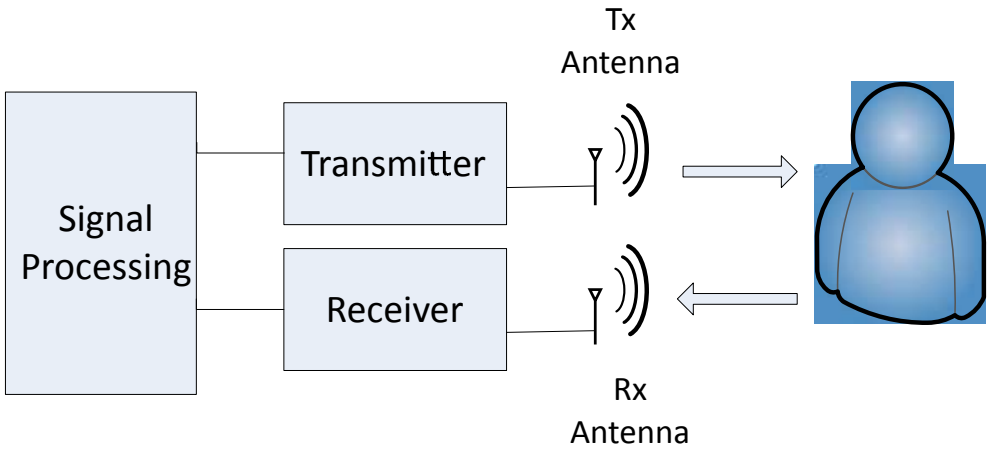

Figure 3.6: Block model of the radar sensor system [16]

3.3 Vital signs sensing using extra wide band $3D$ antennae

3.3.1 System and performance analysis

The block system of Doppler radar sensor is shown in Figure 3.6. In the continuous wave (CW) radar system a single-tone continuous wave signal ($s(t)$) as described by Equation(3.6), with amplitude A_T, frequency f, wavelength λ, and phase noise $\varphi(t)$ is sent to the human body [26],

$$s(t) = A_T \cos(2\pi f t + \varphi(t)) \tag{3.6}$$

This signal is then modulated by the chest movement $x(t)$. When a person breathes the thorax volume change causes the diaphragm, the intercostal(the muscles between the ribs), the neck, and the abdomen muscles move. The main displacement of the chest surface comes from the movements of abdominal and ribs [26]. The amplitude of the chest movement is around 12 mm [151]. The receiving signal at the Rx-antenna ($r(t)$)with the amplitude (A_R) can be acquired as follows [26].

$$r\left(t\right) = A_R \cos\left(2\pi f t - \frac{2\pi}{\lambda}\left(2x\left(t\right) + 2d\right) + \varphi\left(t - \frac{2d}{c}\right)\right) \tag{3.7}$$

where d is the distance from the human location to the radar antennae, and c is the light velocity.

If the intermediate frequency (IF) is used, the radio frequency (RF) signal is down-converted to IF as in the Equation(3.8) and (3.9) [152].

$$f_{IF} = f_{RF} - f_{LO} \tag{3.8}$$

where f_{LO} is frequency of local oscillator.

$$R_{IF}(t) = A_{IF} cos\left(2\pi f_{IF} t + \theta_0 + \frac{4\pi x(t)}{\lambda} + \triangle\varphi(t)\right) \tag{3.9}$$

where A_{IF} and f_{IF} are the amplitude and frequency of the IF signal respectively. $\theta_0 = \frac{4\pi d}{\lambda}$ is the constant phase shift due to the distance from the target to the radar system and $+\xi_0$ is phase shift due to the hardware such as antenna, amplifier, mixer and so on. $\triangle\varphi(t) = \varphi(t) - \varphi\left(t - \frac{2d}{c}\right)$ is the residual phase noise.
After the IF signal is filtered through the low pass filter (LPF) the base band output signal is given as:

$$B(t) = cos\left(\theta_0 + \frac{4\pi x(t)}{\lambda} + \triangle\varphi(t)\right) \tag{3.10}$$

Obviously, when $\theta_0 = n\pi$, n is an integer number, the output $B(t)$ is calculated approximately as [153]:

$$B(t) = 1 - \left(\frac{4\pi x(t)}{\lambda} + \triangle\varphi(t)\right)^2 \tag{3.11}$$

In this case, the receiving signal at the base band is very small, or not proportional linearly with the desired signal ($x(t)$). This issue is called the null point problem. The null point problem can be reduced by the quadrature detector. In the quadrature detector, the IF signal is divided into two parts with the phase difference of 90 degrees. These signals are demodulated by I/Q demodulator, two base band signals $B_I(t)$ and $B_Q(t)$ are created as follows [154]:

$$B_I(t) = cos\left(\frac{4\pi x(t)}{\lambda} + \theta_0 + \triangle\varphi(t)\right) \tag{3.12}$$

$$B_Q(t) = sin\left(\frac{4\pi x(t)}{\lambda} + \theta_0 + \triangle\varphi(t)\right) \tag{3.13}$$

From equations(3.12) and (3.13), the desired signal can be obtained by the arctangent demodulation [26].

$$\triangle\theta = arctan\left[\frac{B_Q(t)}{B_I(t)}\right] = arctan\left[\frac{sin\left(\frac{4\pi x(t)}{\lambda} + \theta_0 + \triangle\varphi(t)\right)}{cos\left(\frac{4\pi x(t)}{\lambda} + \theta_0 + \triangle\varphi(t)\right)}\right] \approx \frac{4\pi x(t)}{\lambda} + \theta_0 + \triangle\varphi(t) \tag{3.14}$$

In Equation (3.14) θ_0 is a constant, if the phase noise is neglected, the constant phase shift is also neglected, the output of arctangent demodulator is linearly proportional with the chest movement ($x(t)$).

$$\triangle\theta(t) \propto \frac{4\pi x(t)}{\lambda} \tag{3.15}$$

3.3.2 Measurement and discussions

Measurement setup

In this section, the performance of the proposed $3D$ antennae at various frequencies is tested using $N5244A\ PNA-X$ Microwave Network Analyzer, $43.5GHz$. The measurement setup is shown in Figure 3.7. On the left-hand side, an object (a person) is required to sit in front of the $3D$ antenna system, where the antennae are connected to two ports of the $N5244A\ PNA-X$ corresponding with the transmitter and receiver. $N5244A\ PNA-X$ send a continuous wave through the transmitting antenna and the changing phase of the receiving signal is determined by arctangent demodulation. The measurement was executed at wide range frequencies (0.953 GHz, 2.198 GHz, 3.362 GHz, 5.556 GHz, and 10 GHz) with the transmitted power of 0 dBm in the normal electronics laboratory environment. To get the stable signal, each measurement is measured in three minutes at a distance of $80cm$. The contact breathing measure equipment $BK-NICO$ [155] was used as a reference to detect the human breathing rate. A similar measurement setup was done with a wood obstacle between the object and the antenna shown on the right-hand side in Figure. 3.7. The extracted data from $N5244A\ PNA-X$ is processed by the common method Fast Fourier Transform -FFT get the respiratory rate [9].

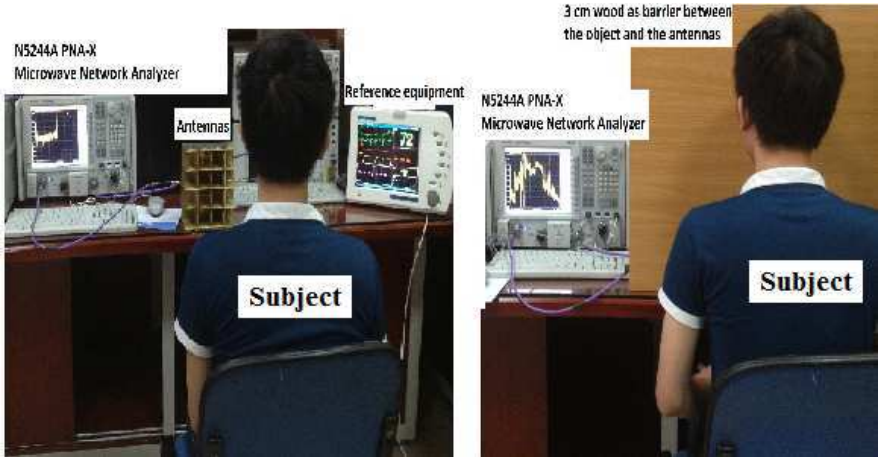

Figure 3.7: The measurement setup to detect the vital signs [16]

Measurement results

This part discusses the impact of antenna gain and the effect of operating frequencies on the breathing rate detection performance. Figure 3.8 shows that the human vital signs can be detected by the designed antenna system at different frequencies with a similar result. An average breathing rate of 17 beats per minute was measured by the commercial equipment BK-NICO [155]. Similarly, the proposed system gives the respiratory rates of 16.5, 18, 18, 15.7 (beats/minute) at the frequencies of 0.953 GHz, 2.198 GHz, 3.362 GHz, and 5.556 GHz respectively. The corresponding gains are 5 dBi, 7 dBi, 5 dBi, and 4 dBi. Figure 3.8 also suggests that the sensitivity of the system at a lower frequency is smaller than that at a higher frequency. This outcome is demonstrated in Equation 3.15. Moreover, the results shown in Figure 3.8 are good recommendations for different applications at different frequencies. For instance, high frequency benefits the medical application because of the high sensitivity of the system. On the other hand, the good penetration capacity through materials of the low frequency system handles the problem of finding survivors under the debris when there are natural hazards.

The performance of the $3D$ antenna system was tested when there was an obstacle (a 3-cm wooden plate) between the human and the antenna system. The object-antenna distance is 40 cm. Figure 3.9 illustrates the measurement results in this situation. The first point to note from this Figure is that when the system operated at low frequency (963.4 MHz), it displays the poor signal to noise ratio (SNR). This result can be explained by Equation. 3.15. Secondly, the system

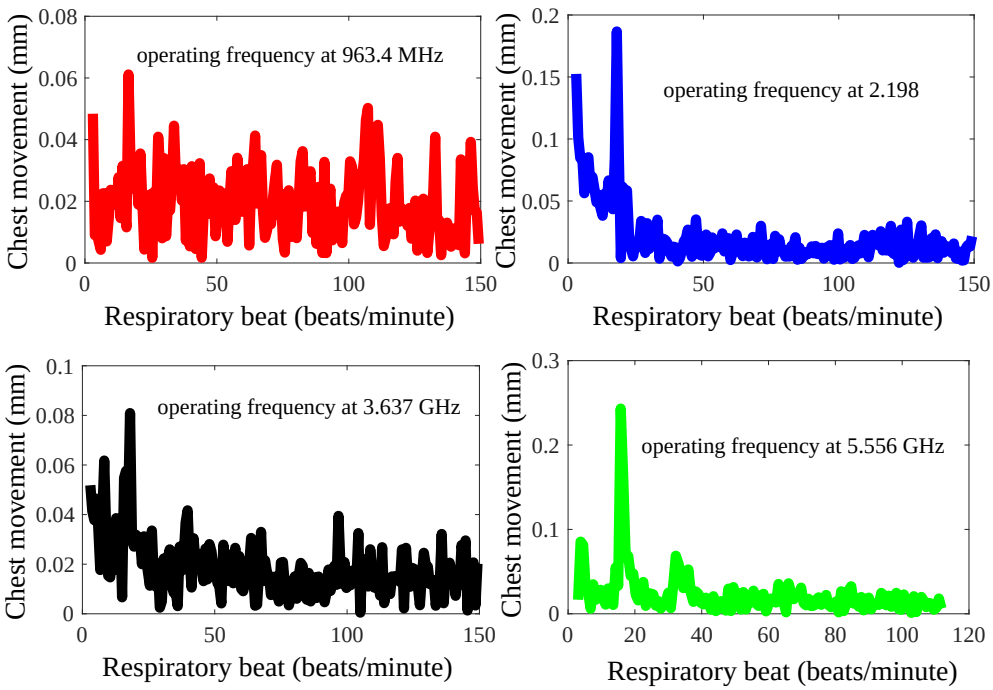

Figure 3.8: Amplitude versus respiratory rate in frequency domain when the distance between the antennae and the object is 80 cm [16]

behaves questionably at the highest operating frequency. Lastly, at two smaller operating frequencies 963.4 MHz and 2.198 GHz, the performance of the system is likely to be downgraded by the GSM and indoor wifi systems.

The receiving signal in time and in the frequency domain for the measurement at X band frequency are displayed in Figure 3.10. The amplitude of receiving signal (0.8 mm) is stronger than the receiving signal when the system runs at smaller frequencies (in Figure 3.8). Undoubtedly, the sensitivity of the radar sensor at the higher frequency band system is enlarged.

3.4 Conclusions

This chapter gives details about the basic principles to develop the patch antennae for the vital signs detecting radar system, and the novel multiple bandwidths $3D$ antenna system which has high potential to be used to detect the human vital signs. The proposed antennae system can work properly at different frequencies in line-of-sign (LOS) and non-line-of-sign (NLOS) environment. This type of

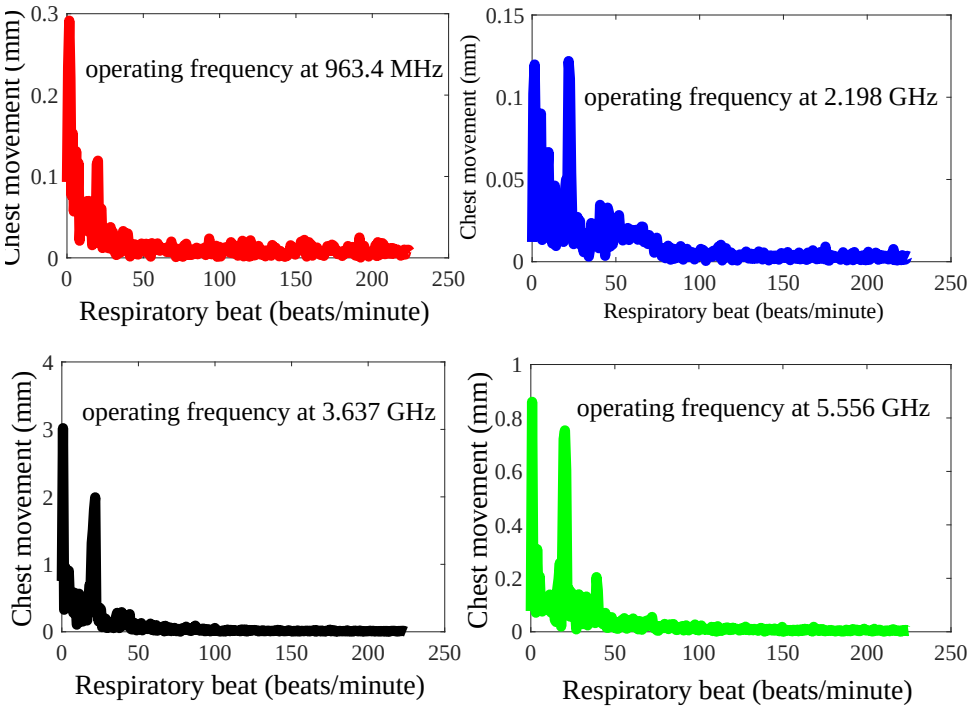

Figure 3.9: Amplitude versus respiratory rate when 3 *cm* of wood between the antennae and the object in frequency domain [16]

antennae allows the vital signs sensing radar system to operate at multiple frequencies simultaneously.
Based on this developed antenna, a smaller size antenna at L band was designed and fabricated for the subsequent chapters.

3.5 Related Publications

- **Van Nguyen Thi Phuoc**, Liqiong Tang, Nguyen Duc Minh, Faraz Hasan, and Subhas Mukhopadhyay. "Extra wide band 3D patch antennae system design for remote vital sign Doppler radar sensor detection." In 2017 Eleventh International Conference on Sensing Technology (ICST),1-5, 2017

- **Van Nguyen Thi Phuoc**, Liqiong Tang, Duc Minh Nguyen, Faraz Hasan, and Subhas Mukhopadhyay. "Wide Band Antennae System for Remote Vital Signs Detecting Doppler Radar Sensor." In Modern Sensing Technologies, pp. 47-62. Springer, Cham, 2019.

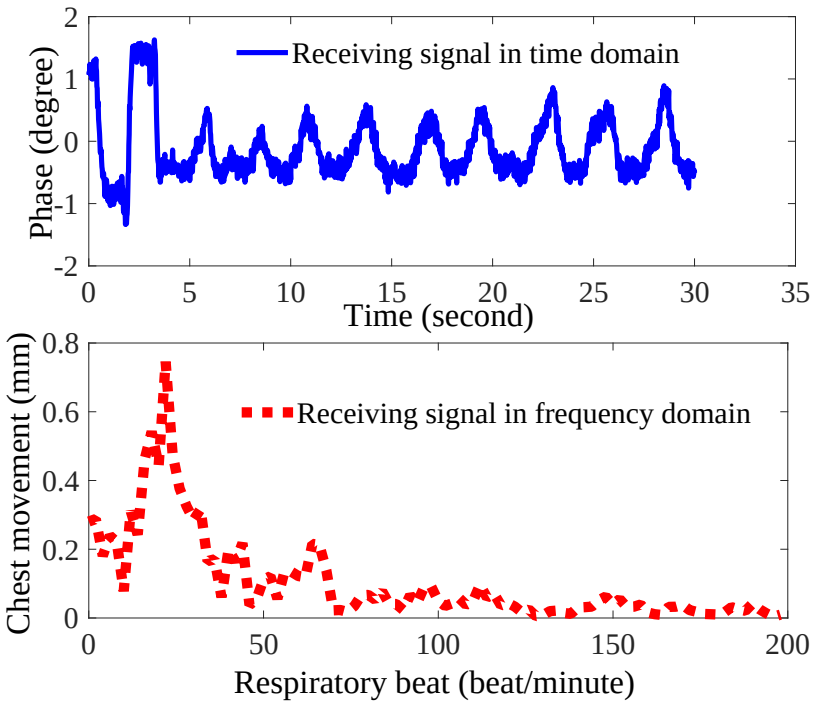

Figure 3.10: Receiving signal in time domain and in frequency domain [16]

Chapter 4

False alarm, Detection Probabilities of Microwave Doppler Sensing System

4.1 Introduction

Finding survivors buried under rubble is a crucial application of a Doppler radar sensor system [8, 9]. In such an application, the microwave beam must penetrate deeply through the debris or rubble to find living victims. Therefore, L and S bands seem to be good choices. Kun-Mu Chen et al. [8] built systems and conducted experiments at two frequencies, 450 and 1150 MHz, and found that the 1150 MHz system operated better when the debris had metallic wires. In 2016, F. JalaliBidgoli et al. [9] proposed a similar system operating at a 1150 MHz frequency with the focus on minimizing clutter and noise. This system is portable and can detect a victim below a depth of 1.5 m. Contrary to the earlier work, the transmission link between the radar system and the human body is a Friis channel model. This model implies a line-of-sight (LOS) connection between the radar sensor system and the subject. For the purpose of finding survivors, the system has to operate through different materials. Clearly, the LOS channel model is not adequate to describe the environment in which the radar system is likely to be used.

This chapter presents research that considers the previous investigations and their drawbacks. In this research work, the SNR is carefully taken into account with respect to the Nakagami-m channel model and its special case (Rayleigh

fading channel model). This model was chosen because it can more adequately describe realistic situations [156]. The Nakagami-m fading channel model can be used for a wide range of radio links, from non-fading channels to land-mobile or indoor-mobile prorogations. This channel can also serve as a LOS/non-line-of-sight (NLOS) channel model [157, 158]. In comparison with previous studies, in terms of a channel radio link between the vital-sign-detecting radar system and the human, this research considers a more realistic and common channel model, the Nakagami-m, for the vital-sign-detecting radar sensor system. To the best of the author's knowledge, this is the first work to use the SNR at the base band under the Nakagami-m radio channel link between a living person and the radar sensor system. Moreover, the detection/false alarm probabilities of the vital-sign-detecting radar sensor system have been established, simulated and analyzed.

4.2 System Model

The working principle of the proposed vital-sign-detecting radar sensor system is presented using the block diagram shown in Figure 4.1. The transmitting antenna sends continuous waves to the human and waits for the reflected signals from the human body. At the human's chest, the RF signal is modulated by the periodic displacement of the chest before being reflected back to the receiving antenna [24]. At the receiver, the signal is amplified by a low-noise amplifier (LNA) and is then sent to the phase detector. In this diagram, the in-phase (I) and quadrature (Q) phase detectors are used to reduce the null-point problem.

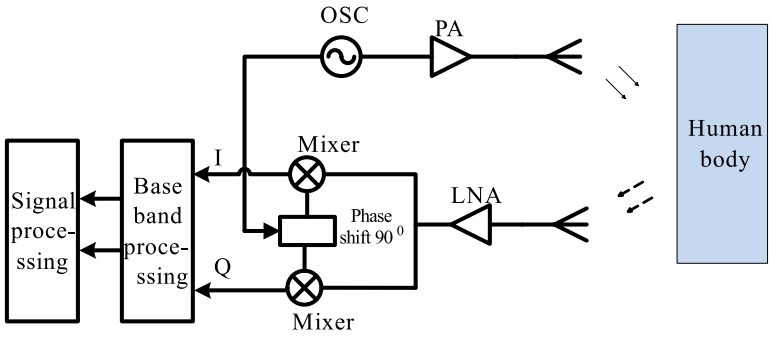

Figure 4.1: System diagram.

The transmitted signal from the vital-sign-detecting radar sensor system can

be described by

$$Y_T = \sqrt{2P_T}\cos\left(2\pi ft + \phi\left(t\right)\right) \tag{4.1}$$

where P_T is the power of the transmitter, f is the carrier frequency, t is the transpiring time, and $\phi\left(t\right)$ is the phase noise. The initial phase of the transmitting signal is assumed to be zero. The signal Y_T is then reflected by the human's chest. The movement of the chest can be considered as the periodic signal $x\left(t\right)$. The distance from the human's location to the antennae of the radar sensor system is d (m). The received signal Y_R can be expressed as follows [106]:

$$Y_R = A_R\cos\left(2\pi ft - \frac{4\pi d}{\lambda} - \frac{4\pi x\left(t\right)}{\lambda} + \phi\left(t - \frac{2d}{c}\right)\right) \tag{4.2}$$

where c is the light velocity, λ is the wavelength of the signal, and A_R is the return signal amplitude that depends on the transmitted power, the gain of the antennae, the radar cross-section, and reflection loss from the human body and environment (channel links from the radar to the human body and from the human body to the radar). In fact, in practice, the transmitting antenna is quite close to the receiving antenna, and thus the leakage noise is unavoidable. Moreover, the radar system also receives the reflected signal from the stationary part of the human and other clusters [24]. Therefore, the stable reflected signal should be considered at the receiving antenna. The received signal can be rewritten as:

$$\begin{aligned} Y_R = {} & A_R\cos\left(2\pi ft - \frac{4\pi d}{\lambda} - \frac{4\pi x\left(t\right)}{\lambda} + \phi\left(t - \frac{2d}{c}\right)\right) \\ & + A_{leak}\cos\left(2\pi f\left(t - t_l\right) + \phi\left(t - t_l\right)\right) \\ & + A_c\cos\left(2\pi ft - \frac{4\pi d}{\lambda} + \phi\left(t - \frac{2d}{c}\right)\right) \end{aligned} \tag{4.3}$$

where A_{leak} is the amplitude of the leakage signal, t_l is the time delay between the transmitting leakage signal and the local oscillator (LO) signal, and A_c is the amplitude of the stationary cluster signal.

In previous studies, channel links between the radar sensor system and the human were considered as in free space [159]. This model implied that there were LOS links between the radar system and the human. However, the vital-sign-detecting radar system has to operate through the NLOS channel. For this

reason, in this study, the Nakagami-m channel model was chosen as the channel model between the radar sensor system and the human. This channel model was considered to be close to the practical situation and could model both LOS and NLOS environments [156]. On the basis of the theory of radar systems [160], the amplitude of the receiving signal A_R $[Volt]$ can be formulated as follows [161]:

$$A_R = \sqrt{\frac{2P_T G_T G_R \sigma_a \rho_r \rho_t r \lambda^2 |g_a|^2 |g_b|^2}{(4\pi)^3 d^{2\alpha}}} \tag{4.4}$$

where $G_T = 10^{\frac{G_T[dBi]}{10}}$ and $G_R = 10^{\frac{G_R[dBi]}{10}}$ are the gains of the transmitting antenna and receiving antenna, respectively; λ (m) is the wavelength of the signal; ρ_r and ρ_t are the radiated efficiencies of the receiving and transmitting antennae; r is the reflection coefficient of the human body; σ_a (m^2) is the radar cross-section (RCS) of the human's chest; and α is the path loss. The channel coefficients for the links from the radar to the human body and from the human body to the radar are g_a and g_b, respectively.

The leakage amplitude can be estimated as follows [130]:

$$A_{leak} = \sqrt{2\eta_{leak} P_T} \tag{4.5}$$

and

$$A_c = \sqrt{\frac{2P_T G_T G_R \sigma_c \rho_r \rho_t r \lambda^2 |g_a|^2 |g_b|^2}{(4\pi)^3 d^{2\alpha}}} \tag{4.6}$$

where σ_c is the RCS of other parts of the human body.
The received signal Y_R is then mixed with the LO signal to obtain the intermediate frequency (IF) signal. As can be seen from Figure 4.1, $I\&Q$ demodulation is applied to reduce the null-point problem [153]. The output signals are then fed to the band pass filter (BPF). The low-and high-end frequencies of the BPF are expressed as f_L and f_H, respectively.

The base band can be written as follows [130]:

$$\begin{aligned} B(t) = & A_R\sqrt{G_{RX}}cos\left[\theta_0 + \frac{4\pi x\left(t\right)}{\lambda} + \triangle\phi_s\left(t\right)\right] \\ & + A_c\sqrt{G_{RX}}cos\left[\theta_0 + \triangle\phi_c\left(t\right)\right] \\ & + A_{leak}\sqrt{G_{RX}}cos\left[\theta_l + \triangle\phi_l\left(t\right)\right] + n(t) + n_{1/f}(t) \end{aligned} \tag{4.7}$$

whereG_{RX} is the gain of the receiver, θ_0 is a constant phase shift due to the distance from the human body to the radar system; θ_l is a constant phase shift that depends on the delay time t_l; $\triangle\phi_s\left(t\right)$, $\triangle\phi_c\left(t\right)$, and $\triangle\phi_l\left(t\right)$ are the residual phase noise of the reflected vital signals (respiratory signal and heart signal), clutter signal, and antennae leakage signal, respectively; $n(t)$ and $n_{1/f}()$ are the additive white Gaussian noise (AWGN) and base-band $1/f$ noise (electronic noise with $1/f$ power density). The residual phase noise in Equation (4.7) can be calculated as follows [130]:

$$\triangle\phi_s\left(t\right) \approx \triangle\phi_c\left(t\right) = \phi\left(t\right) - \phi\left(t - \frac{2d}{c}\right) \tag{4.8}$$

$$\triangle\phi_l\left(t\right) = \phi\left(t\right) - \phi\left(t - \triangle t_l\right) \tag{4.9}$$

In the following sections, the SNR is considered carefully, and the comparison between the theoretical calculation and the measurement is examined.

4.3 SNR Analysis

4.3.1 Signal Power

In the case in which the optimal demodulation is achieved, the receiving power at the output of the mixer can be given as follows [130, 153, 159]:

$$\begin{aligned} S_B &= A_R^2 G_{RX} \left(\frac{4\pi x\left(t\right)}{\lambda} \right)^2 \\ &= \frac{2P_T G_T G_R \sigma_a \rho_r \rho_t r \lambda^2 |g_a|^2 |g_b|^2}{\left(4\pi\right)^3 d^{2\alpha}} G_{RX} \frac{16\pi^2 \overline{x^2\left(t\right)}}{\lambda^2} \\ &= \frac{P_T G_T G_R \sigma_a \rho_r \rho_t r |g_a|^2 |g_b|^2 G_{RX} \overline{x^2\left(t\right)}}{2\pi d^{2\alpha}} \end{aligned} \tag{4.10}$$

In this work, the main sources of noise have been considered carefully: residual phase noise, AWGN, and the base-band $1/f$ noise.

4.3.2 Residual Phase Noise

Clearly, phase noise degrades the performance of the Doppler radar system. The effect of this phenomenon is to spread energy of the clutter into the target frequency range. The spreading of clutter obscures the target signal and reduces the signal-to-clutter ratio [75]. In this section, the residual phase noise power is calculated. The residual phase noise consists of phase noise by the antennae leakage signal and the clutter. As defined in [75, 130, 159], the base-band noise spectral density ($S_{\triangle\phi}(f_0)$) is derived from the RF phase noise spectral density $S_\theta(f_0)$:

$$S_{\triangle\phi_s}(f_0) = S_{\phi_s}(f_0) 4sin^2\left(2\pi\frac{df_0}{c}\right) \approx S_\phi(f_0)\left(\frac{16\pi^2 d^2 f_0^2}{c^2}\right) \tag{4.11}$$

$S_{\phi_s}\left(f_0\right)$ can be derived from the phase noise at 1 Hz, $S_\phi\left(1\right)$, if the close-in phase noise has a -30 dB/decade slope (typical value of an oscillator), as follows [130]:

$$S_{\phi_s}\left(f_0\right) \approx \frac{S_\phi\left(1\right)}{\left(1Hz\right)^{-3}} f_0^{-3} \tag{4.12}$$

On the basis of Equations (4.11) and (4.12), $S_{\triangle\phi_c}(f_0)$ can be given:

$$S_{\triangle\phi_s}(f_0) \approx \frac{S_\phi(1)}{(1Hz)^{-3}} f_0^{-3} \left(\frac{16\pi^2 d^2 f_0^2}{c^2}\right) \tag{4.13}$$

The mean square of the residual phase noise in the time domain is calculated through the integral of the spectrum over the frequency range $[f_L to f_H]$ of the BPF [130]:

$$\overline{\triangle\phi_s(t)^2} = \int_{f_L}^{f_H} S_{\triangle\phi_s}(f_0)\, df_0 = 16\pi^2 (1Hz)^3 S_\phi(1) \frac{d^2}{c^2} ln\left[\frac{f_H}{f_L}\right] \tag{4.14}$$

Finally, the residual phase noise power ($N_{\triangle\phi_s}$) of the received signal can be calculated [130]:

$$\begin{aligned} N_{\triangle\phi_s} &\approx A_R^2 G_{RX} \overline{\triangle\phi_s(t)^2} \qquad (4.15)\\ &\approx \frac{2P_T G_T G_R \sigma_a \rho_r \rho_t r \lambda^2 |g_a|^2 |g_b|^2}{(4\pi)^3 d^{2\alpha}} G_{RX} 16\pi^2 (1Hz)^3 S_\phi(1) \frac{d^2}{c^2} ln\left[\frac{f_H}{f_L}\right] \\ &\approx \frac{P_T G_T G_R \sigma_a \rho_r \rho_t r \lambda^2 |g_a|^2 |g_b|^2}{2\pi d^{2(\alpha-1)} f^2} G_{RX} S_\phi(1)\, ln\left[\frac{f_H}{f_L}\right] \end{aligned}$$

$S_\phi(1)$ is the proportion between energy at spectrum 1 Hz and the whole band energy. By following similar steps to Equation (4.11)–(4.15), the residual phase noise power ($N_{\triangle\phi_c}$) of the clutter signal can be calculated:

$$N_{\triangle\phi_c} \approx \frac{P_T G_T G_R \sigma_c \rho_r \rho_t r \lambda^2 |g_a|^2 |g_b|^2}{2\pi d^{2(\alpha-1)} f^2} G_{RX} S_\phi(1)\, ln\left[\frac{f_H}{f_L}\right] \tag{4.16}$$

This then turns to antennae leakage phase noise; the base-band spectral density of antennae leakage phase noise $S_{\triangle\phi_l}(f_0)$ is given as:

$$S_{\triangle\phi_l}(f_0) \approx \frac{S_\phi(1)}{(1Hz)^{-3}} f_0^{-3} \left(\frac{16\pi^2 \triangle t_l^2 f_0^2}{4}\right) \tag{4.17}$$

The power of the antennae leakage phase noise ($N_{\triangle\phi_l}$) can be expressed as:

$$\begin{aligned} N_{\triangle\phi_l} &\approx A_{leak}^2 G_{RX} \overline{\triangle\phi_l(t)^2} \\ &\approx A_{leak}^2 G_{RX} \int_{f_L}^{f_H} S_{\triangle\phi_l}(f_0)\, df_0 \\ &\approx A_{leak}^2 G_{RX} 16\pi^2 (1Hz)^3 S_\phi(1) \frac{\triangle t_l^2}{2^2} ln\left[\frac{f_H}{f_L}\right] \\ &\approx 32\eta_{leak} P_T G_{RX} \pi^2 S_\phi(1) \frac{\triangle t_l^2}{2^2} ln\left[\frac{f_H}{f_L}\right] \end{aligned} \tag{4.18}$$

4.3.3 Additive White Gaussian Noise

AWGN is the main noise at the receiver's input, and afterwards, this noise is converted to the baseband with the power (N_W) as follows [130, 159]:

$$N_W = 8G_{RX}(kTB)(NF) \tag{4.19}$$

where $G_{RX} = 10^{\frac{G_{RX}[dBi]}{10}}$ is the gain of the receiver, B (Hz) is the bandwidth, T (K) is the absolute temperature, k is Boltzman's constant, and $NF = 10^{\frac{NF[dB]}{10}}$ is the noise figurer of the receiver.

4.3.4 $1/f$ Noise

The mixer is chosen to minimize the $1/f$ noise. The power of the $1/f$ noise ($N_{1/f}$) can be designated by the noise power ($P_{1/f}(1)$) in a 1 Hz bandwidth centered at 1 Hz:

$$N_{1/f} = \int_{f_L}^{f_H} P_{1/f}(1) f^{-1} df = P_{1/f}(1) ln\left(\frac{f_H}{f_L}\right) \tag{4.20}$$

4.3.5 SNR

The noise sources are uncorrelated, and the powers of the noise are added together. The SNR is written as:

$$SNR = \frac{S_B}{N_{\triangle\phi_s} + N_{\triangle\phi_c} + N_{\triangle\phi_l} + N_W + N_{1/f}} \tag{4.21}$$

4.4 Detection and False Alarm Probabilities

In this section, the analysis and simulation results of the detection probability (P_D) and false alarm probability (P_f) of the proposed system are presented. Estimations of the detection/false alarm probabilities are very important for the vital-sign-detecting radar system. The decision hypothesis is detected when the received signal and noise are greater than the threshold value P_{th}. The decision is a false alarm when the power of the noise is greater than the threshold P_{th} [5,160]. The false alarm/detection probabilities are estimated under two hypotheses, H_0 and H_1. H_0 corresponds to the case that the vital signal is not presented, and H_1 is the opposite case.

4.4.1 Detection Probability

The detection probability can be defined as follows:

$$P_D = P_r\left\{S_B + N_{\triangle\phi_s} + N_{\triangle\phi_c} + N_{\triangle\phi_l} + N_W + N_{1/f} \geq P_{th} \mid H_1\right\} \tag{4.22}$$

By using $C = \frac{P_T G_T G_R \sigma_a \rho_r \rho_t r G_{RX} \overline{x^2(t)}}{2\pi d^{2\alpha}}$ and $D = \frac{P_T G_T G_R \rho_r \rho_t r \lambda^2}{2\pi d^{2(\alpha-1)} f^2} G_{RX} S_\phi(1)$, P_D can be rewritten as follows:

$$P_D = P_r\left\{C|g_a|^2|g_b|^2 + D\sigma_a|g_a|^2|g_b|^2 + D\sigma_c|g_a|^2|g_b|^2 + N_{\triangle\phi_l} + N_W + N_{1/f} \geq P_{th}\right\} \tag{4.23}$$

$$= P_r\left\{(C + D\sigma_a + D\sigma_c)\,|g_a|^2|g_b|^2 + N_{\triangle\phi_l} + N_W + N_{1/f} \geq P_{th}\right\}$$

$$= 1 - P_r\left\{|g_a|^2|g_b|^2 \leq \frac{P_{th} - \left(N_{\triangle\phi_l} + N_W + N_{1/f}\right)}{C + D\sigma_a + D\sigma_c}\right\}$$

The channel model between the radar system and the human body is Nakagami-m, where m is the fading severity parameter. We assume that $|g_a^2|$ and $|g_b^2|$ are independent gamma random variables with the severity fading factor m_a and m_b; in the case $m = 1$, the Nakagami-m model becomes the Rayleigh fading channel model. By applying the work from [161], the detection probability can be given

as:

$$P_D = 2\sqrt{\frac{P_{th} - \left(N_{\triangle\phi_l} + N_W + N_{1/f}\right)}{\left(C + D\sigma_a + D\sigma_c\right)\mu_a\mu_b}} K1\left(2\sqrt{\frac{P_{th} - \left(N_{\triangle\phi_l} + N_W + N_{1/f}\right)}{\left(C + D\sigma_a + D\sigma_c\right)\mu_a\mu_b}}\right) \tag{4.24}$$

where μ_a and μ_b are the mean values of $|g_a^2|$ and $|g_b^2|$, respectively. $K1(.)$ is the first-order modified Bessel function of the second kind, $K1\left(x\right) = \int_0^\infty e^{-xcosh(t)} cosh\left(t\right) dt$ [162].

When it comes to the normal case of the Nakagami-m channel model, the detection probability of the sensor system can be calculated on the basis of the distribution of the products of two independent variables $|g_a^2|$ and $|g_b^2|$. Associated with the probability theory in [163], P_D can be calculated as:

$$P_D = 1 - u2^{1-m_a-m_b} Dm_1 + m_2 - 1, m_1 - m_2\left(2\sqrt{\frac{P_{th} - \left(N_{\triangle\phi_l} + N_W + N_{1/f}\right)}{C + D\sigma_a + D\sigma_c}}\right) \tag{4.25}$$

where $u = 2\tau\left(m_1\right)^{-1}\tau\left(m_2\right)^{-1}$ and $D_{\mu,v}(x) = \int_0^x x^\mu K_v(x)dx$; $\tau\left(.\right)$ and $K\left(.\right)$ are the *Gamma* function and Bessel function, respectively. These functions can be found in [164] and calculated by available software such as Matlab or Wolfram. In the special case $m_a = m_b = \mathrm{I} + 1$ (where I = 0, 1, 2, ...), P_D is given as follows [163]:

$$P_D = 2^{-2i}\left(i!\right)^{-1}\sum_{j=0}^{i}\left(2\sqrt{\frac{P_{th} - \left(N_{\triangle\phi_l} + N_W + N_{1/f}\right)}{C + D\sigma_a + D\sigma_c}}\right)^{2i+1-j} \times \tag{4.26}$$
$$K_{j+1}\left(2\sqrt{\frac{P_{th} - \left(N_{\triangle\phi_l} + N_W + N_{1/f}\right)}{C + D\sigma_a + D\sigma_c}}\right) 2^j/(i-j)!$$

where K_{j+1} is the $j+1$ order modified Bessel function of the second kind.

4.4.2 False Alarm Probability

Similarly, the false alarm probability is given as

$$\begin{aligned} P_f &= P_r\left\{N_{\triangle\phi_s} + N_{\triangle\phi_c} + N_{\triangle\phi_l} + N_W + N_{1/f} \geq P_{th} \mid H_0\right\} \\ &= 1 - P_r\left\{|g_a|^2|g_b|^2 \leq \frac{P_{th} - \left(N_{\triangle\phi_l} + N_W + N_{1/f}\right)}{D\sigma_a + D\sigma_c}\right\} \end{aligned} \tag{4.27}$$

Under the Rayleigh fading channel model, the false alarm probability can be expressed as:

$$P_f = 2\sqrt{\frac{P_{th} - \left(N_{\triangle\phi_l} + N_W + N_{1/f}\right)}{\left(D\sigma_a + D\sigma_c\right)\mu_a\mu_b}} K1\left(2\sqrt{\frac{P_{th} - \left(N_{\triangle\phi_l} + N_W + N_{1/f}\right)}{\left(D\sigma_a + D\sigma_c\right)\mu_a\mu_b}}\right) \tag{4.28}$$

Under the Nakagami-m channel model ($m \geq 1/2$), the false alarm probability can be given as:

$$P_f = 1 - u2^{1-m_a-m_b} Dm_1 + m_2 - 1, m_1 - m_2\left(2\sqrt{\frac{P_{th} - \left(N_{\triangle\phi_l} + N_W + N_{1/f}\right)}{D\sigma_a + D\sigma_c}}\right) \tag{4.29}$$

In the case $m_a = m_b = \mathrm{I} + 1$ (where I = 0, 1, 2, ...), P_f can be calculated as follows [163]:

$$\begin{aligned} P_f = 2^{-2i}\left(i!\right)^{-1} \sum_{j=0}^{i} &\left(2\sqrt{\frac{P_{th} - \left(N_{\triangle\phi_l} + N_W + N_{1/f}\right)}{D\sigma_a + D\sigma_c}}\right)^{2i+1-j} \\ &\times K_{j+1}\left(2\sqrt{\frac{P_{th} - \left(N_{\triangle\phi_l} + N_W + N_{1/f}\right)}{D\sigma_a + D\sigma_c}}\right) 2^j/(i-j)! \end{aligned} \tag{4.30}$$

4.5 Simulation Result

In this section, the SNR and detection/false alarm probabilities are discussed in terms of simulation and analysis. The values used for simulation and analysis are given in Table 4.1.

Table 4.1: System parameters used for simulation.

Symbol	Description	Value
P_T	Power of transmitter	0 dBm
G_T	Transmitting antenna gain	5 dBi
G_R	Receiving antenna gain	5 dBi
G_{RX}	Gain of the receiver	10 dB
ρ_r	Radiated efficiency of receiving antenna	0.8
ρ_t	Radiated efficiency of transmitting antenna	0.8
r	Reflection coefficient of the human body	0.5
σ_a	RCS of the human's chest	500 mm^2
NF	Received noise figure	6 dB
$P_{1/f}(1)$	$1/f$ power noise power at 1 Hz	-130 dBm/Hz
T	Absolute noise temperature	300
f_H	High frequency	5 Hz
f_L	Low frequency	0.1 Hz
$S_{\triangle}(1)$	Phase noise at 1 Hz intercept	60 dB/Hz
η_{leak}	Leakage between transmitting and receiving antennae	-20 dB
α	Path loss	2

4.5.1 SNR and Detection/False Alarm Probabilities under Rayleigh Fading Channel

Firstly, a special case of the Nakagami-1 (Rayleigh fading channel) channel model has been considered. This model implied that there was no LOS transmission between the human and the radar system. The power of the received signal and different types of noise are shown in Figure 4.2. The leakage noise was relatively high, around -90 dBm, while the AWGN and $1/f$ noise were lower than 120 dBm. The residual phase noise power of the received signal had less effect on the system than the residual phase noise power of the clutter signal; both decreased when the distance increased. It is noted from this simulation that with the transmitting power of 0 dBm, the receiving power was greater than the power of each type of noise when the distance was less than 3 m. This figure gives an important idea to enhance the system. The most dominant noise was leakage noise; this type of noise is defined by the isolation level between the transmitting

and receiving antennae. Therefore, this noise could be minimized by hardware development and signal processing techniques.

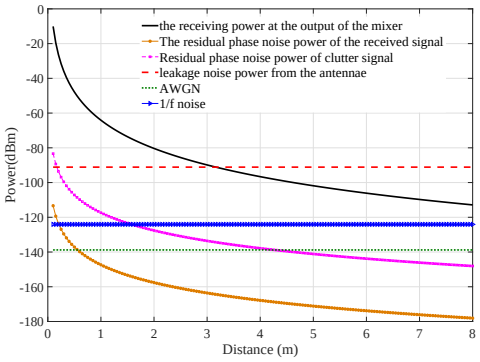

Figure 4.2: Power of signal and noise of the system.

Besides the power of the signal and noise, the SNR is the most important feature of the radar sensor system. The overall SNR of system is displayed in Figure 4.3. The first point to note is that the SNR decreased whenever the distance between the human body to the radar system and the antennae leakage increased. At the level of antennae leakage of -20 dB, the SNR reduced from around 30 dB at a distance of 1 m to -20 dB at a distance of 7 m. When the leakage between the two antennae was at -40 dB, the SNR at the same distance increased to 0 dB.

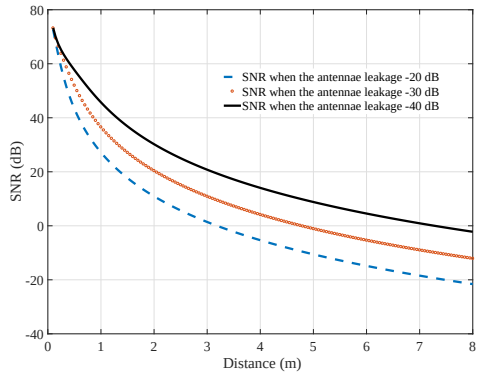

Figure 4.3: Signal-to-noise ratio (SNR) versus the distance from the radar system to the human body.

Figure 4.4 displays the detection probability of the system at three different

levels of the threshold power of the receiver's filter, −70, −80, and −90 dBm. The lowest threshold value gave the highest detection probability. When the distance increased, the detection probability decreased. The threshold power of the receiver's filter defined the steepness of the detection probability line.

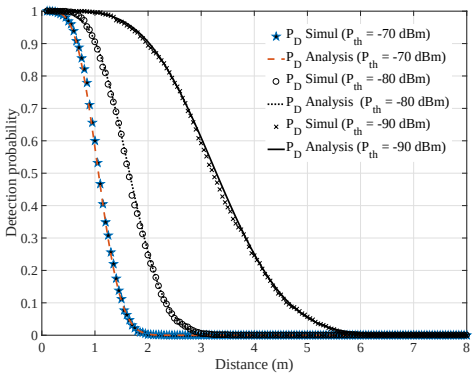

Figure 4.4: Detection probabilities of the system under different threshold levels of receiver filter.

To evaluate the accuracy of the vital-sign-detecting radar sensor, the false alarm should be taken into account. Figure 4.5 shows that when the threshold power of the receiver's filter was set at −90 dBm, the false alarm probability was high at distances of less than 30 cm. This phenomenon was due to the high level of phase noise when the radar was too close to the human body. When this threshold value increases to −70 dBm, the false alarm moved to the zero level. The simulation and analysis results are presented in Figures 4.2–4.6.

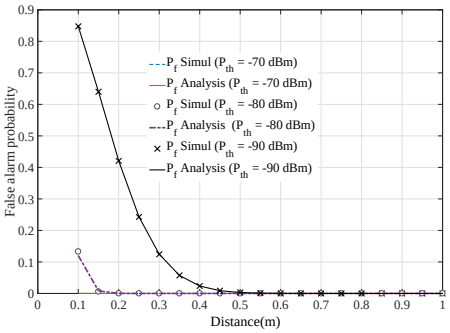

Figure 4.5: False alarm of the system under different threshold levels of receiver filter.

4.5.2 Detection/False Alarm Probabilities of the System under the Nakagami-2 Channel Model

When the quality of the channel increased, for example, when the fading factor $m = 2$, in comparison with the Rayleigh fading link, the detection probability increased significantly. At a distance of around 7 m, the detection probability was approximately 80% as shown in Figure 4.6. The false alarm detection probability was relatively high at a close distance (less than 50 cm) because of the high level of phase noise.

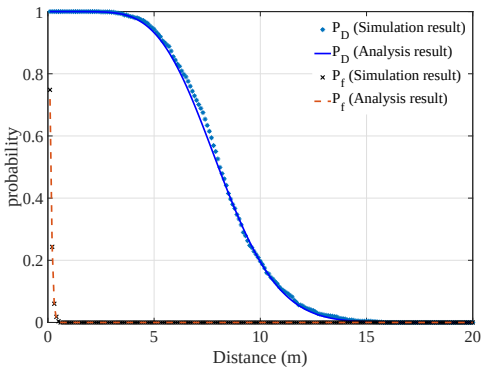

Figure 4.6: False alarm/detection probabilities of the system under Nakagami-2 channel model.

4.6 Measurement Results

This section presents the measurement results of detecting the respiratory rate of humans. The SNR and the detection capability/probability were considered and compared to those of the theoretical models. The measurement was a setup based on the $N5244A\ PNA-X$ Microwave Network Analyzer, 43.5 GHz. Two ports of this device were connected to two antennae, as shown in Figure 4.7. Five people aged from 21 to 25 participated in this experiment. The participants were required to sit in front of the antennae; one antenna played the role of the transmitting antenna, and the other was the receiving antenna. The operating frequency of the system was set up in L band to obtain higher penetration through different environments [165]. In this study, the frequency was chosen as the optimal operating frequency (1.6 GHz) of the microstrip/path antenna. The antennae's size was 10 cm $\times$ 10 cm with a gain of 5 dBi. For each distance (1, 2, 3, and 4 m), objects

were measured over five minutes continuously in the normal electronic lab. The internal phase detector of the $N5244A\ PNA-X$ Microwave Network Analyzer was utilized to find the phase shift of the received signal. This signal was then processed in Matlab to find the breathing rate. At the same time, the person's breathing rate was measured by the wearable sensor *Shimmer* 3 ECG/EMG with five probe leads connected, as shown in Figure 4.7; the output signals of the *Shimmer* 3 were sent to the computer by a Bluetooth connection. The measurement results are shown in Table 4.2. The breathing rates at different distances were close to the reference values. For the rescue detection purpose, the deviation around the beats per minute was acceptable. Regarding the SNR values, at every distance, the measured results were close to the simulation results. The difference was only around 1.5 dBm. The measurement result of the SNR of the second object was the closest to the simulation outcome and the mean values of the five cases. The detailed measured results of object 2 are presented in Figures 4.8 and 4.12.

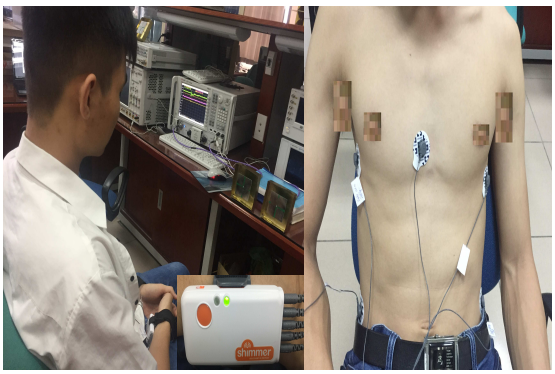

Figure 4.7: Measurement setup to detect the breathing rate.

Table 4.2: Respiratory rates and signal-to-noise ratio (SNR) from five objects at different distances.

Object	Breathing Rate					SNR							
	Ref	1 m	2 m	3 m	4 m	1 m		2 m		3 m		4 m	
						Sim.	Meas.	Sim.	Meas.	Sim.	Meas.	Sim.	Meas.
1	15	16	17	18	18	43.73	43.37	33.67	21.76	27.12	13.5	22.31	15.77
2	16	17	15	18	16	**43.73**	**43.13**	**33.67**	**33.03**	**27.12**	**27.32**	**22.31**	**21.77**
3	16	18	18	19	17	43.73	40.11	33.67	40.44	27.12	30.65	22.31	27.08
4	17	18	16	17	13	43.73	66.25	33.67	43.19	27.12	24.55	22.31	19.55
5	16	18	16	17	16	43.73	34.09	33.67	44.56	27.12	27.12	22.31	18.65
Mean values	16	17.4	16.4	17.8	16	**43.73**	**45.39**	**33.67**	**36.59**	**27.12**	**24.62**	**22.31**	**20.56**

Figure 4.8 shows the reference signal and the measured signal at a distance of 4 m in the time domain by the radar system. These signals were then processed by the fast Fourier transform (FFT) to find the breathing rate. The signals in the frequency domain can be seen in Figure 4.9. The breathing rate of the measured person was 16 beats per minute. The window size of the FFT was 30 s and moved forward every second; the number of samples in each second was 256. The SNR and the detection capability of the system were evaluated at each second after the first 30 s.

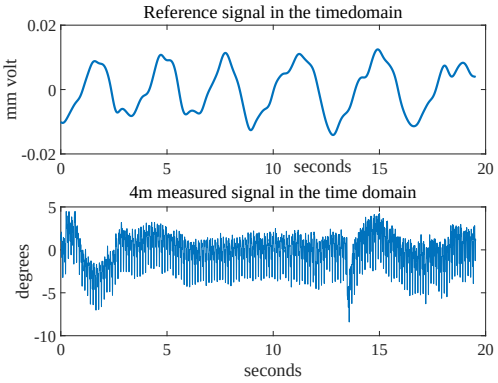

Figure 4.8: Receiving signals in time domain.

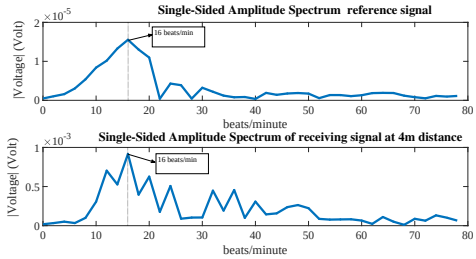

Figure 4.9: Receiving signals in frequency domain.

The SNR of the breathing signal was calculated by the mean value of the signal in the following range: (center frequency − 4 beats) to (center frequency + 4 beats), over the mean value of the remaining signal from 5 to 40 beats/min [26]. The breathing rate of the person was measured at four positions (1, 2, 3, and 4 m). The SNR of the system at each distance was calculated by the mean values of the SNR in each window. Figure 4.10 shows that the measured result was in line with the theoretical analysis in the case of the Nakagami-2 model. In this

situation, the fading parameter was 2, corresponding with the LOS connection between the radar system and the human body. Figure 4.11 presents the detection capability of the system in the time domain.

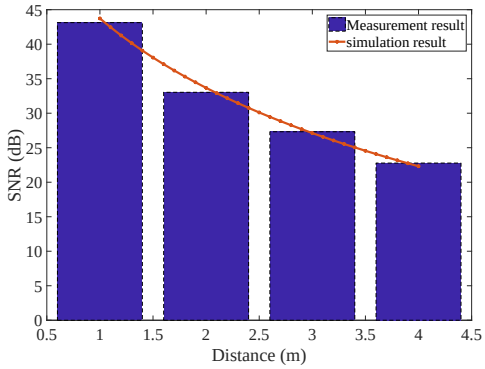

Figure 4.10: Signal-to-noise ratio (SNR) of the system.

In Figure 4.11, the detection capabilities of the system at four distances are presented. When the detection capability equalled 1, the radar system could detect the breathing rate of a human. As can be seen in Figure 4.11, at most time points, the measured result matched with the simulation outcome. However, when the object was closer to the radar system, the detection capability was higher and the false detection in the measured result was distributed over a period of time. For example, at a distance of 3 m, the false detections occurred at around 100 and 150 seconds, while the simulation showed that the false detection occurred randomly at different time points. This phenomenon could be explained by, for some duration in the laboratory environment, the noise level increasing significantly and negatively affecting the radar system; the simulation result, however, followed the statistical distribution—the errors occurred randomly at different time points.

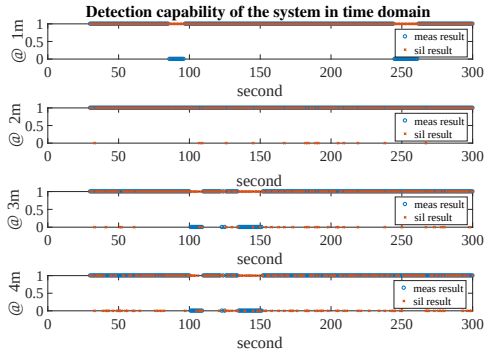

Figure 4.11: Detection capability of the system in time domain.

The detection probability of the system is shown in Figure 4.12. At distances of 2 and 3 m, the measurement results were close to those of the theoretical model, while at a distance of 1 m, the detection probability was higher than that of the simulation result; the opposite result at a distance of 4 m was found. These differences may have appeared because the measuring time was not long enough. However, the theoretical detection probability model is a good reference to evaluate the performance of the radar sensor system in the long term.

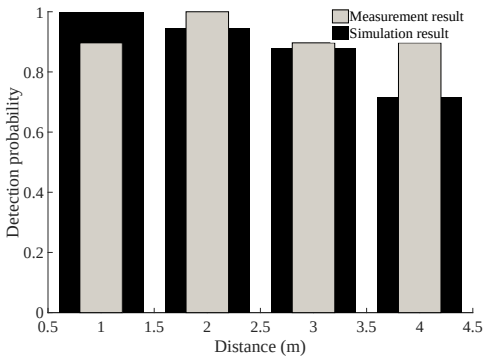

Figure 4.12: Detection probability of the system at different distances.

4.7 Conclusion

In this chapter, the SNR and the detection probability of the vital-sign-detecting radar sensor system have been considered and simulated. The measured result of the SNR was close to the theoretical calculation. This theoretical model is

a basis for hardware development. The designer could optimize their design by choosing different parameters, such as leakage noise, phase noise, and so on, to obtain a high value of the SNR. In addition, on the basis of different types of noise, the detection probability has also been investigated in terms of simulation and analysis. The simulation followed the analytical models. When the system operated at close distances, the phase noise was relatively high and caused a false alarm problem. The threshold power of the receiver's filter affected the alarm/-detection probabilities. This value should be enhanced to improve the detection probability and reduce the false alarm probability. Moreover, the isolation between the transmitting and receiving antennae is an important factor to boost the SNR and detection probability of the system.

4.8 Related Publications

- **Van Nguyen Thi Phuoc**, Liqiong Tang, Subhas Chandra Mukhopadhyay, Duc Minh Nguyen, and Faraz Hasan. "Probabilities of False Alarm for Vital Sign Detection on the Basis of a Doppler Radar System." Sensors 18, no. 3 (2018): 694.

- **Van Nguyen Thi Phuoc**, Liqiong Tang, Nguyen Duc Minh, Faraz Hasan, and Subhas Mukhopadhyay. "Outage Probability of Vital Signs Detecting Radar Sensor System." 12th International Conference on Sensing Technology (ICST), 358-362, 2018

Chapter 5

Nature-inspired Sensor System for Vital Sign Detection

5.1 Introduction

The microbat is an animal, well known for prey detection based on echolocation. It can recognize the difference between its selected prey and other objects [166]. In the microbat, their calls are emitted through their mouth/nostrils. This part plays the role of the transmitter in the radar sensor system. The microbat sends the signal to the environment through its mouth and the echo signal from the surroundings is processed by its two ears. The microbats have a very good hearing system with large ears/pinnae and tragus to limit the receptive field to 30^0 *to* 40^0 [166]. By comparing the emitting signal and received signal (the echo), the bats can locate the exact position of the prey. They can distinguish the difference between the echo from the prey and from other obstacles. Owing to the symmetry of two ears, bats can recognize the direction of the prey by analyzing the sensitivity of the echo from two ears. In comparison with the radar system, two ears of the microbat work as two receivers to detect the exact $3D$ of the chased objects. To detect the prey accurately, microbats emit the signal with a wavelength similar to the length of the object. The transmitting signal could be frequency modulation (FM), continuous frequency (CF), or the combination continuous frequency/frequency modulation (CF/FM) or frequency modulation/-continuous frequency/frequency modulation (FM/CF/FM) pulses.
Beside the type of signals that microbats use to emit to hunt prey, the wavelength of the signal is an important factor. Normally, the wavelength of the signal is

close to the dimension of the prey. This feature should be taken into account when choosing frequency for vital sign detection purposes of the radar sensor system. Microbats also have their own targets for time window and range. For example, the *Noctilio albiventris* bat emits a FM/CF signal with the window 21 ms, the Horsehoe bat *Rhinolophus* uses the combination of FM/CF/FM pulses and $rouxi$ or $Eptesicus\ fuscus$ emits only a FM signal. The time window for them is around 30 ms, giving them the target range of 5 m [166]. Inspired from the natural radar system- microbats, this research proposed that the radar sensor system has one transmitter, and two symmetrical receivers. The system mimics the physical structure of the microbats (see Figure 5.1).

Besides the touching sensing system to detect the human vital signs [167–170]

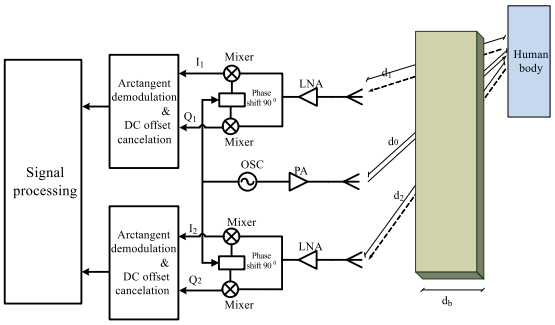

Figure 5.1: System diagram.

or close contactless sensor [171], the microwave Doppler radar sensor system has high potential applications in different areas, including medical appliances, rescue purposes, and smart home. In the early 1970s, the Doppler radar systems were developed to detect the apnoea of a patient [17] and monitor the respiratory rate of infants [31]. The advancement of those systems has been limited by the present technology. The development of semiconductor technology grants more advanced Doppler radar sensor system, enhances medical applications of this sensor. The microwave radar system can also be used to detect breast cancer [172, 173]. In 2016 Stefano Pisa *et al.* summarized the studies of the radar system for medical application [23]. This study highlights the recent work to detect tumors, the heart and respiratory beat of humans at different distances with the different topologies such as continuous wave (CW) radar, ultra wide band (UWB) radar, and frequency modulation continuous wave(FMCW).

Obviously, the vital signs (heart and breathing beats) are very small,with the signal processing part in the Doppler radar sensor system playing an important

role in improving the detected vital sign signal. Jing Li *et al.* have developed a novel signal processing method to extract and classify human vital signs in complicated situations like a human buried under the debris during an earthquake. Some signal processing techniques were used in their proposed method. Firstly, the Curvelet transform was applied to remove the direct wave. The signal is then de-noised by the singular value decomposition (SVD) tool. The last step was to characterize signals by the Hilber-Huang Transform (HHT) and two-dimensional fast Fourier transform ($2-D\ FFT$). Their method was then applied to the UWB radar system and showed promising results. Detecting the human vital signs in the shortest time is another challenge for researchers. The reference [174] proposed a novel method, namely, stepwise atomic norm minimization ($StANM$). Their innovative approach produced accurate vital signs with a small data volume. Recently, Faheem Khan and Sung Ho Cho proposed a new algorithm for detecting vital signs under stationary and non-stationary humans [175]. They compared their method with the conventional filter based harmonic reduction. Their proposed algorithm introduced more stable results in detecting the human vital signs than the conventional filter based method.

When it comes to hardware development, there have been many attempts to improve the performance of radar systems in human vital sign detection [2, 3, 7–9, 24, 116, 152, 153, 176]. Authors in [8] and [9] have developed a microwave life-detection system for finding survivors under natural hazards like earthquakes. Both systems had a similar hardware structure, but the latter [9] concentrated on the elimination of different types of noise including clutter noise and the noise from the environment. The size and the energy consumption of the Doppler radar for vital sign detection can be reduced significantly by Silicon technology. For example, reference [153] produced a 0.25 chip μm silicon $CMOS$ technology operating at 1.6 and 2.4 GHz frequencies. Their system can detect the breathing rate at a distance of 50 cm. The detection range was then increased to 75 cm by a low-power $65-nm\ CMOS$ designed by Shao-Ting Tseng *et al.* [116]. By applying different techniques such as DC offset calibration [176], low-power IF [152], and RF interference rejection [7], the performance of the life-detection radar sensor system has enhanced rapidly. As mentioned in [7], their system can detect the breathing rate at a distance of nine metres.

Most of the previous vital sign detection radar sensor systems consisted of one

transmitter and one receiver. Those systems did not show the capability to detect the direction of alive humans. On the contrary, this work proposes a new Doppler radar sensor system which is inspired from the microbat to improve the directional ability. Moreover, the error probability of the system is investigated and compared with the conventional one transceiver system. The measurement in the system level is set up to validate the performance of the proposed system diagram.

5.2 System Model

5.2.1 Theoretical model

The block diagram of the proposed vital sign detection radar sensor system is shown in Figure 5.1. The system consists of one transmitter, two receivers, arctangent demodulation modules, and a signal processing block. The signal of the radar system may have to go through an obstacle with the thickness of d_b. As mentioned in the Introduction, there are different types of signals which can be used in this system. This work considers the transmitting signal as a continuous wave (CW). The system consists of two symmetrical receivers and a transmitter in the centre. Assuming that the initial phase of the transmitting signal is zero, then the transmitting signal (Y_T) in time domain (t) can be written as [177]:

$$Y_T = \sqrt{2P_T}\cos\left(2\pi ft + \phi\left(t\right)\right) \tag{5.1}$$

where f is the carrier frequency, P_T is the power of the transmitter, and $\phi\left(t\right)$ is the phase noise. The human is assumed to be stable. When the transmitting signal reaches the human body it will be modulated by the chest displacement before reflecting back to the receivers of the radar system. The received signals at receivers can be expressed as:

$$\begin{aligned} Y_{R_i} \quad &= A_{R_i} cos\left(2\pi ft - \tfrac{2\pi}{\lambda}\left(2x\left(t\right) + d_i + d_0 - 2d_b + 2d_b\sqrt{\epsilon_b}\right)\right. \\ &\left. +\phi\left(t - \tfrac{d_0}{c} - \tfrac{d_i}{c}\right)\right) + \sum N(t) \end{aligned} \tag{5.2}$$

where Y_{R_i} are the receiving signals at the receiver order i $(i = 1, 2)$, $x\left(t\right)$ is the chest movement, d_0 and d_i are the distances from the transmitting antenna and receiving antennae to the human body respectively. ϵ_b is the permittivity of the

obstacle, λ is the wavelength of transmitting signal, c is the velocity of light, and $\sum N(t)$ is the total of noises.
Similar to the work in [177] and [159], amplitudes (A_{R_i}) of receiving signal are given as:

$$A_{R_i} = \sqrt{\frac{2P_T G_T G_{Ri} \sigma_a \rho_{ri} \rho_t r \lambda^2 |g_0|^2 |g_i|^2}{(4\pi)^3 d_0^\alpha d_i^\alpha}} \tag{5.3}$$

where G_T, G_{Ri} are the gain of transmitting and receiving antennae respectively. ρ_t and ρ_{ri} are the radiated efficiencies of transmitting and receiving antennae. r is the reflection coefficient of the human body, σ_a is the radar cross section (RCS) of the human's chest, and α is the path loss. The channel coefficients from the transmitter to the human body and from the human body to the receivers are g_0 and g_i. The receiving signal Y_{R_i} are then down-converted to the intermediate frequency by mixers. In each receiver, two mixers are used to get in-phase (I) and quadrature (Q) signals. Those signals then go through the band pass filter (BPF) with the bandwidth $[f_{min}, f_{max}]$. The baseband I signal $B_{Ii}(t)$ at the receiver i $(i = 1, 2)$ can be formulated as:

$$B_{Ii}(t) = A_{Ri}\sqrt{G_{RXi}} cos\left[\theta_{0i} + \frac{4\pi x\,(t)}{\lambda} + \triangle\phi_s\,(t)\right] + \sum N_b\,(t) \tag{5.4}$$

where $\theta_0 i$ is the constant phase shift due to the distance and obstacle between the radar system and the human body. $\triangle\phi_s\,(t)$ is the residual phase noise of reflected vital sign signals. $\sum N_b\,(t)$ is the total noise at the base band. There are three main sources of noise, which are residual phase noise, Additive White Gaussian Noise (AWGN) and $1/f$ noise. Similarly, Q signal at the baseband is expressed as:

$$B_{Qi}(t) = A_{Ri}\sqrt{G_{RXi}} sin\left[\theta_{0i} + \frac{4\pi x\,(t)}{\lambda} + \triangle\phi_s\,(t)\right] + \sum N_b\,(t) \tag{5.5}$$

From Equations (5.4) and (5.5), the vital signal can be extracted by arctangent demodulation. The outputs $\triangle\theta_i$ $(i = 1, 2)$ of arctangent and DC cancelation

block can be expressed as follows

$$\begin{aligned}\triangle\theta_i &= arctan\left[\frac{B_{Qi}(t)}{B_{Ii}(t)}\right] \approx arctan\left[\frac{sin\left[\theta_{0i}+\frac{4\pi x(t)}{\lambda}+\triangle\phi_s\left(t\right)\right]}{cos\left[\theta_{0i}+\frac{4\pi x(t)}{\lambda}+\triangle\phi_s\left(t\right)\right]}\right] \\ &\approx arctan\left[\theta_{0i}+\frac{4\pi x\left(t\right)}{\lambda}+\triangle\phi_s\left(t\right)\right]\end{aligned} \tag{5.6}$$

The final outputs are corresponding directly with the human chest displacement.

$$\triangle\theta_i \approx \frac{4\pi x\left(t\right)}{\lambda} \tag{5.7}$$

5.2.2 System Signal to Noise Ratio (SNR)

In this section, the SNR in the receivers are developed. Three main noise sources are considered: residual phase noise, AWGN, and baseband Flicker noise $(1/f)$.

Power of signal

The received signal power at the mixer of receivers i can be estimated based on the amplitude of signal at the radio frequency (RF) band, the gain of receivers, the wavelength of transmitting wave, and the displacement of the human's chest $x(t)$ [177] [153].

$$S_{Bi} = A_{Ri}G_{RXi}\left(\frac{4\pi x(t)}{\lambda}\right)^2 \tag{5.8}$$

By replacing the value of A_{Ri} in the Equation (5.3) into Equation (5.8) the baseband signal power can be achieved as:

$$S_{Bi} = \frac{P_T G_T G_{Ri}\sigma_a\rho_{ri}\rho_t r|g_0|^2|g_i|^2 G_{RXi}\overline{x(t)^2}}{2\pi d_0^{\alpha} d_i^{\alpha}} \tag{5.9}$$

Residual phase noise

The residual phase noise consists of the phase noise of the receiving signal, clutter signal and the antennae leakage between the transmitting antenna and receiving antenna. The total power of residual phase noise (N_{Si}) of receiver i can be

calculated as [177]:

$$N_{Si} = \frac{P_T G_T G_{Ri} \rho_{ri} \rho_t r |g_0|^2 |g_i|^2 G_{RXi} S_\phi(1) ln(\frac{f_{max}}{f_{min}})}{2\pi f^2 d_0^{\alpha-1} d_i^{\alpha-1}} (\sigma_a + \sigma_c) \\ + 8\eta_{leak} P_T G_{RXi} \pi^2 S_\phi(1) \triangle t_l^2 ln(\frac{f_{max}}{f_{min}}) \tag{5.10}$$

where σ_c is the RCS of the remainder parts of the human body, $S_\phi(1)$ is the phase noise at 1 H_z, and the leakage between transmitting and receiving antenna is η_{leak}.

AWGN

AWGN is the primary RF noise source at the input of the receiver. This type of noise is converted to the baseband noise with power N_{Wi} as follows [159]:

$$N_{Wi} = 8 G_{RXi} (NF_i)(kTB) \tag{5.11}$$

where NF_i is the noise figure of the receiver i, k is Boltzman's constant, T is the absolute temperature, and B is the bandwidth.

$1/f$ noise

The passive mixer and the baseband filtering can be chosen to minimize the $1/f$ noise, and the power of $1/f$ noise ($N_{1/fi}$) at the baseband of the receiver i can be calculated by the noise power in a 1-Hz bandwidth centered at 1 Hz.

$$N_{1/fi} = P_{1/fi}(1) ln(\frac{f_{max}}{f_{min}}) \tag{5.12}$$

SNR

From Equations (5.8-5.12) the SNR_i in each receiver i can be expressed as:

$$SNR_i = \frac{S_{Bi}}{N_{1/fi} + N_{Wi} + N_{Si}} \tag{5.13}$$

5.3 Error detection probability

Evaluating the detection performance of a vital sign detection radar system is critical. In this section, the analytical model of error probability of the proposed system is derived. The error probability of the proposed system is then compared with the conventional model (1 transmitter and 1 receiver). The error probability of the system is developed based on the false alarm and miss detection in each receiver.

False alarm detection probability

A false alarm appears in the radar system when the total noise power is larger than the threshold power (T) which is set to detect the present target [178] [5]. The false alarm probability (P_{FAi}) in the receiver i of the proposed system is written as follows:

$$P_{FAi} = Pr\left\{N_{Si} + N_{Wi} + N_{1/fi} > T\right\} \tag{5.14}$$

Bring in the values of noise power in the Equations (5.10- 5.12), the P_{FAi} can be rewritten as:

$$\begin{aligned} P_{FAi} = & \\ & Pr\left\{\frac{P_T G_T G_{Ri} \rho_{ri} \rho_t r |g_0|^2 |g_i|^2 G_{RXi} S_\phi(1) ln(\frac{f_{max}}{f_{min}})}{2\pi f^2 d_0^{\alpha-1} d_i^{\alpha-1}}\right. \\ & \times (\sigma_a + \sigma_c) > T - 8\eta_{leak} P_T G_{RXi} \pi^2 S_\phi(1) \triangle t_l^2 ln(\frac{f_{max}}{f_{min}}) \\ & \left. -8G_{RXi}(NF_i)(kTB) - P_{1/fi}(1) ln(\frac{f_{max}}{f_{min}})\right\} \end{aligned} \tag{5.15}$$

By setting $C_i = \frac{P_T G_T G_{Ri} \rho_{ri} \rho_t r G_{RXi} S_\phi(1) ln(\frac{f_{max}}{f_{min}})}{2\pi f^2 d_0^{\alpha-1} d_i^{\alpha-1}} (\sigma_a + \sigma_c)$,
$M_i = T - 8\eta_{leak} P_T G_{RXi} \pi^2 S_\phi(1) \triangle t_l^2 ln(\frac{f_{max}}{f_{min}}) - 8G_{RXi}(NF_i)(kTB) - P_{1/fi}(1) ln(\frac{f_{max}}{f_{min}})$,
the false alarm probability is given as:

$$\begin{aligned} P_{FAi} &= Pr\left\{C_i |g_0|^2 |g_1|^2 > M_i\right\} \\ &= 1 - Pr\left\{|g_0|^2 |g_1|^2 \leq \frac{M_i}{C_i}\right\} \end{aligned} \tag{5.16}$$

There are various channel models for links from the transmitter to the human and from the human position to the receiver, such as Rayleigh, Nakagami-m, Rice, log-normal and so on. In this work, the log-normal model is utilized because of its simplicity and it is close to the empirical results [5, 179]. In the Equation (5.16), $|g_0|^2$ and $|g_i|^2$ are two independent log-normal variables with the mean values μ_0 μ_i and variances ν_0^2 ν_i^2, respectively. Their product is a log-normal distribution [180] with the mean value of μ_T and variance ν_T^2.

$$\mu_T = \frac{\mu_0^2}{\sqrt{\mu_0^2 + \nu_0^2}} + \frac{\mu_i^2}{\sqrt{\mu_i^2 + \nu_i^2}} + \sqrt{\frac{\nu_0^2}{\mu_0^2} + 1} + \sqrt{\frac{\nu_i^2}{\mu_i^2} + 1} \tag{5.17}$$

$$\nu_T^2 = \left(\frac{\mu_0^4}{\mu_0^2 + \nu_0^2} + \frac{\mu_i^4}{\mu_i^2 + \nu_i^2}\right)\left(\frac{\nu_0^4}{\mu_0^4} + \frac{\nu_i^4}{\mu_i^4} + \frac{\nu_0^2}{\mu_0^2} + \frac{\nu_i^2}{\mu_i^2}\right) \tag{5.18}$$

The detailed calculation for the mean μ_T and variance ν_T^2 is presented as follows:

The mean and variance of the product of two independent log-normal distributed variables $|g_0|^2$ and $|g_i|^2$

$|g_0|^2$ and $|g_i|^2$ are two log-normal distributed independent variables, $|g_0|^2 \sim LN\left[\mu_0, \nu_0^2\right]$ and $|g_i|^2 \sim LN\left[\mu_i, \nu_i^2\right]$. The product (Z) of $|g_0|^2$ and $|g_0|^2$ can be written as

$$Z = |g_0|^2 |g_0|^2 = e^x e^y \tag{5.19}$$

where x and y are two normal-distributed random variable with the mean values m_x m_y and variances V_x and V_y respectively, $x \sim N\left[m_x, V_x^2\right]$, $y \sim N\left[m_y, V_y^2\right]$.

$$\begin{aligned} m_x &= \ln\left(\frac{\mu_0^2}{\sqrt{\mu_0^2 + \nu_0^2}}\right) \\ m_y &= \ln\left(\frac{\mu_i^2}{\sqrt{\mu_i^2 + \nu_i^2}}\right) \end{aligned} \tag{5.20}$$

$$V_x = \sqrt{\ln\left(\frac{\nu_0^2}{\mu_0^2}+1\right)} \tag{5.21}$$
$$V_y = \sqrt{\ln\left(\frac{\nu_i^2}{\mu_i^2}+1\right)}$$

By applying the result in [181] the mean and variance of Z can be written as:

$$mean(Z) = \exp(m_x + m_y + \frac{1}{2}V_x^2 + \frac{1}{2}V_y^2) \tag{5.22}$$

$$variance(Z) = \exp\left(2m_x + 2m_y\right)\left(\exp\left(2V_x^2 + 2V_y^2\right) - exp\left(V_x^2 + V_y^2\right)\right) \tag{5.23}$$

Replacing the values of m_x, m_y, V_x, and V_y in the Equations (5.21)-(5.22) $mean(Z)$ and $variance(Z)$ are given as

$$mean(Z) = \frac{\mu_0^2}{\sqrt{\mu_0^2+\nu_0^2}} + \frac{\mu_i^2}{\sqrt{\mu_i^2+\nu_i^2}} + \sqrt{\frac{\nu_0^2}{\mu_0^2}+1} + \sqrt{\frac{\nu_i^2}{\mu_i^2}+1} \tag{5.24}$$

$$variance(Z) = \left(\frac{\mu_0^4}{\mu_0^2+\nu_0^2} + \frac{\mu_i^4}{\mu_i^2+\nu_i^2}\right) \tag{5.25}$$
$$\times \left(\left(\frac{\nu_0^2}{\mu_0^2}+1\right)^2 + \left(\frac{\nu_i^2}{\mu_i^2}+1\right)^2 - \left(\frac{\nu_0^2}{\mu_0^2}+1\right) - \left(\frac{\nu_i^2}{\mu_i^2}+1\right)\right) \tag{5.26}$$
$$= \left(\frac{\mu_0^4}{\mu_0^2+\nu_0^2} + \frac{\mu_i^4}{\mu_i^2+\nu_i^2}\right)\left(\frac{\nu_0^4}{\mu_0^4} + \frac{\nu_i^4}{\mu_i^4} + \frac{\nu_0^2}{\mu_0^2} + \frac{\nu_i^2}{\mu_i^2}\right)$$

Based on the probability theory, P_{FAi} can be calculated as.

$$P_{FAi} = 1 - \int_0^{\frac{M_i}{C_i}} \frac{1}{x\sqrt{2\pi\nu_T^2}} \exp\left(-\frac{\left(\ln x - \mu_T\right)^2}{2\nu_T^2)}\right) dx \tag{5.27}$$
$$= \frac{1}{2}\left[1 - erf\left(\frac{\ln M_i - \ln C_i - \mu_T}{\sqrt{2\nu_T^2}}\right)\right]$$

Miss detection probability

Miss detection occurs when the target is presented but the total receiving power signal (including noises) is lower than the threshold power (T) [5]. The miss detection (P_{Mi}) at the receiver i is defined as:

$$\begin{aligned} P_{Mi} &= Pr\left\{S_{Bi} + N_{1/fi} + N_{Wi} + N_{Si} < T\right\} \\ &= Pr\left\{|g_0|^2|g_i|^2(D_i + C_i) < M_i\right\} \\ &= Pr\left\{|g_0|^2|g_i|^2 < \frac{M_i}{(D_i + C_i)}\right\} \end{aligned} \tag{5.28}$$

where $D_i = \frac{P_T G_T G_{Ri} \sigma_a \rho_{ri} \rho_t r G_{RXi} \overline{x(t)^2}}{2\pi d_0^\alpha d_i^\alpha}$, C_i and M_i are stated in the Equation (5.16). Similar to the Equation (5.27), the miss detection probability can be expressed as:

$$P_{Mi} = \frac{1}{2}\left(1 + erf\left(\frac{\ln \frac{M_i}{D_i + C_i} - \mu_T}{\sqrt{2\nu_T^2}}\right)\right) \tag{5.29}$$

Error detection probability

The average error probability (P_{ei}) of the receiver i ($i = 1, 2$) is given by [182]

$$\begin{aligned} P_{ei} &= \frac{1}{2}P_{FAi} + \frac{1}{2}P_{Mi} \\ &= \frac{1}{2} + \frac{1}{4}\left(erf\frac{\ln \frac{M_i}{D_i + C_i} - \mu_T}{\sqrt{2\nu_T^2}} - erf\frac{\ln M_i - \ln C_i - \mu_T}{\sqrt{2\nu_T^2}}\right) \end{aligned} \tag{5.30}$$

The proposed system consists of two independent receivers. The error detection of the system arises when both receivers have an error problem. Therefore, the system error detection (P_E) probability can be evaluated as

$$P_E = P_{e1}P_{e2} \tag{5.31}$$

5.4 Simulation Results

In this section, the simulation results of the SNR and the error probability of the system are presented. The error probability of the conventional system (one

transmitter and one receiver) is compared with the proposed system. The parameters used for the simulation are shown in Table 5.1. In Figure 5.2, the

Table 5.1: Parameters of the proposed system used for simulation

Description	Value
Transmitting signal power (P_T)	0 dBm
Receiving antennae gain (G_{Ri})	8 dBi
Gain of the receiver i (G_{RXi})	10 dB
Absolute noise temperature (T)	300
Received noise figure (NF_i)	6 dB
Radiated efficiency of transmitting antenna (ρ_t)	0.8
Radiated efficiency of receiving antenna (ρ_{ri})	0.8
RCS of the human's chest (σ_a)	500 mm^2
Reflection coefficient of the human body (r)	0.5
$1/f$ power noise power at 1 Hz ($P_{1/f_i}(1)$)	-130 dBm/Hz
Phase noise at 1 Hz intercept ($S_{\triangle}(1)$)	60 dB/Hz
Antennae leakage (η_{leak})	-33 dB
High frequency (f_max)	5 Hz
Low frequency (f_min)	0.1 Hz
Time delay ($\triangle t_l^2$)	5 ns
Path loss (α)	2
Mean value of $\|g_0\|^2$ (μ_0)	2
Standard deviation $\|g_0\|^2$ (ν_0)	1.97
Mean value of channel gain $\|g_i\|^2$ (μ_i)	2
Standard deviation of $\|g_i\|^2$ (ν_i)	1.97

domination of different types of noise to the overall noise is displayed. When the human is close to the radar system, the phase noise dominates the SNR of the system. The influence of the antennae leakage to SNR of the system is essential when the distance increases. The additive noise is quite low and does not cause many problems to the overall SNR. From the simulation, the results suggest that the SNR can be maximized if the phase noise and the antennae leakage can be minimized. Based on the power of different types of noise, the error probability (P_e) of the proposed system is derived and compared with the error probability (P_{e1}) of the conventional system in Figure 5.3.

The first point to note from Figure 5.3 is that the analysis results match per-

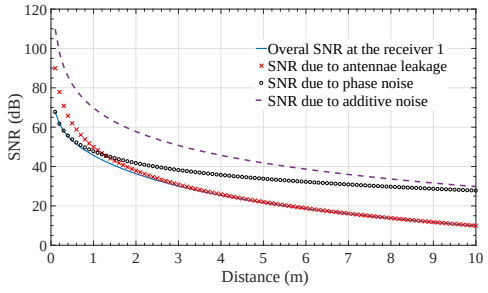

Figure 5.2: SNR at the receiver 1

fectly with the simulation results. Moreover, due to the contribution of phase noise at a very close distance, the error probability (P_{e1}) of the conventional system (1 transmitter and 1 receiver) is quite high, and the error probability of the

system starts to increase dramatically from the distance of 4 m. On the other hand, the error probability of the proposed system is lower than the conventional one, for example, at the distance 0.2 m, $P_{e1} = 0.3$ while $P_e = 0.1$. In addition, the range with zero error probability of the proposed system is also expanded from $[1m - 4m]$ to $[0.5m - 5.5m]$. Moreover, when the distance increases, the error probability of the proposed system also increases gradually and its' slope is lower than the conventional one. For instance, at the distance of 10 m, the error probability of the proposed system is around 0.16, while the error probability of the conventional system is above 0.4.

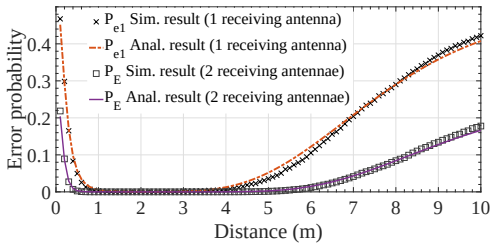

Figure 5.3: Error probability of the system when the distance changes

5.5 Measurement Result

In this section, the measurement results of error probability, directional capability and human breathing rate based on the proposed system are presented. The Microwave Network Analyser $N5244A\ PNA$ -43.5 GHz played a role of radar system, and three antennae (one transmitting and two receiving) were connected to three ports of this device. The measurement setup is shown in Figure 5.5. The object (measured person) was required to sit in front of the antenna system. Five people aged from 21 to 27 participated in the experiment. Each person's breathing rate was measured at the distances of $1m$, $2m$, $3m$, $4m$ and $5m$ right in the middle of the antenna system. A similar process was repeated at the 15 *degrees* acute angle from the middle of the antenna system. A five-lead connected wearable sensor system ($Shimmer\ 3\ ECG/EMG$) was used to collect the reference signal. For each position, the object was measured in five minutes continuously in the electronics lab. The transmitting power was $-10\ dBm$ and the operating frequency was 1.6 GHz. The size of antenna system is 30 cm $\times$ 33

cm, the position of the transmitting antenna was in the middle of two symmetrical receiving antennae, and the leakage between antennae was $-26\ dB$. The schematic diagram of the experimental setup is displayed in Figure 5.4.

The receiving signal at $5m$ distance is presented in Figure 5.6. In comparison

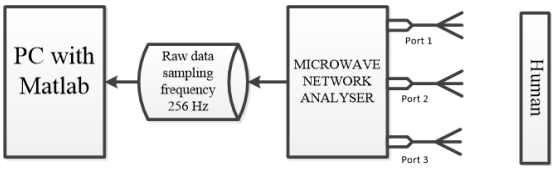

Figure 5.4: Experimental setup

Figure 5.5: Measurement setup for proposed system

with the reference signal, the measured signal is quite noisy. This signal is then put through the Fast Fourier Transform (FFT) to find the spectrum [183]. The receiving signal in frequency domain is shown in Figure 5.7. From this Figure, the peak of spectrum is considered as the breathing rate. In this case, the reference breathing rate is equal to the measured respiratory rate, but the receiving signal consists of some noises at different frequencies.

The breathing rate of a person was measured in five minutes continuously with a sampling frequency of 256. The total samples in five minutes are 76800. The DC value in the raw data is then removed before being applied FFT with the window size of 30 seconds, the window moves forward every second. In each FFT window, the frequency at the peak of spectrum is considered as the breathing rate. The power of signal is calculated as the mean power value for the range ± 4 beats around the central frequency. The power outside this range from 5 to 40 beats/minute is considered as the noise power [26]. The error detection occurs when the power of the receiving signal is lower than the predefined threshold

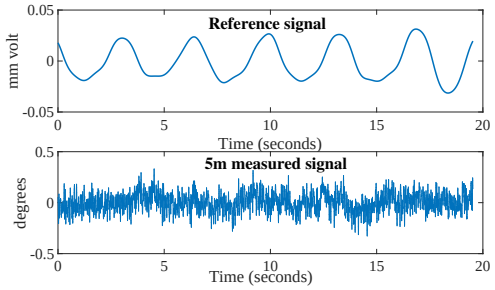

Figure 5.6: Receiving signal in time domain

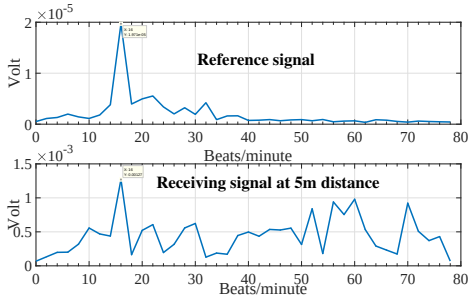

Figure 5.7: Receiving signal in frequency domain

value. In this work, the threshold value was $-90\ dBm$, and this value is the mean of the measured noise of the radar system. The error detection probability is determined as the proportion of error detection over the total trials. The error probability of the system is presented in Figure 5.8. At different distances the measurement results match properly with the developed theoretical model. This measured result suggests that the derived theoretical model is reliable and can be used as a good reference for hardware development.

As mentioned in the Introduction section, the proposed system is auspicious

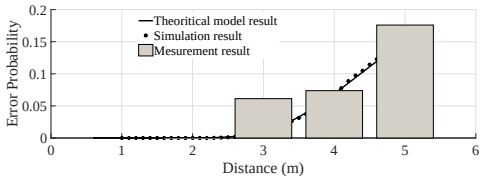

Figure 5.8: Error probability of system vs distance of measurement

for $3D$ detection. In this work, the initial measurement was set up to check this capability. The measured objects were on the left side of the antenna system, and the angle (person-transmitting antennae-middle line) was 15 degrees. The SNR

of breathing rate is estimated based on the spectrum of the receiving signal as in [177]. As can be seen from Figure 5.9, signal on the left side are always larger than the right side. The difference of SNR also increases proportionally with the distance because when the human position is far away from the antenna system, the difference between d_1 and d_2 is expanded. This Figure shows that the person is on the left side of the system at various distances.

The directional detection capability of the system in terms of time at the dis-

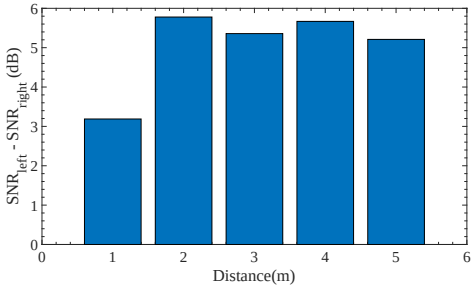

Figure 5.9: $SNR_{left} - SNR_{right}$ at different distances when the object is in the left side

tance of $3m$ is given in Figure. 5.10. Around 90 *percent* of the time, the proposed system gives the correct indicator. At certain times, the indicator was wrong due to the environmental noise. Besides the directional ability, the system also showed high accuracy in detecting the human respiratory rate. The results of the breathing rates measured by the proposed system are displayed in Table 5.2.

The breathing rate measured by the proposed system is the mean values of

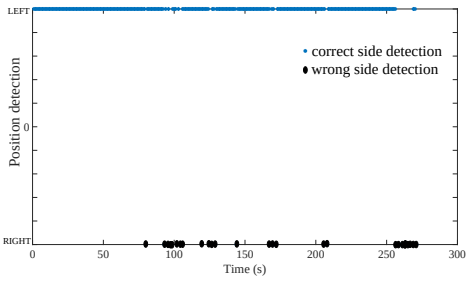

Figure 5.10: Directional detecting capability of the proposed system

respiratory rate at receivers 1 and 2. In almost all positions, the proposed system gives a similar result to the reference signal. However, at the distance of 5 m, the difference of the measured breathing rate and the reference value of object 4

is 2.5 beats/minute. This inclined value is due to the weakness of the receiving signal at the longer distance of measurement.

As can be seen from the measurement result for the error detection probability

Table 5.2: Respiratory rates from five objects at different distances

Object	Breathing rate (Beats/Minute)					
	Ref	1m	2m	3m	4m	5m
1	16.4	15.2	16.8	16.7	16.1	16.8
2	14.8	13.8	13.2	12.0	14.6	13.8
3	16.8	15.9	16.6	17.5	16.7	16.0
4	15.6	15.7	15.1	17.5	16.1	18.1
5	12.0	12.2	13.8	12.7	12.6	13.8

and the breathing rate, the deviation is not a significant issue. Obviously, the remote radar sensor system may be affected by other wireless equipment in the electronics laboratory. Moreover, during the measurement process, the object could move to create the cluster noise.

5.6 Conclusion

This chapter has proposed a novel vital sign detecting radar sensor system inspired by the microbat. In this research, the theoretical model to calculate the error probability of the system is investigated. The analytical result of error probability has a good match with the simulation and measurement results. The error detection of the proposed system is lower than the conventional one. Moreover, due to two symmetrical receivers, the directional ability of proposed system was enhanced significantly. The measurement was set up to validate with 90 percent reliability. If the antennae system is enlarged with the advanced technique, the $3D$ directional detection capability of this system will be improved and show a better result.

Moreover, the proposed system needs two symmetrical receivers; this means that the components in the radar circuit increase. However, with the development of the current integrated circuit, the cost and the entire size of the system could be reduced. This makes a portable system possible.

5.7 Related Publications

- **Van Nguyen Thi Phuoc** Liqiong Tang, Faraz Hasan, Nguyen Duc Minh, and Subhas Mukhopadhyay. "Nature-inspired sensor system for vital signs detection." Sensors and Actuators A: Physical 281 (2018): 76-83.

Chapter 6

Smart Radar Sensing System for Vital Signs Detection

6.1 Introduction

We propose a model to the end users in order to make a more intelligent radar sensor system. This model is to be built, based on an AI technique. The specific machine learning model for the breathing sign detection radar is utilized to categorise different subjects such as humans or pets under the debris, or to diagnose the respiratory disorder of the end user. Based on the training data set, the proposed system can give the instruction to the radar operator to classify the subjects under the debris in a search and rescue application. For example, when the system detects alive creatures under the debris of a collapsed building, the system should tell us that it is a person or a pet (dog or cat). Since the breathing rate, tidal volume and amplitude of chest wall movements of the pets and human are different, the detected signals from them are also distinctive. If we can collect the data of measured signals from various pets and people by the microwave radar sensor, and using this data to build the machine learning model, this model can then be used to classify detected subjects of the radar sensing system. For the medical application, this smart system can give a warning to a person, such as whether they have a high/low/normal breathing rate. This kind of warning is useful for the person to go further in checking out health problems. Moreover, the model could be extended to diagnose different types of respiratory disorders. For example, a person has a dysrhythmic breathing problem when their respiratory system has irregular rhythm of rate and amplitude. This type

of breathing problem relates to a brain stem issue. The rhythm and amplitude of this type changes with the time, and it is difficult to estimate the breathing rate of a person who has this breathing disorder [184] (see Figure 6.1).

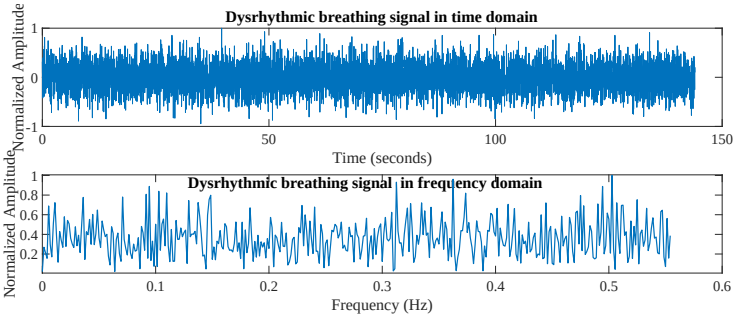

Figure 6.1: Simulation for Dysthymic respiration.

An other example of breathing disorder is the central apnoea respiration. This problem occurs when a person's breathing stops for a duration lasting from 10 to 30 seconds. The apnoea duration corresponds with the time that the brain stops sending signals to the breathing control muscles [185].

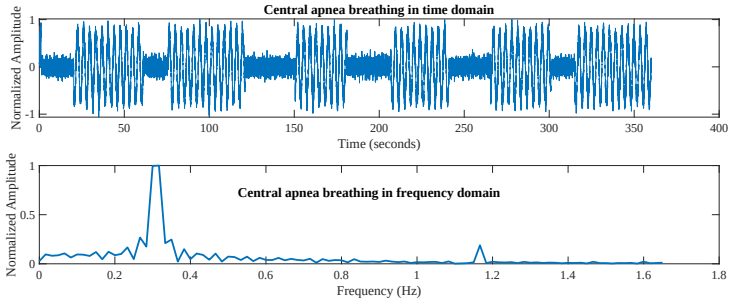

Figure 6.2: Simulation of Cheyne Stokes Respiration signal.

The two above examples show that the breathing disorder can not be classified by simply estimating the peak frequency spectrum of the receiving signal. Therefore, the machine learning technique should be used to diagnose breathing disorder issues.

The measured data was also used to build the machine learning based model. The breathing rate measured by the CW radar sensor system is compared to the reference measurement by the five-point touching Shimmer sensor. The results of the breathing rate are compatible. Two main time-frequency (TF) extraction feature methods, short time Fourier transform ($STFT$) and continuous Wavelet transform (CWT) were implemented in the proposed system. Under these

extraction techniques, some classification approaches were employed and have shown high accuracy in categorizing the respiratory types. The research shows the possibility of building an Artificial Intelligence (AI) module for a non-contact radar sensor system to make this system more intelligent.
In addition, this work collected data from 31 people when they perform high/low/normal respiration by CW radar sensor. This work assists further research in the field by publishing our data set.

This chapter is structured as follows. Section 6.2 presents the discussion on the proposed system diagram and functions of each module in the proposed system. Section 6.3 describes the experimental setup and Section 6.4 discusses the measurement results. The final Section 6.5 is the conclusion and consideration for future work.

6.2 Proposed system

The block diagram of the proposed system is presented in Figure 6.3. The system consists of three main modules, a radar sensor, an AI module, and a personal device.

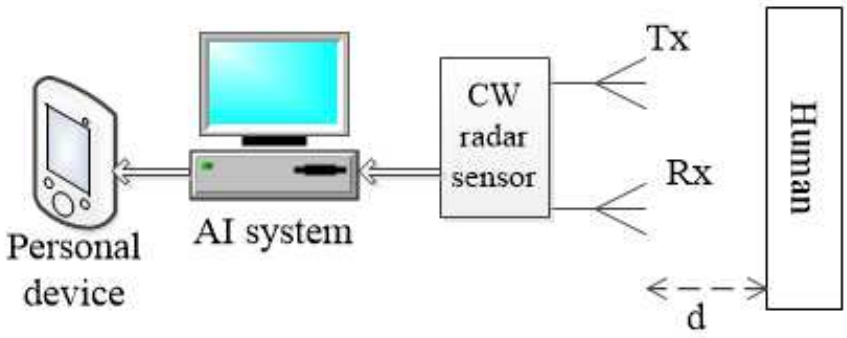

Figure 6.3: Block diagram.

A continuous wave (CW) is sent toward the human position through the transmitting antenna of CW radar sensor, and the reflected signal from the human chest goes back to the sensor system through receiving antenna. The arctangent modulation is applied to the sensor system; the output signal at the sensor is proportional with the chest displacement. This signal is sampled at a frequency of 256 Hz before being sent to the AI module. At the AI module, signals are

processed to provide useful information to the person through their personal devices.

6.2.1 Operating principle of CW radar sensor

In the CW radar sensor, a single sin wave is transmitted toward the human position. Neglecting the amplitude, the transmitting signal is given as follows [93, 177].

$$Y_T = \cos\left(2\pi f t + \phi\left(t\right)\right) \tag{6.1}$$

where f is the operating frequency of the radar sensor and $\phi\left(t\right)$ is the phase noise. When the transmitting signal reaches the chest of the person, this signal is then modulated by the displacement of the chest and reflects back to the receiving antenna of the sensor [93, 177]. The receiving signal can be written as:

$$Y_R = \cos\left(2\pi f t - \frac{4\pi d}{\lambda} - \frac{4\pi x\left(t\right)}{\lambda} + \phi\left(t - \frac{2d}{c}\right)\right) \tag{6.2}$$

where d is the distance from the sensor to the human location, λ is the wavelength of the sending signal, $x(t)$ is the chest displacement of the human, and c is the speed of light. The receiving signal is then down-converted into the intermediate frequency (IF) signal. Two mixers are used in the down-converter to get in phase (I) and quadrature (Q)signals. At the base band, I and Q discrete signals are given as [152]:

$$B_I(n) \approx \cos\left[\theta + \frac{4\pi x(n)}{\lambda} + \triangle\phi(n)\right] \tag{6.3}$$

$$B_Q(n) \approx \sin\left[\theta + \frac{4\pi x(n)}{\lambda} + \triangle\phi(n)\right] \tag{6.4}$$

where θ is the constant phase shift due to the distance from the human position to the radar, and $\triangle\phi(t)$ is the phase noise. At the receiver, the arctangent demodulation is applied and the output signal of the radar sensor system can be

calculated as:

$$\psi(n) = arctan\left[\frac{B_Q(n)}{B_I(n)}\right] = \theta + \frac{4\pi x(n)}{\lambda} + \triangle\phi(n) \tag{6.5}$$

The output signal $\psi(n)$ of the radar sensor is processed by the AI module to extract the breathing rate and classify the breathing problems.

6.2.2 AI module

The framework of the AI module is presented in Figure 6.4. The AI module consists of three main steps; data processing, feature extraction and classification. All the steps are implemented using Matlab $R2018b$ on Intel Core $i5$, 16 GB memory configuration hardware running with Windows 7 OS. In this module, the raw signal is reprocessed to remove the DC value and be filtered by an appropriate filter. The next step is to extract features based on a time frequency technique. Finally, data is classified into different categories.

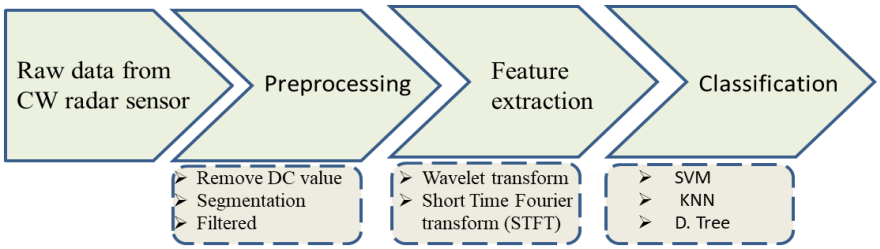

Figure 6.4: The steps implemented in the AI module.

Data preprocessing and feature extraction

After visual inspection, five-minute data (i.e. 76800 data points because of 256 sampling rate) was extracted from the six-minute recording. Firstly, the DC value of the measured data was removed. The data was further bandpass filtered by [0.1 to 2] Hz Butterworth. We used the two most popular time-frequency (TF) methods [186]: short time Fourier transform ($STFT$) and continuous wavelet transform (CWT) to extract time-varying spectral properties of the breathing signal as our features for the classification model. TF features are used for classification and also give an instantaneous breathing rate of the user in the time domain.

In the $STFT$, first, a whole signal is divided into portions of equal window size, then the Fourier Transform (FT) is applied to each portion, respectively [187]. The $STFT$ $F(\tau, \omega)$ of the measured signal $\psi(t)$ is defined as:

$$F(\tau, \omega) = \sum_{-\infty}^{\infty} \psi(n) h(n - \tau) e^{-j\omega n} \tag{6.6}$$

where $h(n-\tau)$ is a window function. Based on Equation. 6.6, the power spectrum density (PSD) of the signal is determined as:

$$P_S(\tau, \omega) = |F(\tau, \omega)|^2 \tag{6.7}$$

The above equations interpret that FT of each portion is captured with the window moving along the time axis of the entire signal. Correspondingly, $P_S(\tau, \omega)$ is a two-dimensional vector that stores power of the input signal according to time and frequency. PSD of $STFT$ has a fixed resolution, because the width of window function is constant for all segments of input signal. Specifically, a wider window function brings a better frequency resolution, while a better time resolution [187] is brought about by the narrow size of window function.
CWT is an alternative feature extraction method to get TF of a signal. This signal processing technique is able to build up time-frequency representation of an input signal with a great time and frequency resolution [188]. The CWT coefficients $W_{\Psi(a,b)}$ signal $\psi(n)$ at a scale $a(a > 0)$ and position b are expressed as follows [188].

$$W_{\Psi(a,b)} = \sum_{-\infty}^{\infty} \psi(n) \overline{\Psi}(\frac{n - b}{a}) \tag{6.8}$$

$\Psi(n)$ is a basis or mother wavelet with zero average and $\overline{\Psi}(n)$ is its conjugated values. PSD $P_{w(a,b)}$ of the CWT can be defined as follows:

$$P_{W(a,b)} = |W_{\Psi(a,b)}|^2 \tag{6.9}$$

Classification

The output signal of the feature extraction block goes through the classification to separate the signal into different categories. There are many classifying techniques

used to allocate signals into various groups. The most popular classifying techniques are support vector network (SVM), artificial neural network (ANN), hidden Markow models (HMM), fuzzy logic (FL), linear discriminant(LN), decision tree ($DTree$), Bayesian classifier (BC) and K- nearest neighbor (KNN) [189]. In these, SVM is kernel-based access and quite popular for non-linear data [189]. KNN is primarily acknowledged for the pattern-recognition approach [190]. Therefore, in this study SVM , $DTree$ and KNN are employed to classify the breathing patterns of people.

SVM

Support Vector Machines (SVM) is a supervised machine learning algorithm which is used for both regression and classification problems. The main concept of SVM is to find the optimum decision boundary to separate two classes [191]. This decision boundary (hyperplane) maximizes the margin between different classes. In SVM, support vectors are the data points nearest to the hyperplane that help in obtaining the optimal position of the hyperplane. The hyperplane, margin support vectors for classification problems are demonstrated in Figure 6.5. In this Figure, two features are chosen to apply the SVM algorithm. The problem to separate different classes becomes finding an optimized hyperplane. The hyperplane decision function for the binary problem is:

$$f(x) = sign\left(\sum_{i=1}^{N} \alpha_i y_i K(x_i, x) + b\right) \tag{6.10}$$

where α represents Lagrange multipliers and is given as $0 \leq \alpha^i \leq C$ and $i = 1, 2, \ldots N$, C is a penalty parameter, which regulates the trade-off between the imposed margins and allows training error. The Kernel function is represented as $K(x_i, x)$ and x_i are the support vectors. Multi-class SVM can be generated using binary $SVMs$.

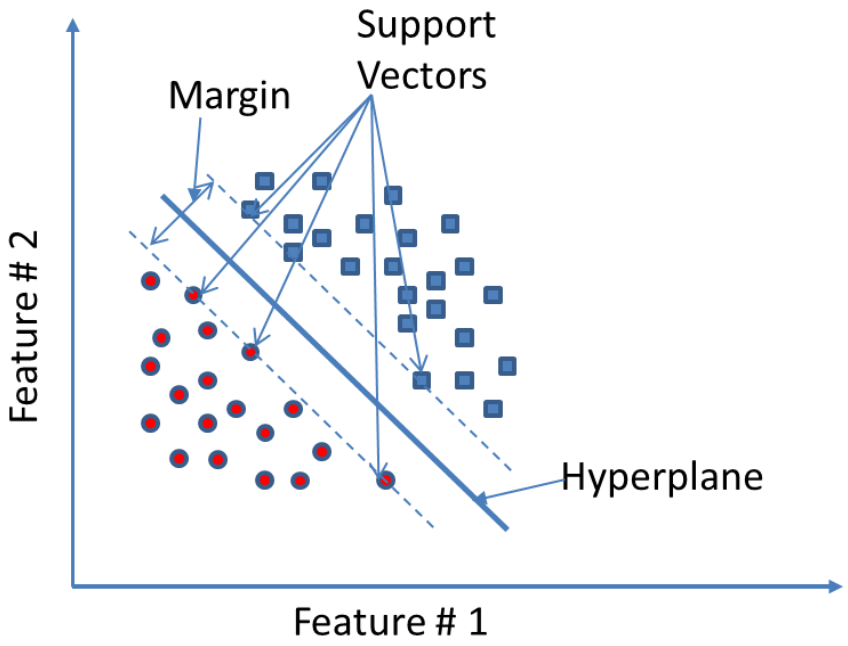

Figure 6.5: Linear Support Vector illustration.

Decision Trees

Similar to $SVMs$, decision tree (DT) is one of the vigorous algorithms. DTs have a tree-like structure, and are simple and close to the logical thinking of humans. The DT is a crucial element of Random Forest - the most compelling algorithm nowadays [192,193]. The DT model consists of different types of nodes as mentioned in Figure 6.6. The starting node is called a root node, the internal nodes are the set of nodes $Child1$ to $Child3$, and the bottom nodes are class labels or leaf nodes. [194]

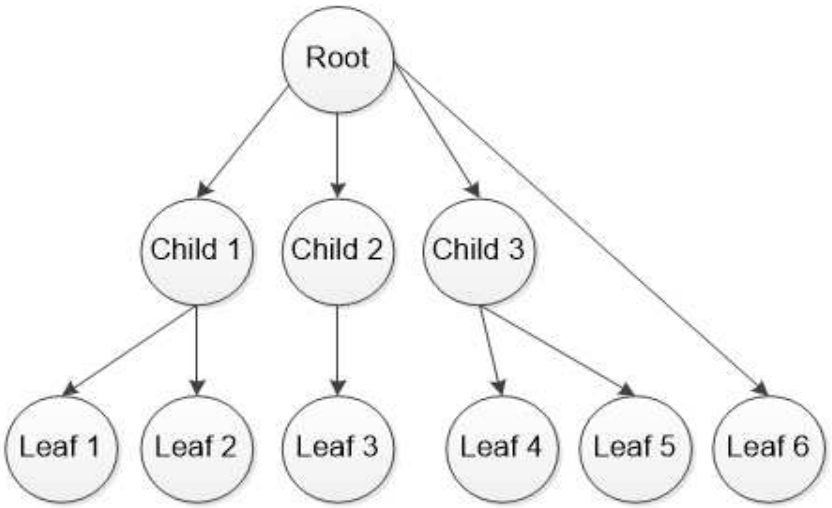

Figure 6.6: Decision tree model.

In the *DT* model, to construct a reasonably good tree and to define attributes for each root note, *Grini impurity* (cost function) is given as follows: [194].

$$G(i) = 1 - \sum_{k=1}^{n} p_{i,k}^2 \tag{6.11}$$

where $G(i)$ is the *Gini* score of i^{th} node, $p_{i,k}$ is the ratio between class k instances and training instance of i^{th} node. In the two-class problem, the best separation is achieved when $G(i) = 0$.
Another alternative to determine the cost function is to calculate the Entropy ($H(i)$) as follows.

$$H(i) = -\sum_{k=1}^{n} p_{i,k} log\left(p_{i,k}\right); p_{i,k} \neq 0 \tag{6.12}$$

Both methods, Entropy and Gini impurity tend to point to analogous trees. There is not a big variation between the two methods.

K Nearest Neighbours

K nearest neighbours (KNN) is called a lazy algorithm that stores all established vectors and class label correlated with each vector and classifies new cases based on a similarity measurement. This algorithm is widely used for practical problems [195, 196] KNN was first mentioned in the 1970s as a non-parametric

method [197]. In the KNN, the input vector is classified/ predicted by determining the similarity between this vector and the training instances (neighbors). Distance functions are used to measure the similarity between a new sample and the training data set. Those distance functions are Euclidean, Manhattan, Minkowski, and Hamming distances. The data used in KNN should be re-scaled before processing to achieve a high accuracy result [198].

6.3 Experiment and Data

6.3.1 Measurement set up

The laboratory equipment - $N5244A\ PNA-X$ Microwave Network Analyzer plays the role of the radar sensor system. The internal transmitter and receiver of $N5244A\ PNA-X$ are utilized for this application. Two antennae are connected to two ports (transmitting and receiving ports) of $N5244A\ PNA-X$. A volunteer is sat in front of antennae as shown in Figure 6.7, and the distance from the antennae to the human position is 1 m. The transmitting power is $-8\ dBm$, the operating frequency is 1.6 Ghz, and the sampling frequency is 256 Hz. The same sampling frequency is set for a reference five-point touching Shimmer sensor.

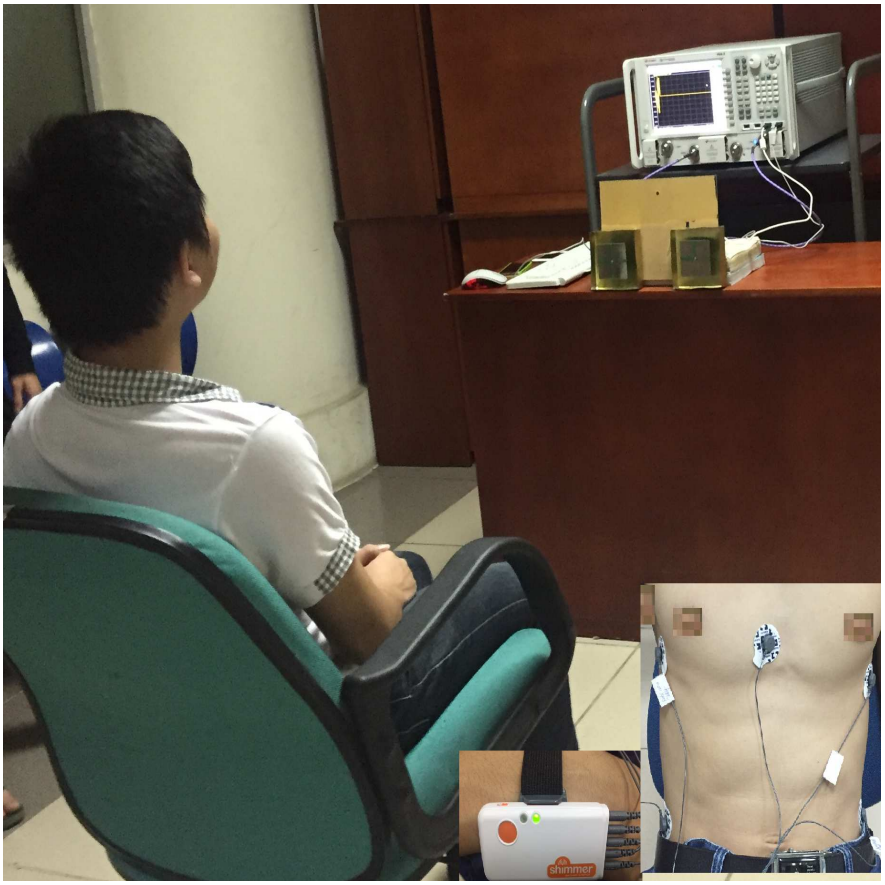

Figure 6.7: Measurement setup.

Thirty-one able-bodied participants (20 males and 11 females, average age 25.4 years) completed three sessions, each of which was approximately six minutes in duration. All sessions occurred on the same day with three-minute break between each session. The procedure of each session is described in Figure 6.8. In the first session, participants were asked to breathe at their normal rate (i.e. 0.2 to 0.33 Hz) while, in the remaining two sessions, they were instructed to breathe at high ($>$ 0.33 Hz) and low ($<$ 0.2 Hz) rates respectively. Participants provided written informed consent, and the experiment was approved by the Head of School of Electronics and Telecommunications, Hanoi University of Science and Technology, Vietnam. The breathing rate of four random participants was measured by the touching-probe Shimmer sensor at the same time they were measured by the remote sensor system in order to check the accuracy of the remote sensor. The remaining participants were only measured by the remote sensor to make sure that the natural signals were obtained.

Table 6.1: Data set description

Data Sets No. of Subjects: 31 | Sampling Freq.: 256 Hz	Segmentation (in seconds)	Trial Size	Train	Test
Data set I	60	15360	348	117
Data set II	30	7680	697	233
Data set III	15	3840	1395	465

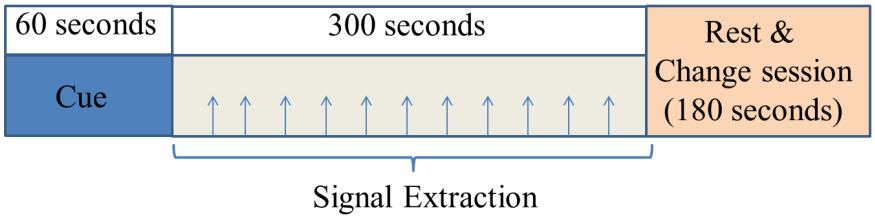

Figure 6.8: Experimental procedure.

6.3.2 Data sets

The five-minute data for each individual per session was slotted into one minute, thirty seconds, and fifteen seconds' recording. Based on the different segment lengths, three data sets were built as shown in Table 6.1.

- Data set I: From each individual, we obtained 15 data samples belonging to low, high and normal (5 for each category). Each data sample has 15360 data points(60 sec × 256 Hz sampling rate). The total data set size is 465 × 15360 having 465 cases of all categories.

- Data set II: Similarly, 30 data samples were obtained from each person and the total data set size is 930 × 7680

- Data set III: This data set has the highest time resolution (15 seconds in each segmentation). The size of data set III is 1860 × 3840

Data sets are labelled into three categories; low, high and normal. Spectral density in the frequency band from 0.1 Hz to 2 Hz is used as a feature. After feature extraction, the data set was divided into two sets; 75% for the training set and 25% for the testing set. The size of train and testing sets in each data set

is displayed in Table 6.1. To avoid the over-fitting problem, 10 × 10 ×fold cross validation is used for the classification of the training set.

6.3.3 Evaluation Metric

In this chapter, classification accuracy is utilized as an evaluation metric. The accuracy in the three classifications case can be determined as follows.

$$Accuracy = \frac{P_{cr}}{P_{cr} + P_{Icr}} \tag{6.13}$$

where

- P_{cr} is the number of correct predictions.
- P_{Icr} is the number of incorrect predictions.

6.4 Results

The measured breathing rate by remote radar sensor system in time and frequency domains are displayed in Figures 6.9 and 6.10.

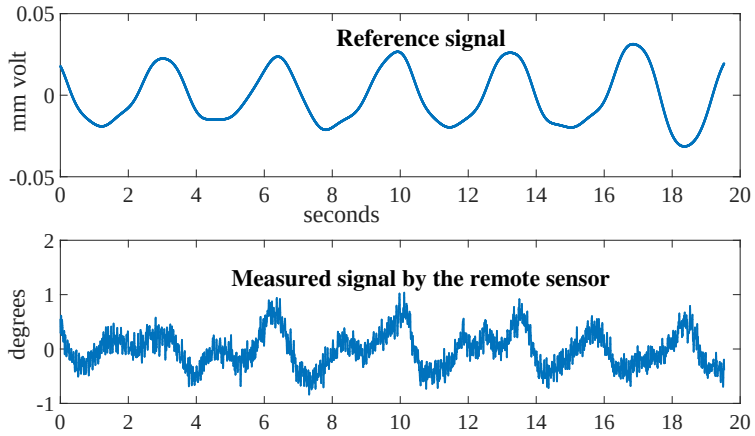

Figure 6.9: Measured signal in the time domain.

The frequency domain signal can give the respiratory rate of a person. In this approach, the corresponding frequency at the highest absolute magnitude of spectrum is considered as breathing frequency. This technique is called peak

position detection [26]. The absolute spectrum of each segment signal can be calculated by $STFT$ as shown in Figure 6.10. Figure 6.10 gives the breathing rate of 18 $beats/minute$, and the signal from the remote sensor is coincided with the signal from the reference touching sensor. From both Figures, one can see that the remote sensor system introduces more noise than the touching sensors, however, the remote radar sensor gives a similar result of breathing rate to the five-probes Shimmer sensor.

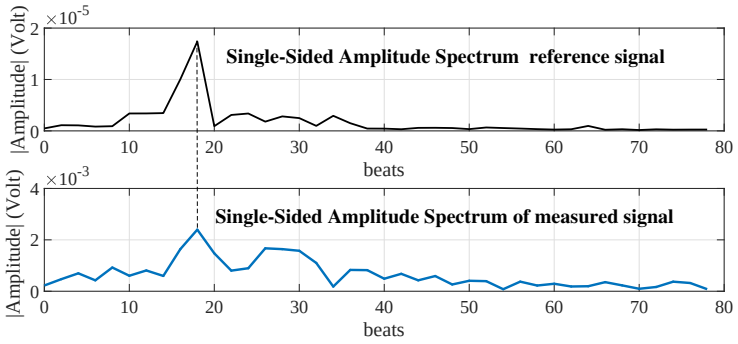

Figure 6.10: Measured signal in the frequency domain.

Figure 6.11 and Figure 6.12 illustrate the relationship between two features in the feature vector of data set I and data set III. It is clear that in data set I (Figure 6.11), three classes are separated properly, while in Figure 6.12, there are some overlaps between classes. This phenomenon comes from time resolutions of each data set. Data set I has the lowest time resolution (60 seconds segmentation), while data set III has the highest time resolution (15 seconds segmentation). The increase in time resolution is compensated to the accuracy of the system as mentioned in Table 6.2.

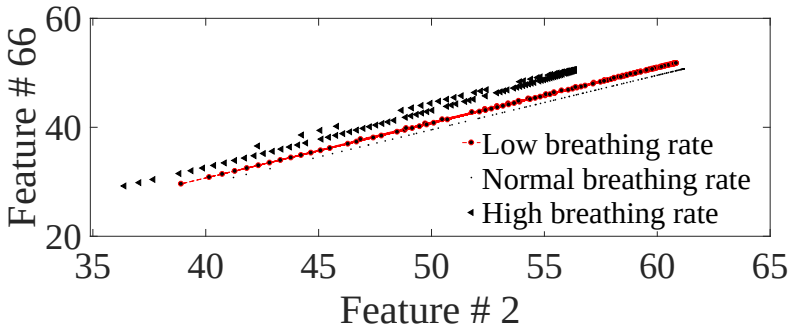

Figure 6.11: Relationship between Feature # 2 and Feature # 66 in the Data set I.

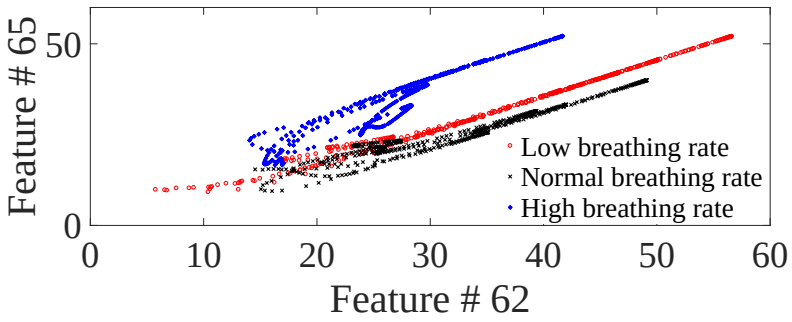

Figure 6.12: Relationship between Feature # 62 and Feature # 65 in the Data set III.

Table 6.2 compares the accuracy of the proposed remote sensing system in classifying breathing rate problems into three categories (fast, normal, and slow) with the conventional method (based on peak position detection). Different classifying techniques are applied and results are shown in Table 6.2. From this Table, we can see that data set I gives very good results (above 99%) with KNN and SVM classifiers. $DTree$ introduces lower accuracy (around 95%). In data set II, the segmentation is half of the segmentation in the data set I. However, SVM and KNN classifications still produce similar results under CWT and $STFT$ extraction methods. For $DTree$ with CWT extraction method, the accuracy is similar to the data set I. There is a large reduction (14%) in accuracy under the $DTree$ classifier when the features are selected by $STFT$. When the segmentation of data reduce to the size of 15 *seconds* in the data set III, the accuracies of the system under the SVM and KNN techniques do not change much. Notwithstanding, $DTree$ delivers a significant reduction of accuracy. In $DTree$ method,

Table 6.2: Classification accuracy of proposed system

Data Sets	Extraction methods	Classification Methods			Conventional method (Peak position detection)
		SVM	DTree	KNN	
Data set I	STFT	99.89 %	94.51%	99.11 %	64.09 %
	CWT	99.95 %	96.58 %	99.88 %	
Data set II	STFT	99.85 %	80.68 %	99.15 %	63.76 %
	CWT	99.87 %	96.13 %	99.45 %	
Data set III	STFT	99.12 %	75.81 %	99.11 %	35.48 %
	CWT	99.67 %	83.01 %	99.55 %	

under $STFT$ and CWT extraction methods, the accuracies of test set III are 75.81% and 83.01% respectively.

The conventional method introduces lower results; for data sets I and II the results are comparable with the recent work of [199]. The accuracy of modified $STFT$ in reference [199] is around 80%, while our results are around 64%. There are several reasons behind that difference. Firstly, the transmitting power of their system was eight times our transmitting power. Their system operated at much higher frequency (around 24 GHz) while the proposed system operated at 1.6 Ghz. The result is that our system is fifteen times less sensitive than their system .

The length of segmentation has a significant effect on the accuracy of breathing rate estimation when the peak position detection method is used. As discussed in the reference [136], this method introduces high accuracy when the segmentation is larger than 60 seconds. Data set III introduces very low accuracy (35.48%) because of the low frequency resolution. In this data set, the 15 seconds' observation window corresponds to $1/15 = 0.067$ Hz frequency resolution. This frequency resolution equals to 4.02 beats/min, therefore, the peak position detection method shows a very poor result (just 35.48%).

Generally, the CWT extraction technique presents better results than $STFT$. The performance of machine learning based methods outperforms the conventional method (peak position detection) because our proposed system used the whole CWT or $STFT$ vector (including peak spectral and its harmonics) for classification, while the conventional method used only one element (peak spectral). The result in Table 6.2 gives a good suggestion for further applications.

6.5 Conclusion

From the measured results, the remote radar sensor system can accurately capture breathing rate, and is more comfortable for the measured person. The remote radar sensor system has high potential to inform the user of their instantaneous breathing rate by the TF feature extraction techniques. Moreover, the AI technique that was applied on the data obtained by the remote radar sensor system, makes this system smarter and gives useful information to the end user. The aim of the proposed machine learning model is to classify the measured signal from the radar sensor system in different categories. This model is then integrated with the radar sensor system and gives a warning to people, for instance, if their breathing rate is abnormal. The system can also be used to predict the type of alive subject under the debris for the search and rescue application. The accuracy of our proposed approach is far greater than the conventional method. The SVM and KNN classifications gave good accuracy on three types of data sets of 31 measured people. The measurement results suggest an alternative high accuracy method in three category types of breathing rate.

6.6 Related Publications

- **Van Nguyen Thi Phuoc**, Liqiong Tang, A. Singh, N. D. Minh, S. C. Mukhopadhyay and S. F. Hasan, "Self-Identification Respiratory Disorder Based on Continuous Wave Radar Sensor System," in IEEE Access, vol. 7, pp. 40019-40026, 2019. doi: 10.1109/ACCESS.2019.2906885

- **Van Nguyen Thi Phuoc**, Liqiong Tang, Faraz Hasan, Subhas Mukhopadhyay, and Nguyen Duc Minh. "Combination of Artificial Intelligence and Continuous Wave Radar Sensor in diagnosing breathing disorder" The 4th International Conference on Research in Intelligent and Computing in Engineering (RICE 2019) - Accepted paper

Chapter 7

Conclusion and Future work

7.1 Conclusion

The microwave Doppler radar sensing systems, which have been developed, show strong potential in search and rescue and health care applications. Such systems can detect live people under debris and obtain health information (breathing rate) without contact and predict the location of the person. The experimental study on the operating of radar sensing systems at different frequencies, is presented in Chapter 3. The extra wide band $3D$ structured antenna system was investigated with high gain, small size and low cost. The performance of the antennae was tested through $LOS/NLOS$ transmission links. The antenna system can operate in five range frequency from L to the X band width.

The lack of a theoretical model to predict the accuracy of the radar sensing system leads the authors to the work presented in Chapter 4. In Chapter 4, the false alarm/ detection probabilities of the radar sensing system in different environments are derived. Moreover, the SNR value is also considered carefully in the various situations from LOS to $NLOS$ transmission links. The analytical results in this chapter are close to the simulation and measurement results. This means that the proposed mathematical model is profitable for the hardware development of a radar sensing system. Based on this model, the performance in distance, power, and accuracy of this system can be estimated in advance.

When it comes to the hardware development, inspired from the Micro Bat animal, the nature-inspired radar sensing system is proposed in Chapter 5. This radar sensing system mimics the physical structure of the Micro Bat animal which uses an echo to detect the position of its prey. In comparison with the conventional

system, the inspired radar sensor system performs better in locating the position of subjects in $3D$ space, improving detection probability and reducing the null point problem. The theoretical model to determine the error probability of the system was investigated and matched properly with the simulation and measurement results. This work took a critical step to develop a sensing system to detect a human position in $3D$ space.
Chapter 6 presents the novel combination between the radar sensing system and AI block to enable the classifying function of the radar sensing system. The machine learning models were built on different algorithms such as SVM , KNN, and DT. The accuracy of the proposed model was higher than 90 %. The Doppler sensor system can be combined with machine learning/deep learning techniques to enable more capabilities such as early warning of a heart attack or asthma attack in medical applications. In addition, smarter and adaptive sensing systems for search and rescue purposes can be built based on the AI technique. The data can be collected when the radar sensor operates in different environments. This data can then be used to build an AI model to enhance the accuracy and reduce the calibration complexity which leads to a smarter radar sensing system.

7.2 Future studies

It is obvious that there are many challenges in the research field of microwave radar sensing system. The research presented in this thesis considered hardware, theoretical models, system configurations and more improvements are expected. For instance, the signal processing techniques/algorithms could be enhanced to improve the quality of the radar sensor. First, the null point problem in the microwave radar sensor appears when the phase shift due to the distance from the target to the sensor is an even multiple of $\frac{\pi}{2}$. In this case, the received signal approximates to zero value. To overcome this problem, the I/Q microwave radar is a good solution. Droitcour *et al.* [153] showed in their work that the null points' issue can be reduced by using a quadrature receiver in the radar sensor system. Moreover, other methods that can be used to dispense with this problem are double-sideband transmission [200], complex signal demodulation [127] and arctangent demodulation [201].

Secondly, the vital sign detection quality of microwave radar sensor is affected negatively by the motion artifacts' noise or multiple subjects' interferences. Multiple-input, multiple-output ($MIMO$) or single-input, multiple-output ($SIMO$) methods could be used to alleviate these problems [72,202,203]. The $SIMO/MIMO$ antenna system was combined with the $SIMO/MIMO$ signal processing technique to differentiate between multiple subjects. Moreover, the random body movement and motion artifacts' noises can be cancelled by using two detecting transceivers [203]. To enhance the detecting multiple targets and the sensitivity of the radar sensing system, a hybrid system which has two operation modes was proposed. In this system, the Doppler mode was used to detect the vital signs and $FMCW$ mode took the responsibility to find the absolute range of the target [204]. The shadowing effect is another large issue of the radar sensing system. This problem was diminished by applying a proposed algorithm based on Wavelet Entropy in bistatic UWB radar [205]. In this algorithm, the difference between periodic respiration and random noise and the entropy of human target are utilized to detect two people at the same time. One person is closer to the radar and one person is in the shadowing region. This method can be combined with the multiple channel system to detect multiple subjects under the debris/-ruble at the same time.

It is obvious that a more efficient signal processing method is needed, which can reduce multiple types of noises and interferences of the radar sensing system. Moreover, this technique should concentrate on the real time application.

As mentioned in Chapter 6, the radar sensing system can combine with the AI technique to make it more intelligent. To make that combined system works perfectly, the radar sensor, itself, should be optimized in the hardware development. There is a design hardware in the reference [206] which tried to reduce the interferences that the microwave search and rescue sensor have to deal with. Those interferences are caused by an operator around the radar antennae and the noise in the shadowing area. Reference [206] introduced a dual-frequency CW radar operated at 5.57 and 35 GHz frequencies to suppress the interference from the radar operator. The radar sensor consists of two transceivers operated at two frequencies at the same time. The lower frequency signal of this system can penetrate through rubble while the higher frequency signal cannot go too far and is used to detect the breathing rate of the operator. The receiving signal at the higher frequency transceiver was used to remove the operator interference in the

lower frequency part. This system showed high potential application for search and rescue purposes because it showed efficient suppression of interference from the operator. However, there are several issues that the hardware developer for the radar sensing system still have to deal with simultaneously, such as antennae isolation, power consumption, detecting distance, and cost. Further investigation could be carried out on optimizing the hardware structure of the radar sensor. New algorithms based on machine learning/deep learning is a direction to process signals of the system more precisely, and in a shorter time.

References

[1] X. Liang, J. Deng, H. Zhang, and T. A. Gulliver, "Ultra-wideband impulse radar through-wall detection of vital signs," *Scientific reports*, vol. 8, no. 1, p. 13367, 2018.

[2] T.-M. Shen, T.-Y. J. Kao, T.-Y. Huang, J. Tu, J. Lin, and R.-B. Wu, "Antenna design of 60-ghz micro-radar system-in-package for noncontact vital sign detection," *IEEE Antennas and Wireless Propagation Letters*, vol. 11, pp. 1702–1705, 2012.

[3] M. S. Rabbani and H. Ghafouri-Shiraz, "Ultra-wide patch antenna array design at 60 ghz band for remote vital sign monitoring with doppler radar principle," *Journal of Infrared, Millimeter, and Terahertz Waves*, vol. 38, no. 5, pp. 548–566, 2017.

[4] J. Yan, H. Hong, H. Zhao, Y. Li, C. Gu, and X. Zhu, "Through-wall multiple targets vital signs tracking based on vmd algorithm," *Sensors*, vol. 16, no. 8, p. 1293, 2016.

[5] J. W. Choi, S. S. Nam, and S. H. Cho, "Multi-human detection algorithm based on an impulse radio ultra-wideband radar system," *IEEE Access*, vol. 4, pp. 10 300–10 309, 2016.

[6] C. Li, X. Yu, D. Li, L. Ran, and J. Lin, "Software configurable 5.8 ghz radar sensor receiver chip in 0.13 μm cmos for non-contact vital sign detection," in *2009 IEEE Radio Frequency Integrated Circuits Symposium*. IEEE, 2009, pp. 97–100.

[7] N. Andersen, K. Granhaug, J. A. Michaelsen, S. Bagga, H. A. Hjortland, M. R. Knutsen, T. S. Lande, and D. T. Wisland, "A 118-mw 23.3-gs/s dual-band 7.3-ghz and 8.7-ghz impulse-based direct rf sampling radar soc in

55-nm cmos," in *2017 IEEE International Solid-State Circuits Conference (ISSCC)*. IEEE, 2017, pp. 138–139.

[8] K.-M. Chen, Y. Huang, J. Zhang, and A. Norman, "Microwave life-detection systems for searching human subjects under earthquake rubble or behind barrier," *IEEE transactions on biomedical engineering*, vol. 47, no. 1, pp. 105–114, 2000.

[9] F. JalaliBidgoli, S. Moghadami, and S. Ardalan, "A compact portable microwave life-detection device for finding survivors," *IEEE Embedded Systems Letters*, vol. 8, no. 1, pp. 10–13, 2016.

[10] M. Ritchie, M. Ash, Q. Chen, and K. Chetty, "Through wall radar classification of human micro-doppler using singular value decomposition analysis," *Sensors*, vol. 16, no. 9, p. 1401, 2016.

[11] G. Wang, C. Gu, T. Inoue, and C. Li, "A hybrid fmcw-interferometry radar for indoor precise positioning and versatile life activity monitoring," *IEEE Transactions on Microwave Theory and Techniques*, vol. 62, no. 11, pp. 2812–2822, 2014.

[12] L. Liu and S. Liu, "Remote detection of human vital sign with stepped-frequency continuous wave radar," *IEEE journal of selected topics in applied earth observations and remote sensing*, vol. 7, no. 3, pp. 775–782, 2014.

[13] C.-P. Lai and R. M. Narayanan, "Ultrawideband random noise radar design for through-wall surveillance," *IEEE Transactions on Aerospace and Electronic Systems*, vol. 46, no. 4, pp. 1716–1730, 2010.

[14] S. Bisht, S. Saini, V. Prakash, and B. Nautiyal, "Study the various feeding techniques of microstrip antenna using design and simulation using cst microwave studio," *International Journal of Emerging Technology and Advanced Engineering*, vol. 4, no. 9, 2014.

[15] A. B. Constantine *et al.*, "Antenna theory: analysis and design," *MICROSTRIP ANTENNAS, third edition, John wiley & sons*, pp. 64–65, 2005.

[16] N. T. P. Van, L. Tang, N. D. Minh, F. Hasan, and S. Mukhopadhyay, "Extra wide band 3d patch antennae system design for remote vital sign

doppler radar sensor detection," in *2017 Eleventh International Conference on Sensing Technology (ICST)*. IEEE, 2017, pp. 1–5.

[17] C. Caro and J. Bloice, "Contactless apnoea detector based on radar," *The Lancet*, vol. 298, no. 7731, pp. 959–961, 1971.

[18] T. Kobayashi, Y. Morishita, and H. Yarai, "Detailed crustal deformation and fault rupture of the 2015 gorkha earthquake, nepal, revealed from scansar-based interferograms of alos-2," *Earth, Planets and Space*, vol. 67, no. 1, p. 201, 2015.

[19] F. JalaliBidgoli, S. Moghadami, and S. Ardalan, "A compact portable microwave life-detection device for finding survivors," *IEEE Embedded Systems Letters*, vol. 8, no. 1, pp. 10–13, 2015.

[20] C. Li, F. Chen, F. Qi, M. Liu, Z. Li, F. Liang, X. Jing, G. Lu, and J. Wang, "Searching for survivors through random human-body movement outdoors by continuous-wave radar array," *PloS one*, vol. 11, no. 4, p. e0152201, 2016.

[21] H. Aumann and N. Emanetoglu, "Doppler radar microphone with logarithmic square-law detector," *Electronics Letters*, vol. 52, no. 12, pp. 1061–1063, 2016.

[22] R. M. Narayanan, "Earthquake survivor detection using life signals from radar micro-doppler," in *Proceedings of the 1st International Conference on Wireless Technologies for Humanitarian Relief*. ACM, 2011, pp. 259–264.

[23] S. Pisa, E. Pittella, and E. Piuzzi, "A survey of radar systems for medical applications," *IEEE Aerospace and Electronic Systems Magazine*, vol. 31, no. 11, pp. 64–81, 2016.

[24] H.-C. Kuo, C.-C. Lin, C.-H. Yu, P.-H. Lo, J.-Y. Lyu, C.-C. Chou, and H.-R. Chuang, "A fully integrated 60-ghz cmos direct-conversion doppler radar rf sensor with clutter canceller for single-antenna noncontact human vital-signs detection," *IEEE Transactions on Microwave Theory and Techniques*, vol. 64, no. 4, pp. 1018–1028, 2016.

[25] G. R. Wang, H. G. Han, S. Y. Kim, and T. W. Kim, "Wireless vital sign monitoring using penetrating impulses," *IEEE Microwave and Wireless Components Letters*, 2016.

[26] A. Tariq, "Vital signs monitoring using doppler radar and on-body antennas," Ph.D. dissertation, University of Birmingham, 2013.

[27] R. Y. Moon, R. S. Horne, and F. R. Hauck, "Sudden infant death syndrome," *The Lancet*, vol. 370, no. 9598, pp. 1578–1587, 2007.

[28] C. Will, K. Shi, S. Schellenberger, T. Steigleder, F. Michler, R. Weigel, C. Ostgathe, and A. Koelpin, "Local pulse wave detection using continuous wave radar systems," *IEEE Journal of Electromagnetics, RF and Microwaves in Medicine and Biology*, vol. 1, no. 2, pp. 81–89, 2017.

[29] Z. Park, C. Li, and J. Lin, "A broadband microstrip antenna with improved gain for noncontact vital sign radar detection," *IEEE Antennas and Wireless Propagation Letters*, vol. 8, pp. 939–942, 2009.

[30] J. C. Lin, "Microwave sensing of physiological movement and volume change: A review," *Bioelectromagnetics*, vol. 13, no. 6, pp. 557–565, 1992.

[31] C. Franks, B. Brown, and D. Johnston, "Contactless respiration monitoring of infants," *Medical and biological engineering*, vol. 14, no. 3, pp. 306–312, 1976.

[32] G. S. Kaplan and A. S. Clorfeine, "Respiration monitor," Nov. 23 1976, uS Patent 3,993,995.

[33] J. Y. Lee and J. C. Lin, "A microcprocessor-based noninvasive arterial pulse wave analyzer," *IEEE transactions on biomedical engineering*, no. 6, pp. 451–455, 1985.

[34] M. Nowogrodzki and D. D. Mawhinney, "Dual frequency heart rate monitor utilizing doppler radar," Apr. 30 1985, uS Patent 4,513,748.

[35] G. J. Schmidt, "Method of and apparatus for detecting living bodies," Aug. 4 1998, uS Patent 5,790,032.

[36] J. Geisheimer, "Rvsm [radar vital signs monitor]," *IEEE Potentials*, vol. 17, no. 5, pp. 21–24, 1998.

[37] F. Lemaitre and J.-C. Poussieres, "Method and system for sensing and locating a person, eg under an avalanche," Feb. 29 2000, uS Patent 6,031,482.

[38] S. M. Sharpe, J. Seals, A. H. MacDonald, and S. R. Crowgey, "Non-contact vital signs monitor," Sep. 25 1990, uS Patent 4,958,638.

[39] F. Sterzer, "Apparatus and method for monitoring the waveform of cyclic movement within the thorax of an individual," Nov. 6 1990, uS Patent 4,967,751.

[40] T. E. Mcewan, "Ultra-wideband radar motion sensor," Nov. 1 1994, uS Patent 5,361,070.

[41] D. V. Hablov, O. I. Fisun, L. N. Lupichev, V. V. Osipov, V. A. Schestiperov, and R. Schimko, "Electronic life detection system," Sep. 5 1995, uS Patent 5,448,501.

[42] T. E. McEwan, "Body monitoring and imaging apparatus and method," Nov. 12 1996, uS Patent 5,573,012.

[43] S. Gabriel, R. Lau, and C. Gabriel, "The dielectric properties of biological tissues: Ii. measurements in the frequency range 10 hz to 20 ghz," *Physics in medicine & biology*, vol. 41, no. 11, p. 2251, 1996.

[44] T. P. Dinh, H. Perrault, P. Calabrese, A. Eberhard, and G. Benchetrit, "New statistical method for detection and quantification of respiratory sinus arrhythmia," *IEEE transactions on biomedical engineering*, vol. 46, no. 9, pp. 1161–1165, 1999.

[45] T. E. McEwan, "Differential pulse radar motion sensor," Oct. 12 1999, uS Patent 5,966,090.

[46] H.-N. Teodorescu and D. J. Mlynek, "Respiration and movement monitoring system," Jan. 4 2000, uS Patent 6,011,477.

[47] J. Geisheimer and E. Greneker, "Remote detection of deception using radar vital signs monitor technology," in *Proceedings IEEE 34th Annual 2000 International Carnahan Conference on Security Technology (Cat. No. 00CH37083)*. IEEE, 2000, pp. 170–173.

[48] S. B. Corn, "Sleep apnea detector system," May 16 2000, uS Patent 6,062,216.

[49] A. Droitcour, V. Lubecke, J. Lin, and O. Boric-Lubecke, "A microwave radio for doppler radar sensing of vital signs," in *2001 IEEE MTT-S International Microwave Sympsoium Digest (Cat. No. 01CH37157)*, vol. 1. IEEE, 2001, pp. 175–178.

[50] E. M. Staderini, "Uwb radars in medicine," *IEEE aerospace and electronic systems magazine*, vol. 17, no. 1, pp. 13–18, 2002.

[51] V. Lubecke, O. Boric-Lubecke, and E. Beck, "A compact low-cost add-on module for doppler radar sensing of vital signs using a wireless communications terminal," in *2002 IEEE MTT-S International Microwave Symposium Digest (Cat. No. 02CH37278)*, vol. 3. IEEE, 2002, pp. 1767–1770.

[52] A. D. Droitcour, O. Boric-Lubecke, V. M. Lubecke, and J. Lin, "0.25/spl mu/m cmos and bicmos single-chip direct-conversion doppler radars for remote sensing of vital signs," in *2002 IEEE International Solid-State Circuits Conference. Digest of Technical Papers (Cat. No. 02CH37315)*, vol. 1. IEEE, 2002, pp. 348–349.

[53] Y. Yin, J. Qian, J. Lu, and Y. Huang, "On the operation mechanism of the microwave sensor for measuring human heartbeats and respirations," in *SENSORS, 2003 IEEE*, vol. 1. IEEE, 2003, pp. 565–568.

[54] X. Yun, R. Johnston, and E. Fear, "Radar-based microwave imaging for breast cancer detection: Tumor sensing with cross-polarized reflections," in *IEEE Antennas and Propagation Society Symposium, 2004.*, vol. 3. IEEE, 2004, pp. 2432–2435.

[55] S. Li, "Vehicle occupant detection system and method using radar motion sensor," Jun. 22 2004, uS Patent 6,753,780.

[56] X. Yun, E. C. Fear, and R. H. Johnston, "Compact antenna for radar-based breast cancer detection," *IEEE Transactions on Antennas and Propagation*, vol. 53, no. 8, pp. 2374–2380, 2005.

[57] C. G. Bilich, "Bio-medical sensing using ultra wideband communications and radar technology: A feasibility study," in *Pervasive Health Conference and Workshops, 2006.* IEEE, 2006, pp. 1–9.

[58] C. Li and J. Lin, "Random body movement cancellation in doppler radar vital sign detection," *IEEE Transactions on Microwave Theory and Techniques*, vol. 56, no. 12, pp. 3143–3152, 2008.

[59] E. Cianca and B. Gupta, "Fm-uwb for communications and radar in medical applications," *Wireless Personal Communications*, vol. 51, no. 4, pp. 793–809, 2009.

[60] D. Gibbins, M. Klemm, I. J. Craddock, J. A. Leendertz, A. Preece, and R. Benjamin, "A comparison of a wide-slot and a stacked patch antenna for the purpose of breast cancer detection," *IEEE transactions on antennas and propagation*, vol. 58, no. 3, pp. 665–674, 2010.

[61] D. Zito, D. Pepe, M. Mincica, F. Zito, A. Tognetti, A. Lanatà, and D. De Rossi, "Soc cmos uwb pulse radar sensor for contactless respiratory rate monitoring," *IEEE Transactions on Biomedical Circuits and Systems*, vol. 5, no. 6, pp. 503–510, 2011.

[62] S. M. Salvador, E. C. Fear, M. Okoniewski, and J. R. Matyas, "Exploring joint tissues with microwave imaging," *IEEE Transactions on Microwave Theory and Techniques*, vol. 58, no. 8, pp. 2307–2313, 2010.

[63] X. Li, J. Yan, M. Jalilvand, and T. Zwick, "A compact double-elliptical slot-antenna for medical applications," in *2012 6th European Conference on Antennas and Propagation (EUCAP).* IEEE, 2012, pp. 3677–3680.

[64] G. A. Zito, E. M. Staderini, and S. Pisa, "A twin spiral planar antenna for uwb medical radars," *International Journal of Antennas and Propagation*, vol. 2013, 2013.

[65] C. Li, V. M. Lubecke, O. Boric-Lubecke, and J. Lin, "A review on recent advances in doppler radar sensors for noncontact healthcare monitoring," *IEEE Transactions on microwave theory and techniques*, vol. 61, no. 5, pp. 2046–2060, 2013.

[66] L. E. Solberg, Ø. Aardal, T. Berger, I. Balasingham, E. Fosse, and S.-E. Hamran, "Experimental investigation into radar-based central blood pressure estimation," *IET Radar, Sonar & Navigation*, vol. 9, no. 2, pp. 145–153, 2015.

[67] S. Smith, R. M. Narayanan, and E. Messaris, "Medical radar considerations for detecting and monitoring crohn's disease," in *Radar Sensor Technology XVIII*, vol. 9077. International Society for Optics and Photonics, 2014, p. 90770W.

[68] T. Hall, D. Lie, T. Nguyen, J. Mayeda, P. Lie, J. Lopez, and R. Banister, "Non-contact sensor for long-term continuous vital signs monitoring: A review on intelligent phased-array doppler sensor design," *Sensors*, vol. 17, no. 11, p. 2632, 2017.

[69] S. Thakur, S. Abdul, H.-Y. Chiu, R. Roy, P.-Y. Huang, S. Malwade, A. Nursetyo, and Y.-C. Li, "Artificial-intelligence-based prediction of clinical events among hemodialysis patients using non-contact sensor data," *Sensors*, vol. 18, no. 9, p. 2833, 2018.

[70] J. Park, D. Choi, and S. Park, "Wireless vital signal detection systems and its applications at 1.9 ghz and 10ghz [biomedical applications]," in *IEEE Antennas and Propagation Society International Symposium. Digest. Held in conjunction with: USNC/CNC/URSI North American Radio Sci. Meeting (Cat. No. 03CH37450)*, vol. 4. IEEE, 2003, pp. 747–750.

[71] C. R. Williams and N. E. Yankielun, "Motion detection and alerting system," Mar. 2 2004.

[72] O. Boric-Lubecke, V. M. Lubecke, A. Host-Madsen, D. Samardzija, and K. Cheung, "Doppler radar sensing of multiple subjects in single and multiple antenna systems," in *TELSIKS 2005-2005 uth International Conference on Telecommunication in ModernSatellite, Cable and Broadcasting Services*, vol. 1. IEEE, 2005, pp. 7–11.

[73] E. F. Greneker III, O. D. Asbell, and J. L. Geisheimer, "Radar detection device employing a scanning antenna system," Apr. 3 2007, uS Patent 7,199,749.

[74] N. T. P. Van, L. Tang, A. Singh, N. D. Minh, S. C. Mukhopadhyay, and S. F. Hasan, "Self-identification respiratory disorder based on continuous wave radar sensor system," *IEEE Access*, vol. 7, pp. 40 019–40 026, 2019.

[75] M. Budge and M. Burt, "Range correlation effects on phase and amplitude noise," in *Southeastcon'93, Proceedings., IEEE*. IEEE, 1993, pp. 5–p.

[76] O. V. Rostislavovich and I. G. Saidkhakimovich, "Method for discovering the location of a living object and microwave location device for realizing the same," Mar. 27 2001, uS Patent 6,208,286.

[77] M. Mahler, H.-O. Ruob, and W. Menzel, "Radar sensors to determine position and physiological parameters of a person in a vehicle," in *2002 32nd European Microwave Conference*. IEEE, 2002, pp. 1–4.

[78] Y. M. T. Haj-Yousef, "Method and device for detecting and monitoring concealed bodies and objects," Mar. 19 2002, uS Patent 6,359,597.

[79] A. D. Droitcour, O. Boric-Lubecke, V. M. Lubecke, J. Lin, and G. T. Kovacs, "Range correlation effect on ism band i/q cmos radar for non-contact vital signs sensing," in *IEEE MTT-S International Microwave Symposium Digest, 2003*, vol. 3. IEEE, 2003, pp. 1945–1948.

[80] S. Venkatesh, C. R. Anderson, N. V. Rivera, and R. M. Buehrer, "Implementation and analysis of respiration-rate estimation using impulse-based uwb," in *MILCOM 2005-2005 IEEE Military Communications Conference*. IEEE, 2005, pp. 3314–3320.

[81] D. Nguyen, S. Yamada, B.-K. Park, V. Lubecke, O. Boric-Lubecke, and A. Host-Madsen, "Noise considerations for remote detection of life signs with microwave doppler radar," in *2007 29th Annual International Conference of the IEEE Engineering in Medicine and Biology Society*. IEEE, 2007, pp. 1667–1670.

[82] A. Høst-Madsen, N. Petrochilos, O. Boric-Lubecke, V. M. Lubecke, B.-K. Park, and Q. Zhou, "Signal processing methods for doppler radar heart rate monitoring," in *Signal processing techniques for knowledge extraction and information fusion*. Springer, 2008, pp. 121–140.

[83] A. Lazaro, D. Girbau, R. Villarino, and A. Ramos, "Vital signs monitoring using impulse based uwb signal," in *2011 41st European Microwave Conference*. IEEE, 2011, pp. 135–138.

[84] C. Gu, G. Wang, T. Inoue, and C. Li, "Doppler radar vital sign detection with random body movement cancellation based on adaptive phase compensation," in *2013 IEEE MTT-S International Microwave Symposium Digest (MTT)*. IEEE, 2013, pp. 1–3.

[85] L. Chioukh, H. Boutayeb, D. Deslandes, and K. Wu, "Noise and sensitivity of harmonic radar architecture for remote sensing and detection of vital signs," *IEEE Transactions on Microwave Theory and Techniques*, vol. 62, no. 9, pp. 1847–1855, 2014.

[86] S. Kazemi, A. Ghorbani, H. Amindavar, and C. Li, "Cyclostationary approach to doppler radar heart and respiration rates monitoring with body motion cancelation using radar doppler system," *Biomedical Signal Processing and Control*, vol. 13, pp. 79–88, 2014.

[87] A. Lazaro, D. Girbau, and R. Villarino, "Techniques for clutter suppression in the presence of body movements during the detection of respiratory activity through uwb radars," *Sensors*, vol. 14, no. 2, pp. 2595–2618, 2014.

[88] L. Ren, H. Wang, K. Naishadham, O. Kilic, and A. E. Fathy, "Phase-based methods for heart rate detection using uwb impulse doppler radar," *IEEE Transactions on Microwave Theory and Techniques*, vol. 64, no. 10, pp. 3319–3331, 2016.

[89] X. Hu and T. Jin, "Short-range vital signs sensing based on eemd and cwt using ir-uwb radar," *Sensors*, vol. 16, no. 12, p. 2025, 2016.

[90] M.-C. Huang, J. J. Liu, W. Xu, C. Gu, C. Li, and M. Sarrafzadeh, "A self-calibrating radar sensor system for measuring vital signs," *IEEE transactions on biomedical circuits and systems*, vol. 10, no. 2, pp. 352–363, 2016.

[91] S. Kazemi, A. Ghorbani, H. Amindavar, and D. R. Morgan, "Vital-sign extraction using bootstrap-based generalized warblet transform in heart and respiration monitoring radar system," *IEEE Transactions on Instrumentation and Measurement*, vol. 65, no. 2, pp. 255–263, 2016.

[92] X. Liang, H. Zhang, S. Ye, G. Fang, and T. A. Gulliver, "Improved denoising method for through-wall vital sign detection using uwb impulse radar," *Digital Signal Processing*, vol. 74, pp. 72–93, 2018.

[93] Z. Yu, D. Zhao, and Z. Zhang, "Doppler radar vital signs detection method based on higher order cyclostationary," *Sensors*, vol. 18, no. 1, p. 47, 2018.

[94] L. Qu, S. Lian, Y. Sun, and L. Zhang, "Doppler radar vital sign detection based on complex continuous basis pursuit algorithm," in *2018 Progress in Electromagnetics Research Symposium (PIERS-Toyama)*. IEEE, 2018, pp. 2371–2377.

[95] M. Li and J. Lin, "Wavelet-transform-based data-length-variation technique for fast heart rate detection using 5.8-ghz cw doppler radar," *IEEE Transactions on Microwave Theory and Techniques*, vol. 66, no. 1, pp. 568–576, 2018.

[96] O. Boric-Lubecke, A. D. Droitcour, V. M. Lubecke, J. Lin, and G. T. Kovacs, "Wireless ic doppler radars for sensing of heart and respiration activity," in *6th International Conference on Telecommunications in Modern Satellite, Cable and Broadcasting Service, 2003. TELSIKS 2003.*, vol. 1. IEEE, 2003, pp. 337–344.

[97] A. Droitcour, O. BORIC-LUBECKE, V. M. Lubecke, J. Lin, and G. T. KOVACS, "Chest motion sensing with modified silicon base station chips," *IEICE transactions on electronics*, vol. 87, no. 9, pp. 1524–1531, 2004.

[98] J. Lin and C. Li, "Wireless non-contact detection of heartbeat and respiration using low-power microwave radar sensor," in *2007 Asia-Pacific Microwave Conference*. IEEE, 2007, pp. 1–4.

[99] J.-H. Cheng, Y.-H. Lin, W.-J. Lin, J.-H. Tsai, T.-W. Huang, and H. Wang, "An integrated dual-band transmitter for vital sign detection radar applications in 0.18-μm cmos," in *Microwave Integrated Circuits Conference (EuMIC), 2016 11th European*. IEEE, 2016, pp. 109–112.

[100] C.-C. Chou, W.-C. Lai, Y.-K. Hsiao, and H.-R. Chuang, "60-ghz cmos doppler radar sensor with integrated v-band power detector for clutter monitoring and automatic clutter-cancellation in noncontact vital-signs sensing,"

IEEE Transactions on Microwave Theory and Techniques, vol. 66, no. 3, pp. 1635–1643, 2018.

[101] C.-H. Chan, C.-C. Chou, and H.-R. Chuang, "Integrated packaging design of low-cost bondwire interconnection for 60-ghz cmos vital-signs radar sensor chip with millimeter-wave planar antenna," *IEEE Transactions on Components, Packaging and Manufacturing Technology*, vol. 8, no. 2, pp. 177–185, 2018.

[102] C.-H. Tseng and Y.-H. Lin, "24-ghz self-injection-locked vital-sign radar sensor with cmos injection-locked frequency divider based on push–push oscillator topology," *IEEE Microwave and Wireless Components Letters*, vol. 28, no. 11, pp. 1053–1055, 2018.

[103] V. M. Lubecke, O. Boric-Lubecke, A. Host-Madsen, and A. E. Fathy, "Through-the-wall radar life detection and monitoring," in *2007 IEEE/MTT-S International Microwave Symposium*. IEEE, 2007, pp. 769–772.

[104] I. Akiyama, N. Yoshizumi, A. Ohya, Y. Aoki, and F. Matsuno, "Search for survivors buried in rubble by rescue radar with array antennas-extraction of respiratory fluctuation," in *2007 IEEE International Workshop on Safety, Security and Rescue Robotics*. IEEE, 2007, pp. 1–6.

[105] C. Li, X. Yu, C.-M. Lee, D. Li, L. Ran, and J. Lin, "High-sensitivity software-configurable 5.8-ghz radar sensor receiver chip in 0.13− *mu* m cmos for noncontact vital sign detection," *IEEE Transactions on Microwave Theory and Techniques*, vol. 58, no. 5, pp. 1410–1419, 2010.

[106] D. Girbau, A. Lazaro, A. Ramos, and R. Villarino, "Remote sensing of vital signs using a doppler radar and diversity to overcome null detection," *IEEE Sensors Journal*, vol. 12, no. 3, pp. 512–518, 2012.

[107] J. Li, Z. Zeng, J. Sun, and F. Liu, "Through-wall detection of human being's movement by uwb radar," *IEEE Geoscience and Remote Sensing Letters*, vol. 9, no. 6, pp. 1079–1083, 2012.

[108] F.-K. Wang, T.-S. Horng, K.-C. Peng, J.-K. Jau, J.-Y. Li, and C.-C. Chen, "Single-antenna doppler radars using self and mutual injection locking for

vital sign detection with random body movement cancellation," *IEEE Transactions on Microwave Theory and Techniques*, vol. 59, no. 12, pp. 3577–3587, 2011.

[109] X. Yu, C. Li, and J. Lin, "Two-dimensional noncontact vital sign detection using doppler radar array approach," in *2011 IEEE MTT-S International Microwave Symposium*. IEEE, 2011, pp. 1–4.

[110] T.-Y. J. Kao, Y. Yan, T.-M. Shen, A. Y.-K. Chen, and J. Lin, "Design and analysis of a 60-ghz cmos doppler micro-radar system-in-package for vital-sign and vibration detection," *IEEE Transactions on Microwave Theory and Techniques*, vol. 61, no. 4, pp. 1649–1659, 2013.

[111] G. Vinci, S. Lindner, F. Barbon, S. Mann, M. Hofmann, A. Duda, R. Weigel, and A. Koelpin, "Six-port radar sensor for remote respiration rate and heartbeat vital-sign monitoring," *IEEE Transactions on Microwave Theory and Techniques*, vol. 61, no. 5, pp. 2093–2100, 2013.

[112] T. P. Van Nguyen, L. Tang, F. Hasan, N. D. Minh, and S. Mukhopadhyay, "Nature-inspired sensor system for vital signs detection," *Sensors and Actuators A: Physical*, vol. 281, pp. 76–83, 2018.

[113] C. Franks, J. Watson, B. Brown, and E. Foster, "Respiratory patterns and risk of sudden unexpected death in infancy." *Archives of disease in childhood*, vol. 55, no. 8, pp. 595–599, 1980.

[114] C. Li, J. Lin, and Y. Xiao, "Robust overnight monitoring of human vital signs by a non-contact respiration and heartbeat detector," in *2006 International Conference of the IEEE Engineering in Medicine and Biology Society*. IEEE, 2006, pp. 2235–2238.

[115] E. M. Staderini, "An uwb radar based stealthy 'lie detector'," in *Ultra-Wideband, Short-Pulse Electromagnetics 6*. Springer, 2003, pp. 537–552.

[116] S.-T. Tseng, Y.-H. Kao, C.-C. Peng, J.-Y. Liu, S.-C. Chu, G.-F. Hong, C.-H. Hsieh, K.-T. Hsu, W.-T. Liu, Y.-H. Huang *et al.*, "A 65-nm cmos low-power impulse radar system for human respiratory feature extraction and diagnosis on respiratory diseases," *IEEE Transactions on Microwave Theory and Techniques*, vol. 64, no. 4, pp. 1029–1041, 2016.

[117] T.-Y. Huang, J. Lin, and L. Hayward, "Non-invasive measurement of laboratory rat's cardiorespiratory movement using a 60-ghz radar and nonlinear doppler phase modulation," in *2015 IEEE MTT-S 2015 International Microwave Workshop Series on RF and Wireless Technologies for Biomedical and Healthcare Applications (IMWS-BIO)*. IEEE, 2015, pp. 83–84.

[118] C. Li, Z. Peng, T.-Y. Huang, T. Fan, F.-K. Wang, T.-S. Horng, J.-M. Muñoz-Ferreras, R. Gómez-García, L. Ran, and J. Lin, "A review on recent progress of portable short-range noncontact microwave radar systems," *IEEE Transactions on Microwave Theory and Techniques*, vol. 65, no. 5, pp. 1692–1706, 2017.

[119] C. A. Balanis, *Antenna theory: analysis and design*. John wiley & sons, 2016.

[120] Y. S. Lee, P. N. Pathirana, C. L. Steinfort, and T. Caelli, "Monitoring and analysis of respiratory patterns using microwave doppler radar," *IEEE journal of translational engineering in health and medicine*, vol. 2, pp. 1–12, 2014.

[121] L. Crocco and V. Ferrara, "A review on ground penetrating radar technology for the detection of buried or trapped victims," in *2014 International Conference on Collaboration Technologies and Systems (CTS)*. IEEE, 2014, pp. 535–540.

[122] M. Loschonsky, C. Feige, O. Rogall, S. Fisun, and L. Reindl, "Detection technology for trapped and buried people," in *2009 IEEE MTT-S International Microwave Workshop on Wireless Sensing, Local Positioning, and RFID*. IEEE, 2009, pp. 1–6.

[123] M. Baldi, G. Cerri, F. Chiaraluce, L. Eusebi, and P. Russo, "Non-invasive uwb sensing of astronauts' breathing activity," *Sensors*, vol. 15, no. 1, pp. 565–591, 2015.

[124] K. V. Madhav, M. R. Ram, E. H. Krishna, K. N. Reddy, and K. A. Reddy, "Estimation of respiratory rate from principal components of photoplethysmographic signals," in *2010 IEEE EMBS Conference on Biomedical Engineering and Sciences (IECBES)*. IEEE, 2010, pp. 311–314.

[125] K. V. Madhav, M. R. Ram, E. H. Krishna, N. R. Komalla, and K. A. Reddy, "Robust extraction of respiratory activity from ppg signals using modified mspca," *IEEE Transactions on Instrumentation and Measurement*, vol. 62, no. 5, pp. 1094–1106, 2013.

[126] Z. Wang, Y. Zhao, and Y. Yuan, "An emd based breathing and heartbeat monitoring system," in *2013 7th Asia Modelling Symposium*. IEEE, 2013, pp. 55–58.

[127] C. Li and J. Lin, "Complex signal demodulation and random body movement cancellation techniques for non-contact vital sign detection," in *2008 IEEE MTT-S International Microwave Symposium Digest*. IEEE, 2008, pp. 567–570.

[128] L. Anishchenko, V. Razevig, and M. Chizh, "Blind separation of several biological objects respiration patterns by means of a step-frequency continuous-wave bioradar," in *2017 IEEE International Conference on Microwaves, Antennas, Communications and Electronic Systems (COMCAS)*. IEEE, 2017, pp. 1–4.

[129] T.-W. Lee, "Independent component analysis: theory and applications," Ph.D. dissertation, 1997.

[130] B.-J. Jang, S.-H. Wi, J.-G. Yook, M.-Q. Lee, and K.-J. Lee, "Wireless bio-radar sensor for heartbeat and respiration detection," *Progress In Electromagnetics Research C*, vol. 5, pp. 149–168, 2008.

[131] D. Zhang, M. Kurata, and T. Inaba, "Fmcw radar for small displacement detection of vital signal using projection matrix method," *International Journal of Antennas and Propagation*, vol. 2013, 2013.

[132] N. Maaref, P. Millot, C. Pichot, and O. Picon, "Fmcw ultra-wideband radar for through-the-wall detection of human beings," in *2009 International Radar Conference" Surveillance for a Safer World"(RADAR 2009)*. IEEE, 2009, pp. 1–5.

[133] M. Mercuri, P. J. Soh, L. Boccia, D. Schreurs, G. A. Vandenbosch, P. Leroux, and G. Amendola, "Optimized sfcw radar sensor aiming at fall detection in a real room environment," in *2013 IEEE Topical Conference on*

Biomedical Wireless Technologies, Networks, and Sensing Systems. IEEE, 2013, pp. 4–6.

[134] R. Narayanan, X. Xu, and J. Henning, "Radar penetration imaging using ultra-wideband (uwb) random noise waveforms," *IEE Proceedings-Radar, Sonar and Navigation*, vol. 151, no. 3, pp. 143–148, 2004.

[135] R. M. Narayanan, "Through-wall radar imaging using uwb noise waveforms," *Journal of the Franklin Institute*, vol. 345, no. 6, pp. 659–678, 2008.

[136] A. Gunasekara, "Contactless estimation of breathing rate using uwb radar," Ph.D. dissertation, Université d'Ottawa/University of Ottawa, 2017.

[137] L. Sakkila, Y. Elhillali, A. Rivenq, C. Tatkeu, and J. Rouvaen, "Short range automotive radar based on uwb pseudo-random coding," in *2007 7th International Conference on ITS Telecommunications*. IEEE, 2007, pp. 1–6.

[138] J. Sachs, M. Helbig, R. Herrmann, M. Kmec, K. Schilling, and E. Zaikov, "Remote vital sign detection for rescue, security, and medical care by ultra-wideband pseudo-noise radar," *Ad Hoc Networks*, vol. 13, pp. 42–53, 2014.

[139] J. Sun and M. Li, "Life detection and location methods using uwb impulse radar in a coal mine," *Mining Science and Technology (China)*, vol. 21, no. 5, pp. 687–691, 2011.

[140] R. Garg, P. Bhartia, I. J. Bahl, and A. Ittipiboon, *Microstrip antenna design handbook*. Artech house, 2001.

[141] K. Carver and J. Mink, "Microstrip antenna technology," *IEEE transactions on antennas and propagation*, vol. 29, no. 1, pp. 2–24, 1981.

[142] K. Luk, C. Mak, Y. Chow, and K. Lee, "Broadband microstrip patch antenna," *Electronics letters*, vol. 34, no. 15, pp. 1442–1443, 1998.

[143] J. S. Sainath and K. Karthikeyan, "Design and analysis of multiband hybrid coupler pentagon micro strip antenna for l-band applications," in *2015 IEEE 9th International Conference on Intelligent Systems and Control (ISCO)*. IEEE, 2015, pp. 1–5.

[144] S. Bist, S. Saini, V. Prakash, and B. Nautiyal, "Study the various feeding techniques of microstrip antenna using design and simulation using cst microwave studio," *International Journal of Emerging Technology and Advanced Engineering*, vol. 4, no. 9, 2014.

[145] M. S. Rabbani and H. Ghafouri-Shiraz, "Ultra-wide patch antenna array design at 60 ghz band for remote vital sign monitoring with doppler radar principle," *Journal of Infrared, Millimeter, and Terahertz Waves*, pp. 1–19.

[146] P. Das, P. Kumar *et al.*, "Designing microstrip antenna with octagonal bounded elliptical slots," in *2016 10th International Conference on Intelligent Systems and Control (ISCO)*. IEEE, 2016, pp. 1–3.

[147] M. A. Sultan, "The radiation characteristics of open-and closed-ring microstrip antennas," 1986.

[148] J. R. James, P. S. Hall *et al.*, *Handbook of microstrip antennas*. IET, 1989, vol. 1.

[149] A. M. Abbosh, "Design of ultra-wideband three-way arbitrary power dividers," *IEEE Transactions on Microwave Theory and Techniques*, vol. 56, no. 1, pp. 194–201, 2008.

[150] S. W. Wong and L. Zhu, "Ultra-wideband power divider with good in-band splitting and isolation performances," *IEEE Microwave and Wireless Components Letters*, vol. 18, no. 8, pp. 518–520, 2008.

[151] D. Obeid, S. Samad, S. Sadek, G. Zaharia, and G. El Zein, "Position-free vital sign monitoring: Measurements and processing," *Advanced Biosignal Processing and Diagnostic Methods*, p. 31, 2016.

[152] H. Zhao, H. Hong, L. Sun, Y. Li, C. Li, and X. Zhu, "Noncontact physiological dynamics detection using low-power digital-if doppler radar," *IEEE Transactions on Instrumentation and Measurement*, vol. 66, no. 7, pp. 1780–1788, 2017.

[153] A. D. Droitcour, O. Boric-Lubecke, V. M. Lubecke, J. Lin, and G. T. Kovacs, "Range correlation and i/q performance benefits in single-chip silicon

doppler radars for noncontact cardiopulmonary monitoring," *IEEE Transactions on Microwave Theory and Techniques*, vol. 52, no. 3, pp. 838–848, 2004.

[154] H. Bo, L. Xu, L. Hao, Y. Dou, L. Zhao, and W. Yu, "A single-channel non-orthogonal i/q rf sensor for non-contact monitoring of vital signs," *Appl. Comput. Electromagn. Soc. J*, vol. 31, no. 6, pp. 603–611, 2016.

[155] "BK-NICO medical center hanoi university of technology," http://bme.hust.edu.vn, accessed: 2017-01-01.

[156] M. K. Mishra, N. Sood, and A. K. Sharma, "Efficient ber analysis of ofdm system over nakagami-m fading channel," *International Journal of Advanced Science and Technology*, vol. 37, pp. 37–46, 2011.

[157] M.-S. Alouini and M. K. Simon, "Performance of coherent receivers with hybrid sc/mrc over nakagami-m fading channels," *IEEE Transactions on Vehicular Technology*, vol. 48, no. 4, pp. 1155–1164, 1999.

[158] H. A. Suraweera, P. J. Smith, and J. Armstrong, "Outage probability of cooperative relay networks in nakagami-m fading channels," *IEEE Communications Letters*, vol. 10, no. 12, pp. 834–836, 2006.

[159] A. D. Droitcour, O. Boric-Lubecke, and G. T. Kovacs, "Signal-to-noise ratio in doppler radar system for heart and respiratory rate measurements," *IEEE transactions on microwave theory and techniques*, vol. 57, no. 10, pp. 2498–2507, 2009.

[160] B. R. Mahafza, *Radar Systems Analysis and Design Using MATLAB Third Edition*. CRC press, 2013.

[161] N. T. P. Van, S. F. Hasan, X. Gui, S. Mukhopadhyay, and H. Tran, "Three-step two-way decode and forward relay with energy harvesting," *IEEE Communications Letters*, vol. 21, no. 4, pp. 857–860, 2017.

[162] M. Kreh, "Bessel functions: project for the penn state–gttingen summer school on number theory," *Available form: http://www. math. psu. edu/papikian/Kreh. pdf*, 2017.

[163] C. S. Withers and S. Nadarajah, "On the product of gamma random variables," *Quality & Quantity*, vol. 47, no. 1, pp. 545–552, 2013.

[164] A. Jeffrey and D. Zwillinger, *Table of integrals, series, and products*. Elsevier, 2007.

[165] G. Grandjean, N. Baghdadi, P. Paillou, P. Dreuillet, P. Dubois, J. Souyris, and J. Achache, "Radar penetration in soils: Towards a new system for subsurface earth observation," in *SAR workshop: CEOS Committee on Earth Observation Satellites*, vol. 450, 2000, p. 267.

[166] J. D. Altringham, J. D. Altringham *et al.*, *Bats: biology and behavior*. Oxford University Press Inc., New York, 1999, no. Sirsi) i9780198503224.

[167] Y.-Y. Chiu, W.-Y. Lin, H.-Y. Wang, S.-B. Huang, and M.-H. Wu, "Development of a piezoelectric polyvinylidene fluoride (pvdf) polymer-based sensor patch for simultaneous heartbeat and respiration monitoring," *Sensors and Actuators A: Physical*, vol. 189, pp. 328–334, 2013.

[168] B. Du, D. Yang, X. She, Y. Yuan, D. Mao, Y. Jiang, and F. Lu, "Mos2-based all-fiber humidity sensor for monitoring human breath with fast response and recovery," *Sensors and Actuators B: Chemical*, vol. 251, pp. 180–184, 2017.

[169] E. Koch and A. Dietzel, "Skin attachable flexible sensor array for respiratory monitoring," *Sensors and Actuators A: Physical*, vol. 250, pp. 138–144, 2016.

[170] J. Weiss, E. Jondeau, A. Giani, B. Charlot, and P. Combette, "Static and dynamic calibration of a mems calorimetric shear-stress sensor," *Sensors and Actuators A: Physical*, vol. 265, pp. 211–216, 2017.

[171] O. Thiabgoh, T. Eggers, and M.-H. Phan, "A new contactless magneto-lc resonance technology for real-time respiratory motion monitoring," *Sensors and Actuators A: Physical*, vol. 265, pp. 120–126, 2017.

[172] S. K. Davis, E. J. Bond, S. Hagness, and B. Van Veen, "Microwave imaging via space-time beamforming for early detection of breast cancer: Beamformer design in the frequency domain," *Journal of Electromagnetic Waves and Applications*, vol. 17, no. 2, pp. 357–381, 2003.

[173] E. C. Fear, J. Bourqui, C. Curtis, D. Mew, B. Docktor, and C. Romano, "Microwave breast imaging with a monostatic radar-based system: A study of application to patients," *IEEE transactions on microwave theory and techniques*, vol. 61, no. 5, pp. 2119–2128, 2013.

[174] L. Sun, H. Hong, Y. Li, C. Gu, F. Xi, C. Li, and X. Zhu, "Noncontact vital sign detection based on stepwise atomic norm minimization," *IEEE Signal Processing Letters*, vol. 22, no. 12, pp. 2479–2483, 2015.

[175] F. Khan and S. Cho, "A detailed algorithm for vital sign monitoring of a stationary/non-stationary human through ir-uwb radar," *Sensors*, vol. 17, no. 2, p. 290, 2017.

[176] H. Zhao, H. Hong, L. Sun, F. Xi, C. Li, and X. Zhu, "Accurate dc offset calibration of doppler radar via non-convex optimisation," *Electronics Letters*, vol. 51, no. 16, pp. 1282–1284, 2015.

[177] N. Phuoc Van, L. Tang, S. Mukhopadhyay, D. Nguyen, and F. Hasan, "Probabilities of false alarm for vital sign detection on the basis of a doppler radar system," *Sensors*, vol. 18, no. 3, p. 694, 2018.

[178] X.-Y. Hou, N. Morinaga, and T. Namekawa, "Direct evaluation of radar detection probabilities," *IEEE Transactions on aerospace and electronic systems*, no. 4, pp. 418–424, 1987.

[179] M. Hamid, N. Björsell, and S. B. Slimane, "Empirical statistical model for lte downlink channel occupancy," *Wireless personal communications*, vol. 96, no. 1, pp. 855–866, 2017.

[180] E. L. Crow and K. Shimizu, *Lognormal distributions*. Marcel Dekker New York, 1987.

[181] C. Gary Schurman MBE, "The mean and variance of the product of two lognormally-distributed random variates," *Available online: http://www.appliedbusinesseconomics.com/files%5Cgvsplndrn01.pdf*, 2012.

[182] S. Theodoridis and K. Koutroumbas, "Pattern recognition. 2003," *Elsevier Inc*, 2009.

[183] H.-f. Hu, S.-j. Sun, R.-q. Lv, and Y. Zhao, "Design and experiment of an optical fiber micro bend sensor for respiration monitoring," *Sensors and Actuators A: Physical*, vol. 251, pp. 126–133, 2016.

[184] Y. S. Lee, P. N. Pathirana, and C. L. Steinfort, "Respiration rate and breathing patterns from doppler radar measurements," in *2014 IEEE Conference on Biomedical Engineering and Sciences (IECBES)*. IEEE, 2014, pp. 235–240.

[185] G. Yuan, N. A. Drost, and R. A. McIvor, "Respiratory rate and breathing pattern," *McMaster University Medical Journal*, vol. 10, no. 1, pp. 23–25, 2013.

[186] B. Boashash and S. Ouelha, "Efficient software platform tfsap 7.1 and matlab package to compute time–frequency distributions and related time-scale methods with extraction of signal characteristics," *SoftwareX*, vol. 8, pp. 48–52, 2018.

[187] J. M. d. Haan, "A survey on methods for time-frequency analysis," 1998.

[188] J. B. Tary, R. H. Herrera, and M. van der Baan, "Analysis of time-varying signals using continuous wavelet and synchrosqueezed transforms," *Philosophical Transactions of the Royal Society A: Mathematical, Physical and Engineering Sciences*, vol. 376, no. 2126, p. 20170254, 2018.

[189] N. Nazmi, M. Abdul Rahman, S.-I. Yamamoto, S. Ahmad, H. Zamzuri, and S. Mazlan, "A review of classification techniques of emg signals during isotonic and isometric contractions," *Sensors*, vol. 16, no. 8, p. 1304, 2016.

[190] Y. Q. Chen, R. I. Damper, and M. S. Nixon, "On neural-network implementations of k-nearest neighbor pattern classifiers," *IEEE Transactions on Circuits and Systems I: Fundamental Theory and Applications*, vol. 44, no. 7, pp. 622–629, 1997.

[191] C. Venkatesan, P. Karthigaikumar, A. Paul, S. Satheeskumaran, and R. Kumar, "Ecg signal preprocessing and svm classifier-based abnormality detection in remote healthcare applications," *IEEE Access*, vol. 6, pp. 9767–9773, 2018.

[192] H. Lan. (2017) Decision trees and random forests for classification and regression. [Online]. Available: https://towardsdatascience.com/decision-trees-and-random-forests-for-classification-and-regression-pt-2-2b1fcd03e342

[193] A. Géron, *Hands-on machine learning with Scikit-Learn and TensorFlow: concepts, tools, and techniques to build intelligent systems.* " O'Reilly Media, Inc.", 2017.

[194] R. Rivera-Lopez and J. Canul-Reich, "Construction of near-optimal axis-parallel decision trees using a differential-evolution-based approach," *IEEE Access*, vol. 6, pp. 5548–5563, 2018.

[195] Y. Bao, X. Du, M. Deng, and N. Ishii, "An efficient method for computing all reducts," *Transactions of the Japanese Society for Artificial Intelligence*, vol. 19, no. 3, pp. 166–173, 2004.

[196] W. Wu, J. Liu, H. Rong, H. Wang, and M. Xian, "Efficient k-nearest neighbor classification over semantically secure hybrid encrypted cloud database," *IEEE Access*, vol. 6, pp. 41 771–41 784, 2018.

[197] E. A. Patrick and F. P. Fischer III, "A generalized k-nearest neighbor rule," *Information and control*, vol. 16, no. 2, pp. 128–152, 1970.

[198] J. Brownlee. (2016) K-nearest neighbors for machine learning. [Online]. Available: https://machinelearningmastery.com/k-nearest-neighbors-for-machine-learning/

[199] M. Mabrouk, S. Rajan, M. Bolic, M. Forouzanfar, H. R. Dajani, and I. Batkin, "Human breathing rate estimation from radar returns using harmonically related filters," *Journal of Sensors*, vol. 2016, 2016.

[200] D. Girbau, A. Lázaro, Á. Ramos, and R. Villarino, "Remote sensing of vital signs using a doppler radar and diversity to overcome null detection," *IEEE Sensors Journal*, vol. 12, no. 3, pp. 512–518, 2011.

[201] F.-K. Wang, C.-H. Fang, T.-S. Horng, K.-C. Peng, J.-Y. Li, and C.-C. Chen, "Concurrent vital sign and position sensing of multiple individuals using self-injection-locked tags and injection-locked i/q receivers with arctangent demodulation," *IEEE Transactions on Microwave Theory and Techniques*, vol. 61, no. 12, pp. 4689–4699, 2013.

[202] Q. Zhou, J. Liu, A. Host-Madsen, O. Boric-Lubecke, and V. Lubecke, "Detection of multiple heartbeats using doppler radar," in *2006 IEEE International Conference on Acoustics Speech and Signal Processing Proceedings*, vol. 2. IEEE, 2006, pp. II–II.

[203] C. Li, J. Cummings, J. Lam, E. Graves, and W. Wu, "Radar remote monitoring of vital signs," *IEEE Microwave Magazine*, vol. 10, no. 1, pp. 47–56, 2009.

[204] Z. Peng, J. M. Muñoz-Ferreras, Y. Tang, C. Liu, R. Gómez-García, L. Ran, and C. Li, "A portable fmcw interferometry radar with programmable low-if architecture for localization, isar imaging, and vital sign tracking," *IEEE transactions on microwave theory and techniques*, vol. 65, no. 4, pp. 1334–1344, 2016.

[205] H. Xue, M. Liu, Y. Zhang, F. Liang, F. Qi, F. Chen, H. Lv, and J. Wang, "An algorithm based wavelet entropy for shadowing effect of human detection using ultra-wideband bio-radar," *Sensors*, vol. 17, no. 10, p. 2255, 2017.

[206] Y. Zhang, T. Jiao, H. Lv, S. Li, C. Li, G. Lu, X. Yu, Z. Li, and J. Wang, "An interference suppression technique for life detection using 5.75-and 35-ghz dual-frequency continuous-wave radar," *IEEE Geoscience and Remote Sensing Letters*, vol. 12, no. 3, pp. 482–486, 2014.

MASSEY UNIVERSITY
GRADUATE RESEARCH SCHOOL

STATEMENT OF CONTRIBUTION
DOCTORATE WITH PUBLICATIONS/MANUSCRIPTS

We, the candidate and the candidate's Primary Supervisor, certify that all co-authors have consented to their work being included in the thesis and they have accepted the candidate's contribution as indicated below in the *Statement of Originality*.

Name of candidate:	Nguyen Thi Phuoc Van
Name/title of Primary Supervisor:	Liqiong Tang
Name of Research Output and full reference:	
Van Nguyen Thi Phuoc, Liqiong Tang, Veysel Demir, Faraz Hasan, Duc Minh Nguyen, and Subhas Chandra Mukhopadhyay,. " Review-Microwave Radar Sensing Systems for Search and Rescue Purpose" Sensors 2019, 19(13), 2879,	
In which Chapter is the Manuscript /Published work:	Chapter 2
Please indicate:	
• The percentage of the manuscript/Published Work that was contributed by the candidate:	80%
and	
• Describe the contribution that the candidate has made to the Manuscript/Published Work:	
The candidate was responsible for research conceptualization and write the majority of the manuscript.	
For manuscripts intended for publication please indicate target journal:	
Candidate's Signature:	Nguyen Thi Phuoc Van Digitally signed by Nguyen Thi Phuoc Van Date: 2019.10.29 10:16:10 +13'00'
Date:	
Primary Supervisor's Signature:	Liqiong Tang Digitally signed by Liqiong Tang Date: 2019.10.29 14:04:16 +13'00'
Date:	

(This form should appear at the end of each thesis chapter/section/appendix submitted as a manuscript/ publication or collected as an appendix at the end of the thesis)

MASSEY UNIVERSITY
GRADUATE RESEARCH SCHOOL

STATEMENT OF CONTRIBUTION
DOCTORATE WITH PUBLICATIONS/MANUSCRIPTS

We, the candidate and the candidate's Primary Supervisor, certify that all co-authors have consented to their work being included in the thesis and they have accepted the candidate's contribution as indicated below in the *Statement of Originality*.

Name of candidate:	Nguyen Thi Phuoc Van
Name/title of Primary Supervisor:	Dr. Liqiong Tang
Name of Research Output and full reference:	
"Wide Band Antennae System for Remote Vital Signs Detecting Doppler Radar Sensor." Van Nguyen Thi Phuoc, Liqiong Tang, Duc Minh Nguyen, Faraz Hasan, and Subhas Mukhopadhyay. In Modern Sensing Technologies, pp. 47-62. Springer, Cham,	
In which Chapter is the Manuscript /Published work:	Chapter 3
Please indicate:	
• The percentage of the manuscript/Published Work that was contributed by the candidate:	80%
and	
• Describe the contribution that the candidate has made to the Manuscript/Published Work:	
The candidate was responsible for research conceptualization, setup the measurement, design the antennae system and write the majority of manuscript.	
For manuscripts intended for publication please indicate target journal:	
Candidate's Signature:	Nguyen Thi Phuoc Van Digitally signed by Nguyen Thi Phuoc Van Date: 2019.10.29 10:05:05 +13'00'
Date:	29/10/2019
Primary Supervisor's Signature:	Liqiong Tang Digitally signed by Liqiong Tang Date: 2019.10.29 14:07:34 +13'00'
Date:	

(This form should appear at the end of each thesis chapter/section/appendix submitted as a manuscript/ publication or collected as an appendix at the end of the thesis)

MASSEY UNIVERSITY
GRADUATE RESEARCH SCHOOL

STATEMENT OF CONTRIBUTION
DOCTORATE WITH PUBLICATIONS/MANUSCRIPTS

We, the candidate and the candidate's Primary Supervisor, certify that all co-authors have consented to their work being included in the thesis and they have accepted the candidate's contribution as indicated below in the *Statement of Originality*.

Name of candidate:	Nguyen Thi Phuoc Van
Name/title of Primary Supervisor:	Dr. Liqiong Tang
Name of Research Output and full reference:	
Van Nguyen Thi Phuoc, Liqiong Tang, Subhas Chandra Mukhopadhyay, Duc Minh Nguyen, and Faraz Hasan. "Probabilities of False Alarm for Vital Sign Detection on the Basis of a Doppler Radar System." Sensors 18, no. 3 (2018): 694.	
In which Chapter is the Manuscript /Published work:	Chapter 4
Please indicate:	
• The percentage of the manuscript/Published Work that was contributed by the candidate:	80%
and	
• Describe the contribution that the candidate has made to the Manuscript/Published Work:	
The candidate was responsible for research conceptualization and write the majority of the manuscript.	
For manuscripts intended for publication please indicate target journal:	
Candidate's Signature:	Nguyen Thi Phuoc Van Digitally signed by Nguyen Thi Phuoc Van Date: 2019.10.29 10:30:07 +13'00'
Date:	29/10/2019
Primary Supervisor's Signature:	Liqiong Tang Digitally signed by Liqiong Tang Date: 2019.10.29 14:08:23 +13'00'
Date:	

(This form should appear at the end of each thesis chapter/section/appendix submitted as a manuscript/ publication or collected as an appendix at the end of the thesis)

MASSEY UNIVERSITY
GRADUATE RESEARCH SCHOOL

STATEMENT OF CONTRIBUTION
DOCTORATE WITH PUBLICATIONS/MANUSCRIPTS

We, the candidate and the candidate's Primary Supervisor, certify that all co-authors have consented to their work being included in the thesis and they have accepted the candidate's contribution as indicated below in the *Statement of Originality*.

Name of candidate:	Nguyen Thi Phuoc Van
Name/title of Primary Supervisor:	Dr. Liqiong Tang
Name of Research Output and full reference:	
Van Nguyen Thi Phuoc Liqiong Tang, Faraz Hasan, Nguyen Duc Minh, and Subhas Mukhopadhyay. "Nature-inspired sensor system for vital signs detection." Sensors and Actuators A: Physical 281 (2018): 76-83.	
In which Chapter is the Manuscript /Published work:	Chapter 5
Please indicate:	
• The percentage of the manuscript/Published Work that was contributed by the candidate:	80%
and	
• Describe the contribution that the candidate has made to the Manuscript/Published Work:	
The candidate was responsible for research conceptualization and write the majority of the manuscript.	
For manuscripts intended for publication please indicate target journal:	
Candidate's Signature:	Nguyen Thi Phuoc Van Digitally signed by Nguyen Thi Phuoc Van Date: 2019.10.29 10:25:46 +13'00'
Date:	29/10/2019
Primary Supervisor's Signature:	Liqiong Tang Digitally signed by Liqiong Tang Date: 2019.10.29 14:10:04 +13'00'
Date:	

(This form should appear at the end of each thesis chapter/section/appendix submitted as a manuscript/ publication or collected as an appendix at the end of the thesis)

MASSEY UNIVERSITY
GRADUATE RESEARCH SCHOOL

STATEMENT OF CONTRIBUTION
DOCTORATE WITH PUBLICATIONS/MANUSCRIPTS

We, the candidate and the candidate's Primary Supervisor, certify that all co-authors have consented to their work being included in the thesis and they have accepted the candidate's contribution as indicated below in the *Statement of Originality*.

Name of candidate:	Nguyen Thi Phuoc Van
Name/title of Primary Supervisor:	Dr. Liqiong Tang
Name of Research Output and full reference:	
Liqiong Tang, A. Singh, N. D. Minh, S. C. Mukhopadhyay and S. F. Hasan, "Self-Identificaticon Respiratory Disorder Based on Continuous Wave Radar Sensor System," in IEEE Access, vol. 7, pp. 40019-40026, 2019. doi: 10.1109/ACCESS.2019.29068	
In which Chapter is the Manuscript /Published work:	Chapter 6
Please indicate:	
• The percentage of the manuscript/Published Work that was contributed by the candidate:	80%
and	
• Describe the contribution that the candidate has made to the Manuscript/Published Work:	
The candidate was responsible for research conceptualization, design the measurement setup, collect and process data and write the majority of the manuscript.	
For manuscripts intended for publication please indicate target journal:	
Candidate's Signature:	Nguyen Thi Phuoc Van Digitally signed by Nguyen Thi Phuoc Van Date: 2019.10.29 10:22:11 +13'00'
Date:	29/10/2019
Primary Supervisor's Signature:	Liqiong Tang Digitally signed by Liqiong Tang Date: 2019.10.29 14:11:08 +13'00'
Date:	

(This form should appear at the end of each thesis chapter/section/appendix submitted as a manuscript/ publication or collected as an appendix at the end of the thesis)